CRITICAL SOUND ATTENUATION IN THE SYSTEM GA-BI

ATTENUATION AND VELOCITY OF ULTRASOUND
NEAR
THE CRITICAL POINT OF GALLIUM-BISMUTH

By

MANFRED PAUL PULS, B.A.Sc., M.A.Sc.

A Thesis

Submitted to the School of Graduate Studies

in Partial Fulfilment of the Requirements

for the Degree

Doctor of Philosophy

McMaster University

May, 1970

DOCTOR OF PHILOSOPHY (1970)

McMASTER UNIVERSITY
Hamilton, Ontario

TITLE: Attenuation and Velocity of Ultrasound Near the Critical Point of Gallium-Bismuth

AUTHOR: Manfred Paul Puls, B.A.Sc. (University of British Columbia)
M.A.Sc. (University of British Columbia)

SUPERVISOR: Professor J.S. Kirkaldy

NUMBER OF PAGES: x, 147.

SCOPE AND CONTENTS:

Attenuation measurements were performed on a liquid Ga-Bi mixture above its miscibility gap and at the frequencies 16.6, 25.5, 37.6 and 49.7 MHz. The attenuation measurements were made over a composition range from 0.20 to 0.75 weight-fraction Bismuth and in the temperature range 0.3 to 9.9^{o}C above the critical temperature of the mixture. For a mixture at the critical composition, attenuation measurements were also made 27.2^{o}C above the critical temperature. The velocity of sound was measured at 25.5 MHz and at each of the above temperature and composition points. The critical temperature and composition of the Ga-Bi system have been determined to improved accuracy as 263.1^{o}C and 0.60 weight-fraction Bismuth, respectively. The attenuation results have been tested against current theories and these theories have been subjected to critical analysis.

ACKNOWLEDGMENTS

I would like to express my appreciation to Professor J.S. Kirkaldy for his encouragement and guidance throughout the course of this work. I would also like to thank the many members of the Metallurgy Department for helpful comments and advice.

Financial support for this project by an Ontario Graduate Fellowship to the author and a National Research Council of Canada research grant to Professor Kirkaldy is gratefully acknowledged.

TABLE OF CONTENTS

LIST OF TABLES

LIST OF ILLUSTRATIONS*

---

* Illustrations have been placed at end of thesis.

CHAPTER 1

INTRODUCTION

When a system undergoes a first order phase transition, such as the boiling of water, certain thermodynamic variables of the system change discontinuously at the transition point. As a consequence, the transition is characterized by a finite and discontinuous change in energy and entropy. By contrast, the onset of a critical phase transition is characterized by the gradual and continuous disappearance of a thermodynamic variable of the system, often identified as the order parameter, which becomes zero at the phase transition point (the critical point). Only small changes in the order parameter are required to change the state of the system drastically when the system is close to the critical point, this situation resulting in correspondingly small amounts of energy being needed to effect this change. This means that the thermodynamic stability of the state of a system near a critical point is of a lower order than that of a system near a first order transition point. Evidence of this lower stability can be gleaned from the large increase in the possible fluctuations of the order parameter that can occur in a system near a critical point. The increased fluctuations manifest themselves in the anomalously large values achieved by certain thermodynamic derivatives that depend on this order parameter (e.g., the specific heat).

In recent years interest has been focussed on the study of critical phase transitions for two reasons. Firstly, it was discovered that earlier

theories (classical theories) of critical phase transitions (some of which were called second order phase transitions) gave predictions which didn't agree with the results of modern experiments. Secondly, the realization developed that a great similarity exists between critical phase transitions in such different substances as a liquid-gas system and a ferromagnetic system. Hence, efforts have been aimed at understanding this similarity and at finding a unified theory. With respect to the equilibrium properties of critical phase transitions, both of these directions of enquiry have led to substantial success.

The increase in the fluctuations of the order parameter near a critical point also causes anomalies to occur in certain hydrodynamic transport modes that are coupled to this order parameter. For instance, in a liquid-liquid system near the critical point anomalous increases are found in the coefficients of shear and bulk viscosities, the sound attenuation coefficient and in the inverse of the diffusion coefficient. For this system, the order parameter is the difference in composition between the equilibrium composition of the system and the critical composition.

The insights and results obtained in the study of equilibrium properties of critical phase transitions gave workers a new impetus towards seeking solutions to the more difficult dynamical problems. Sound attenuation is one of the many properties associated with transport which bears on the dynamical problems. Some time ago, a moderately successful theory explaining the anomalous absorption of sound in the region above the phase separation curve for a liquid-liquid system was given by Fixman. Using a different approach, substantially the same result was obtained

later by Kawasaki. A more recent work by Swift draws on an analogy between variables describing a liquid-liquid and liquid-gas system and makes use of the results of Kadanoff and Swift on the anomalous transport coefficients of a liquid-gas system. He obtains a considerably different result for the sound attenuation coefficient than does Fixman and Kawasaki.

Very few experimental results are available that are extensive enough and accurate enough to serve as a test of the above theories. Furthermore, of the few mixtures for which experimental results on the sound attenuation are available, all of them are made up of complex organic molecules. It is feared that the true anomalous absorption due to the critical fluctuations might be obscured in these mixtures due to the relatively large sizes and complexities of the constituent molecules which might lead to many non-critical dissipation effects. A better system for testing the theories is one comprised of simple monatomic molecules such as found in liquid metal mixtures. However a number of difficulties not usually found with organic mixtures arise when trying to perform accurate sound attenuation measurements in liquid metals. To begin with, their critical temperatures are usually much higher than those for liquid organic systems. This eliminates a lot of possible systems, as too high a critical temperature means reduced accuracy in temperature measurement, sound transmission and temperature control. Oxidation in air at these high temperatures and lack of wettability of most substances are two other common properties of liquid metals that can inhibit or seriously reduce the transmission of sound into the mixture. Fortunately a system was found wherein the above difficulties

were surmountable. This is the system Ga-Bi.

The experimental work consists of the measurement of the velocity and attenuation of sound as a function of temperature, frequency and composition in the system Ga-Bi. The design of the experimental apparatus is described in detail. The results of the experiment are tested against the current theories of critical sound attenuation and a critical evaluation of these theories is given.

CHAPTER 2

THEORY OF CRITICAL PHENOMENA

2.1 Equilibrium Theory

2.1.1 Introduction

In the past ten years renewed interest has been generated in the field of critical phase transitions[1]. This has come about because it was recognized from new experiments and more sophisticated theoretical analyses that the classical ideas as they had been enunciated by Landau, Ehrenfest, Weiss, van der Waals and others, were either wrong or only partially correct.

Examples of the systems and phenomena that fall into the category of critical transitions are: binary liquid or solid systems that are totally miscible above or below a certain critical temperature and only partially miscible below or above it; one-component liquid systems in equilibrium with their vapours at a critical temperature, pressure and density; systems that become ferromagnetic or antiferromagnetic in zero external field at a critical temperature; the superfluid transition in liquid He^4; some order-disorder transitions in solids; the onset of superconductivity in a variety of metals and alloys.

With the exception of the first two systems, all of the above were identified as second order phase transitions following a classification first put forward by Ehrenfest. Unfortunately, this classification never properly described these transitions and, indeed, probably

added to the confusion and difficulties which arose when attempts were made to conceptualize the mechanisms.

Critical phase transitions are characterized by the continuous loss or gain, as the system approaches the transition temperature, of a certain variable of the system which is called the order parameter. In terms of increasing temperature, examples are: the disappearance of the spontaneous magnetization in zero field of a ferromagnet such as Ni or Fe; the disappearance of the meniscus of a liquid-gas system (difference in density between two phases disappears); appearance or disappearance of total miscibility in a two-component system; the disappearance of an ordered structure such as in beta-brass. At the same time anomalously large values are recorded for the specific heat and the response function of the system as the critical temperature is approached. Examples of response functions are the isothermal compressibility in a liquid-gas system, the inverse of the derivative of the difference in chemical potential with respect to composition in a two-component system and the isothermal susceptibility in a ferromagnet.

Of the early theories the most noteworthy are the Weiss theory for ferromagnetism, the van der Waals theory for a liquid-gas system and the Landau theory of order-disorder. Viewed from the modern perspective, these theories can now all be grouped under the general heading of molecular field theories and can be treated in a unified way provided they are properly characterized by a specific order parameter[2]. For a liquid-gas, a liquid-liquid (or solid-solid) and a ferromagnetic system these are defined in Table I*(listed under $\langle p \rangle$). Also given

*Tables (except for Table VI) have been placed at the end of each section in which they are mentioned.

in Table I are the thermodynamic conjugates of these order parameters. These are listed under the heading h and are defined by the relation $h = \partial F / \partial \langle p \rangle$ where F is the Helmholtz free energy.

Also of note is the theory of Ornstein and Zernicke (O-Z)[3,4] which attempts to derive correlation functions and relate them to thermodynamic data. This theory is of particular value in explaining the results of scattering experiments near liquid system critical points.

The above theories are now called "classical" theories and the results obtained from them are referred to as "classical" results. Briefly the features of a molecular field theory are as follows:

The system is described by a thermodynamic potential such as the Helmholtz (F) or Gibbs (G) free energy formulated as a function of the order parameter and temperature and perhaps an "external field" which can be made vanishingly small near the critical point. In the case of a binary liquid-liquid system with a miscibility gap the order parameter as shown in Table I is $C_1 - C_1^c$ or $C_2 - C_2^c$ where C stands for concentration of component 1 or 2 and the "external field" is in this case given by the difference in chemical potential between component 1 and component 2, $\mu_1 - \mu_2$ (written often as μ_{12}).

To obtain the functional dependence of F, say, very near the critical point, two approaches are usually used. One is microscopic and makes use of statistical mechanics to calculate the free energy of the system. To make the problem tractable, a mean field is said to act upon each molecule, this being a suitable average of the effect of all molecules surrounding the first. Only long range ordering is considered, short range order and possible correlations being ignored.

The other approach is a phenomenological one in which the thermodynamic potential is expanded in a Taylor series around the critical point and the various orders are investigated by invoking the requirements of thermodynamic stability. These imply that for a stable state of the system the first non-zero derivative of F for any displacement of the order parameter from its equilibrium value must be the fourth or any higher even derivative. This means that we have, at least

$$dF = 0,\ d^2F = 0,\ d^3F = 0,\ d^4F \geq 0$$

where the above derivatives stand for the first, second, third and fourth order terms of the Taylor expansion

$$\Delta F = dF + d^2F + d^3F + d^4F + \ldots .$$

Considering specifically the cases of liquid-gas, liquid-liquid and solid-solid systems and for comparison purposes, a ferromagnetic system, and following either of the above calculations, one then obtains the results summarized in Tables II and III. Similar results are obtained for analogous quantities in other systems having critical points. The results are supposed to be valid only in a certain temperature range near the critical point and, as shown in Table II, are conveniently put into power law form. The various exponents in the power laws are called critical indices. The results of theory and experiments near critical points are now usually put into this form to facilitate comparison. Table II gives a list of the critical indices and how they

are used in the above-named systems. Table III gives the values of the indices for the various theories and experimental observations.

The major faults of the above derivations are that in the first instance the mean field is substituted for the correlated fluctuations of the atoms, while in the second instance it is assumed that a Taylor series expansion about the critical point is a valid procedure and hence that the thermodynamic potential exhibits no singularities. What this amounts to in both cases is ignoring the possibility of fluctuations in the order parameter, i.e., the molecular field theories say that the equilibrium order parameter is the only one and no fluctuations about the equilibrium value near the critical point are allowed. It turns out that all of the above assumptions are correct, and hence the results derived from them, if the systems considered have really long range forces. This is hardly ever the case in fact. More sophisticated theories such as those based on the Ising or Heisenberg models, show that for systems with short range forces (inter-molecular range) it is these fluctuations and their correlations which account for the behaviour of systems undergoing critical transitions and hence that the thermodynamic potentials have singularities around the critical point. It is for this reason that the molecular field theories are expected to give incorrect results. Experimental findings, moreover, confirm this conclusion as indicated in Table III.

With a view to applying certain results of the equilibrium theory to the dynamical problem of critical behaviour, the next section will give a short account of the O-Z theory and the O-Z-Debye theory. A brief discussion on their range of validity, a comparison of their predictions

with experiments and some possible ways of correcting the inadequacies of the O-Z theory are presented. Following this is presented a section on "scaling laws" which propose to make predictions on the relationships between critical indices and on the form of the various correlation functions. These laws are of fairly recent vintage in the study of critical phenomena and stem from a recognition of the mathematical importance[4] of the concept of a correlation length and its general applicability to all systems exhibiting critical phase transitions. These laws are now finding increasing favour with workers in the field. Since the scaling laws give relations between critical indices, they are capable of predicting values for some of the indices different from "classical" theories, and indeed, their predictions for the long-range correlation function differ from the results of the original O-Z theory and the O-Z-Debye theory. Their experimental verification has generated considerable interest.

There are a number of excellent review articles in this field giving good background to both the theoretical and experimental aspects of the problem. Fisher[5] has recently reviewed the theoretical situation while Heller[6] has a corresponding article on the experimental situation. An interesting review article by Kadanoff et al[2] considers both the theoretical and experimental features of equilibrium critical phenomena with emphasis on the "scaling laws".

Table I*. Specific forms for the order parameter.

Phase transition	Meaning of order parameter <p>	h thermodynamic conjugate of <p>
Liquid-gas	Density difference: $\rho_{L,G} - \rho^c$	Chemical potential: μ
Ferromagnetic	Magnetization: $\langle \vec{M} \rangle$	Applied magnetic field: H, along easy (anisotropic) axis
Liquid-liquid	Concentration difference: $C_1 - C_1^c$ (in this case written as mass concentration)	A difference in chemical potentials: $\mu_{12} \equiv (\mu_1/m_1 - \mu_2/m_2)$

* Reprinted (with slight changes) from reference 2.

Table II.* Critical point exponents.

Exponent[a,b]	Liquid-gas	Liquid-liquid[c]	Ferromagnet[d]
Below T_c	At coexistence curve as $T \to T_c^-$	At coexistence curve as $T \to T_c^-$	At $H = 0$, $T \to T_c^-$
α'	$C_v \sim \lvert\varepsilon\rvert^{-\alpha'}$	$C_p \sim \lvert\varepsilon\rvert^{-\alpha'}$	$C_H \sim \lvert\varepsilon\rvert^{-\alpha'}$
β	$(\rho_{L,G} - \rho^c) \sim \lvert\varepsilon\rvert^{\beta}$	$(C_1 - C_1^c) \sim \lvert\varepsilon\rvert^{\beta}$	$M(T) \sim \lvert\varepsilon\rvert^{\beta}$
γ'	$K_T \sim \lvert\varepsilon\rvert^{-\gamma'}$	$\partial C_1/\partial \mu_{12} \sim \lvert\varepsilon\rvert^{-\gamma'}$	$\partial M(T)/\partial H = X(T) \sim \lvert\varepsilon\rvert^{-\gamma'}$
ν'	$\kappa(T) \sim \lvert\varepsilon\rvert^{\nu'}$	$\kappa(T) \sim \lvert\varepsilon\rvert^{\nu'}$	$\kappa(T) \sim \lvert\varepsilon\rvert^{\nu'}$
At $T = T_c$	As $\rho \to \rho^c$	As $C_1 \to C_1^c$	As $H \to 0$
δ	$\lvert\rho-\rho^c\rvert \sim \lvert p-p_c\rvert^{1/\delta}$	$\lvert C_1-C_1^c\rvert \sim \lvert\mu_{12}\rvert^{1/\delta}$	$\lvert M\rvert \sim \lvert H\rvert^{1/\delta}$
η	At $\rho = \rho^c$ as $r \to \infty$ $G(r) \sim \frac{1}{r^{d-2+\eta}}$	At $C_1 = C_1^c = 1 - C_2^c$ as $r \to \infty$ $G(r) \sim \frac{1}{r^{d-2+\eta}}$	At $H = 0$ as $r \to \infty$ $\langle S_0^z S_r^z \rangle \sim \frac{1}{r^{d-2+\eta}}$
Above T_c	Along the critical isochore $\rho = \rho^c$ with $T \to T_c^+$	At the critical concentration and with $T \to T_c^+$	At $H = 0$ as $T \to T_c^+$
α	$C_v \sim \varepsilon^{-\alpha}$	$C_p \sim \varepsilon^{-\alpha}$	$C_H \sim \varepsilon^{-\alpha}$
γ	$K_T \sim \varepsilon^{-\gamma}$	$\partial C_1/\partial \mu_{12} \sim \varepsilon^{-\gamma}$	$\partial M(T)/\partial H \sim \varepsilon^{-\gamma}$
ν	$\kappa(T) \sim \varepsilon^{\nu}$	$\kappa(T) \sim \varepsilon^{\nu}$	$\kappa(T) \sim \varepsilon^{\nu}$

Table II (continued).

a. This table has been included as a reference to define the various critical exponents. Most of the quantities given will be used in the text and defined at the appropriate places. However, it might be useful to give the meaning of the symbol ε now:

$$\varepsilon = \frac{T - T_c}{T_c}$$

b. To be specific, a critical exponent is defined by $\lim_{x \to 0^+} \ell n\, f(x)/\ell n\, x = \lambda$ so that $f(x) \sim x^{\lambda}$ as $x \to 0^+$. Using this definition, if $\lambda = 0$, this can mean either $f(x) \sim |\ell n\, x|$ or else, if $f(0)$ is finite, that it is either continuous or discontinuous as x goes through zero.

c. In the column on the liquid-liquid transition either C_1 or C_2 can be used. Use of C_2 in the expressions just means that 1 would have to be interchanged with 2 wherever it appears.

d. Since the relations given for the ferromagnet will not be explicitly used in the text, definitions of the symbols used are given below.

C_H = specific heat at constant magnetization

M, $M(T)$ = magnetization and spontaneous magnetization, respectively

$X(T)$ = isothermal susceptibility

H = magnetic field

S_r^z = spin variable at site r

$\langle S_o^z S_r^z \rangle$ = spin-spin correlation function

* Reprinted (with slight changes and the addition of a column) from reference 43.

Table III.* Values of critical exponents.

Exponent	Molecular field theories	Ising model		Observation	
		d (dimension) = 2	d = 3	All fluids[a]	Ferromagnet
α'	0 (discontinuous)	0 (logarithmic ∞)	Not sure -- either log. or very small	0.12 ± 0.12	≤ 0.16
β	$\frac{1}{2}$	1/8	$\approx 5/16 = 0.312$	0.346 ± 0.01	0.33 ± 0.03
γ'	1	1 3/4	1.23 - 1.32	1.0 ± 0.3	
ν'	$\frac{1}{2}$				
δ	3	15	5.20 ± 0.15	4.4 ± 0.4	4.1 ± 0.1
η	0	$\frac{1}{4}$	$0.059 \approx 1/18 \pm 0.006$		0.07 ± 0.07
α	0 (discontinuous)	0 (logarithmic ∞)	≥ 0 ≤ 0.2	0.2 ± 0.2	≤ 0.16
γ	1	1 3/4	$1\frac{1}{4}$	1.37 ± 0.2	1.33 ± 0.03
ν	$\frac{1}{2}$	1	0.644 ± 0.002	0.65 ± 0.05	0.65 ± 0.03

a. Most of the values are for the liquid-gas transition. Not as much comprehensive information is available on liquid-liquid systems. However, values of the indices for the two systems are very similar.

* Concept of the table and theoretical values obtained from reference 43 while most of the experimental values were obtained from reference 2.

2.1.2 The Theory of Ornstein and Zernicke

Intermediate between molecular field theories and theories based on the Ising or Heisenberg models is the O-Z theory. This theory was presented by Ornstein and Zernicke[3,4] in 1914 and represented the first attempt to incorporate correlated density fluctuations into correlation function expressions in order to explain the results of light scattering experiments on liquid-gas systems near critical points (critical opalescence).

There are now many approaches to the O-Z method, all substantially equivalent. The following outline of the major results and discussion of the difficulties of the O-Z theory is taken mainly from Fisher's review article[7]. The derivation given below is for a one-component liquid-gas system.

As the first step, consider the correlation function defined for a uniform system by

$$g(\bar{r}_{12}) = \frac{n_2(\bar{r}_1,\bar{r}_2)}{n_1(\bar{r}_1)\, n_2(\bar{r}_2)} = \frac{n_2(\bar{r}_{12})}{\rho^2} \qquad (2\text{-}1)$$

where $n_2(\bar{r}_1,\bar{r}_2)$ and $n_1(\bar{r}_1)$ are pair and singlet distribution functions, respectively, and ρ is the density. For a system in one phase (as a shorthand notation we will use $\bar{r}_{12} \equiv \bar{r}$)

$$g(\bar{r}) \to 1 \qquad (\bar{r} \to \infty)$$

Hence, using the net or complementary correlation function (also called the reduced radial distribution function) one obtains

$$G(\bar{r}) = g(\bar{r}) - 1 \qquad (2\text{-}2)$$

so that now $G(\bar{r}) \to 0$ as $\bar{r} \to \infty$. Thus the deviation of $G(\bar{r})$ from zero is a direct measure of the influence of one molecule on another. From statistical mechanics one obtains the result (particle fluctuations in the grand canonical ensemble) that

$$k_B T \left(\frac{\partial \rho}{\partial p}\right)_T \equiv k_B T \rho K_T = 1 + \rho \int G(\bar{r}) d\bar{r} \tag{2-3}$$

However, $K_T \to \infty$ as $T \to T_c$ which means that the integral diverges as well. Now, since $G(\bar{r})$ is bounded for small $\bar{r}$-values (minimum distance of approach for two molecules) then $\int G(\bar{r}) d\bar{r}$ can only diverge at its upper limit. This means $G(\bar{r})$ must become longranged in the sense that, in three dimensions, it goes to zero slower than $1/r^3$.

Experimentally one way of obtaining information about $G(\bar{r})$ is through the light or X-ray scattering equation (1^{st} Born approximation)

$$\frac{I(\bar{k})}{I_o(\bar{k})} \equiv X(\bar{k}) = 1 + \rho \hat{G}(\bar{k}) \tag{2-4}$$

where $I(\bar{k})$ = scattered intensity in the presence of correlations

$I_o(\bar{k})$ = scattered intensity in the absence of correlations

$|\bar{k}| = 4\pi/\lambda \sin \theta/2$

$\hat{G}(\bar{k}) = \int e^{i\bar{k}.\bar{r}} G(\bar{r}) d\bar{r}$, the Fourier transform of $G(\bar{r})$

Comparing equations (2-3) and (2-4) we obtain that

$$X(0) = \lim_{\bar{k} \to 0} \frac{I(\bar{k})}{I_o(\bar{k})} = 1 + \rho \hat{G}(0) = k_B T \rho K_T \tag{2-5}$$

This predicts that the relative scattering equation (2-4) for zero angle scattering is proportional to the isothermal compressibility. Since

$K_T \rightarrow \infty$ as $T \rightarrow T_c$, low angle scattering becomes large as T_c is approached.

To calculate the functional dependence of $G(\bar{r})$ near T_c, Ornstein and Zernicke used the following approach. They assumed that the contributions to $G(\bar{r}_{12})$ were caused jointly by:

1) A direct influence of molecule 1 on 2 described by a <u>direct</u> correlation function $C(\bar{r}_{12})$. This function should be quite short-ranged and remain so even near T_c.
2) An indirect influence propagated <u>directly</u> from molecule 1 to 3 which in turn propagates it to 2.

Mathematically the above is stated as

$$G(\bar{r}_{12}) = C(\bar{r}_{12}) + \rho \int C(\bar{r}_{13}) G(\bar{r}_{32}) d\bar{r}_3 \tag{2-6}$$

It was hoped that $C(\bar{r}_{12})$ could be obtained from fundamental molecular data so that the above equation could then be solved precisely for $G(\bar{r}_{12})$. Unfortunately this has so far not been found possible and some additional assumptions have to be introduced to facilitate solution of the above equation. Hence, as it stands, equation (2-6) can only be considered as the defining equation for $C(\bar{r})$. Mathematically, equation (2-6) is a convolution; hence Fourier transformation gives

$$1 + \rho \hat{G}(\bar{k}) = \frac{1}{1 - \rho \hat{C}(\bar{k})} \tag{2-7}$$

where $\hat{G}(\bar{k})$ and $\hat{C}(\bar{k})$ are the Fourier transforms of $G(\bar{r})$ and $C(\bar{r})$, respectively. Now since

$$1 + \rho \hat{G}(0) = k_B T \rho K_T \rightarrow \infty \qquad (T \rightarrow T_c) \tag{2-8}$$

then

$$1 - \rho\,\hat{C}(0) = 1 - \rho\int C(\bar{r})d\bar{r} = 0 \qquad (T = T_c) \tag{2-9}$$

which shows that the zeroth moment of $C(\bar{r})$ remains finite at T_c. This at least shows that $C(\bar{r}) \to 0$ more rapidly than $G(\bar{r})$ and agrees with the expectation that it is relatively short-ranged. The most crucial assumption of the theory now follows.

We must make the assumption that $C(\bar{r})$ is strictly short-ranged at and near T_c in the sense that its transform $\hat{C}(\bar{k})$ has a Taylor series expansion in powers of k^2. In particular, we must assume that its second moment

$$R^2 = \frac{1}{2}\,\rho\,\langle\cos^2\theta\rangle\int r^2\,C(\bar{r})d\bar{r} \tag{2-10}$$

exists at T_c and does not vary <u>rapidly</u> near it. Furthermore, unless $C(\bar{r})$ can be calculated independently, R^2 will have the status of a phenomenological parameter to be guessed at or fitted by experiment.

Expanding $\hat{C}(\bar{k})$ in powers of k^2 and neglecting terms of $O(k^4)$ gives the Lorentzian scattering curve (dropping the vector notation)

$$\hat{X}(k) = 1 + \rho\,\hat{G}(k) \cong \frac{1}{R^2(\kappa^2 + k^2)} \qquad (k^2 \to 0) \tag{2-11a}$$

where

$$\kappa^2 = \frac{1 - \rho\,\hat{C}(0)}{R^2} \tag{2-11b}$$

Fourier inversion (in three dimensions) of the above gives the famous O-Z correlation function

$$G(r) \simeq \frac{1}{4\pi\rho R^2}\,\frac{e^{-\kappa r}}{r} \qquad (r \to \infty) \tag{2-12}$$

Now from (2-11), (2-7) and (2-8) κ is related to the isothermal compressibility by

$$K_T = \frac{A}{\kappa^2} \qquad (T \to T_c) \tag{2-13a}$$

where

$$A = \frac{1}{k_B T \rho R^2} \tag{2-13b}$$

and is approximately constant in the critical region. Relations (2-13) imply that

$$\kappa(T) \to 0 \qquad (T \to T_c) \tag{2-14}$$

and hence

$$G(r) \simeq \frac{D}{r} \qquad (r \to \infty, T = T_c) \tag{2-15}$$

Equation (2-13) also suggests that $\kappa(T)$ takes the form

$$\kappa(T) = \kappa_0 \left| 1 - \frac{T}{T_c} \right|^{\nu} \tag{2-16}$$

From Table II

$$K_T \to |T - T_c|^{-\gamma} \quad \text{as} \quad T \to T_c \tag{2-17}$$

thus implying that $\nu = \frac{1}{2}\gamma$.

If the classical value of $\gamma = 1$ (Table III) is assumed one would have $\nu = 1/2$. However there is nothing in the above derivation which demands using this value and hence equally suitable would be the non-classical value $\gamma > 1$, say between 1.1 and 1.3. This would give $\nu > \frac{1}{2}$ by a small amount. Now a study of the scattering equation shows that

the graphs of $1/\hat{X}(k)$ vs k^2 for small values of k^2 should be equi-spaced for different temperatures if $\gamma = 1$ and, moreover, should be straight, with the line for $T = T_c$ going through the origin. This is shown in Fig. 1. If, however, $\gamma > 1$ were correct, the lines as shown in Fig. 2 would still be straight with the $T = T_c$ lines going through the origin, but the lines $T > T_c$ would be spread increasingly further apart with increasing temperature away from the critical temperature. Experimentally, this latter result is in fact what is found, showing that the O-Z theory can accommodate non-classical indices within its framework. There appears, however, to be some experimental evidence that the lines of $1/\hat{X}(k)$ vs k^2 become curved downwards for graphs with T very near T_c and for very small k^2 values. Theoretically this curvature is thought to arise from the incorrectness of assuming that the second moment of $\hat{C}(k)$ exists and can be expanded as a Taylor series in k^2. This, therefore, suggests a failure in the O-Z approach.

Still staying within the framework of the O-Z theory (i.e., assuming that the critical correlations for large r can be described by <u>two</u> lengths; a long range correlation length which goes as $\kappa(T)^{-1}$ and goes to infinity at the critical point, and a short range length representing an effective direct interaction range, which must remain finite at the critical point) Fisher[7] takes account of the above deviative behaviour by writing a more general form for the correlation function, viz.,

$$G(r) \simeq \frac{De^{-\kappa r}}{r^{d-2+\eta}} \left(1 + Q(\kappa r)\right) \quad \left\{\begin{matrix} r \to \infty \\ \rho = \rho_c \end{matrix}\right\} \tag{2-18}$$

where $D = D(T)$ varies relatively slowly with T and $Q(x) \to 0$ as $x \to 1$ and grows less fast than exponentially as $x \to \infty$. A non-Lorentzian

critical scattering curve is obtained where

$$\hat{X}(k) \simeq \frac{\tilde{D}}{(k^2 + \kappa^2)^{1-\eta/2}} \qquad (k^2 \to 0) \tag{2-19}$$

and where $\tilde{D}$ can vary only slowly with T and k. Assuming, as before, that

$$\kappa(T) = \kappa_0 \left| 1 - \frac{T}{T_c} \right|^{\nu} \tag{2-16}$$

and comparing equation (2-19) with the expression for the compressibility Fisher obtains the result that

$$\gamma = (2 - \eta)\nu \tag{2-20}$$

Experimentally and from machine calculations of Ising models in three dimensions it has generally been found that η is small ($\eta \sim 0.06$ might be a reasonable estimate) and hence its addition to the correlation function would not usually affect the results significantly until one gets within millidegrees of the critical point. Of course the exact range inside which this deviation might be important would vary from system to system. From a mathematical point of view it should be noted that any non-zero value of η means that C(r) (for $r \to \infty$) as well as G(r) becomes long-ranged as $T \to T_c$ (meaning that their second moments don't exist). However, C(r) still diverges less rapidly than G(r).

There are many variants of the above interpretation of the O-Z method. Below we present one in particular which will later be used to develop a sound absorption expression, following Fixman. This is the approach used by Debye[8] to explain the angular asymmetry of the scattered

light near a critical point of a binary mixture. Debye's approach is semi-phenomenological and classical in spirit in that fluctuations are calculated via Taylor expansions of certain extensive thermodynamic quantities about their normal values. In particular, for a liquid-gas, as was the case with the original O-Z derivation, he defines two lengths. One is a range of molecular interactions length ℓ defined by the relation

$$\ell^2 = \frac{\int r^2 \, \varepsilon(r) \, d\tau}{\int \varepsilon(r) \, d\tau} \tag{2-21}$$

In this equation it is assumed that the energy of interaction between two molecules ($-\varepsilon(r)$) is a function only of their distance apart r. The integration over the volume $d\tau$ extends over all space up to the distance of closest approach between the two molecules. The other length is called a correlation, or persistence length L and is defined in terms of a correlation function C(r) (in Debye's notation) which describes the correlations between fluctuations at two points 1 and 2 in the system. This is written as

$$L^2 = \frac{\int r^2 C(r) d\tau}{\int C(r) d\tau} \tag{2-22}$$

Similar quantities are defined for the binary system. In particular one has here an average length ℓ defined by

$$\ell^2 = \Omega^{-1} \left[\ell_{11}^2 \frac{W_{11}}{V_1} + \ell_{22}^2 \frac{W_{22}}{V_2} - 2\ell_{12}^2 \frac{W_{12}}{V_1^{\frac{1}{2}} V_2^{\frac{1}{2}}} \right] \tag{2-23}$$

and

$$\Omega = \frac{W_{11}}{V_1} + \frac{W_{22}}{V_2} - 2\frac{W_{12}}{V_1^{\frac{1}{2}} V_2^{\frac{1}{2}}} \tag{2-24}$$

where V_1, V_2 = volumes/molecule

$$W_{11} = \int \varepsilon_{11}\, d\tau$$

$$\ell^2 W_{11} = \int r^2\, \varepsilon_{11}\, d\tau, \text{ etc}$$

Ω is also given by the critical temperature of the system as

$$\Omega = k_B T_c \left[(V_1\, \phi_1)^{-1} + (V_2\, \phi_2)^{-1} \right] \tag{2-25}$$

where the ϕ's are volume fractions.

Debye then shows that if one relates the two expressions for the scattered intensities of light -- the one obtained from a calculation of the excess free energy taking account of critical fluctuations, and the other from the correlation function C(r), one obtains the relation

$$L^2 = \ell^2 \frac{T_c}{|T - T_c|} \tag{2-26}$$

This can be written as

$$\frac{1}{L} = \frac{1}{\ell} \left| 1 - \frac{T}{T_c} \right|^{\frac{1}{2}} \tag{2-27}$$

which is similar to Fisher's expression (2-16) given earlier. Debye's derivation of relation (2-27) however precludes any other values of γ and ν than $\gamma = 1$ and $\nu = \frac{1}{2}$.

Debye's calculations on a binary critical system raise an important question. This is to the effect that to predict results of scattering experiments in binary systems it becomes apparent that more than one correlation function is needed to describe a system, since there are now possible three distinct correlations. Notwithstanding, a number of

authors[9,10] have shown that when the system is near a critical point the three correlation functions ordinarily needed to describe the system become substantially equal to each other. Thus the O-Z formalism for the calculations of correlation functions of a system near a liquid-gas critical point is adequate to the description of the critical behaviour of a binary system.

2.1.3 Equilibrium Scaling Laws

The success of Ising model calculations in giving quantitative descriptions of critical point behaviour of both magnetic systems and liquid-gas or liquid-liquid systems is highly suggestive. Theoretically, this information and the concept of a correlation length, which is an attribute of all critical systems, led several workers to the derivation of some general relations among critical indices. The unifying principle upon which these derivations are based is the idea of "scaling laws"[11,12,13].

Before giving a description of these "scaling laws" some comments must first be made about the temperature range (often called the critical region) inside which it is expected that a classical picture will fail to be a correct description of the physical behaviour of a system. This should also define the region of validity of "scaling laws" and help the experimenter to decide which theories may be expected to fit his data.

Making use of the Landau version of molecular field theory, Ginzburg[14] and Levanyuk[15] predicted the latter's range of validity. The result was that the theory could only be valid in that temperature range for which the reduced temperature interval $\varepsilon = (T - T_c)/T_c$

was much larger than a critical value ε_c which they calculated to be proportional to λ^{-6} where λ was a zero temperature coherence length (range of direct molecular interactions). If $|\varepsilon| << \varepsilon_c$, then fluctuations in the order parameter become important and the molecular field theory can no longer be valid. Thus one expects the molecular field theory to be valid for

$$1 >> |\varepsilon| >> \varepsilon_c$$

This means that one can use the results of a molecular field theory to correctly describe the results of an experiment if one is either far enough away from T_c, or the range of molecular interactions is very long. This point was also mentioned in the introduction where it was pointed out that for a system with infinitely long-ranged forces the molecular field theories correctly describe its critical behaviour. An example of such a system is a van der Waals gas with infinite interaction range.

Another criterion for the range of validity of the molecular field theories was given by Brout[16] who based his calculations on a magnetic model. He obtained the result that the above theories should be valid whenever $|\varepsilon| >> 1/z$ where z is the number of equally interacting spins (or molecules if one carries this over to other systems). Hence in liquid-liquid systems z would be the co-ordination number.

It is worth noting in connection with the above criteria for setting a limit on the critical region that they are formulated in terms of the parameter ε and hence systems with approximately equal z but different T_c would show a widely different $(T - T_c)$ region within which

the classical critical behaviour is expected to fail. For instance the critical $(T - T_c)$ region for liquid metal mixtures should be appreciably larger than for liquid organic mixtures since the critical temperatures are usually much higher for the former.

The "scaling laws" are the results of plausibility arguments applied to an Ising model[13,2]. The arguments are based on the idea that near a critical point the exact nature of short-ranged molecular interactions become unimportant and the important variable now is a length ξ (earlier denoted by κ^{-1} and L in connection with the O-Z and O-Z-Debye theories) which represents the "effective" range of molecular interactions (long-range correlation length). On this basis the system can be "scaled". This means that the system can be subdivided into boxes of dimensions La_o where a_o is the lattice constant and La_o is chosen so as to be large compared to a_o but small compared to ξ, viz.,

$$1 << L << \xi/a_o$$

Then one has a new Ising model problem which should have a similar solution to that for molecular interactions. However, instead of interactions among spins one has interactions among the boxes, each of which contains many spins. As long as the suppositions hold, this box model should give the same answer as the molecular spin problem, except for scaling of the values of parameters ε and h, where h represents an "external" field. We designate these scaled values as $\tilde{\varepsilon}$ and $\tilde{h}$, different from ε and h for the molecular problem. However, as the external field goes to zero one should have that $h \sim \tilde{h}$. One further expects that the proportionality between h and $\tilde{h}$ will depend on the

magnitude of the scaling. It is reasonable to guess that

$$\tilde{h} = L^{x}h$$

and similarly that

$$\tilde{\varepsilon} = L^{y}\varepsilon$$

The exponents x and y are unknowns. Notice that the final form of quantities calculated from the box problem should not have any dependence on L. On comparing the results of the Ising box and spin models, this homogeneity condition on L determines the form of these functions in their dependence on the parameters ε and h.

Thus, using the above arguments with the Ising model, we arrive at relations among the critical indices and find that the nine original indices can now be expressed in terms of the two "fundamental" ones, x and y. These relations among critical indices are (where d is the dimensionality of the system) that

$$\begin{aligned} \beta &= (d - x)/y \\ \gamma &= \gamma' \\ \alpha &= \alpha' \\ \text{and} \quad \frac{d}{y} &= 2 - \alpha = \gamma + 2\beta = \beta(\delta + 1) \end{aligned} \tag{2-28}$$

We obtain further that the spin-spin correlation function is of the form

$$g(R,\varepsilon,h) = |\varepsilon|^{2(d-x)/y}\, \tilde{g}\,(R|\varepsilon|^{1/y},\ \varepsilon/|h|^{y/x}) \tag{2-29}$$

for $R = \dfrac{|\bar{r}-\bar{r}'|}{a_0} >> 1$ and $|\varepsilon| << 1$ and $|h| << 1$.

Table IV*. Comparison of scaling law equalities for Ising model and experimental results[a].

	$2 - \alpha$	$2 - \alpha'$	$d\nu$	$d\nu'$	$d\gamma/(2-n)$	$\gamma + 2\beta$	$\gamma' + 2\beta$	$\beta(\delta+1)$	y	$2x/y$
Two-dimensional Ising model	2	2	2	2	2	2	2	2	1	3.75
Three-dimensional Ising model	1.87 ± 0.12	1.93 + 0.04 - 0.16	1.93 ± 0.01		1.933 ± 0.008	1.87 ± 0.01	1.94 ± 0.05	1.93 ± 0.05	1.55 ± 0.01	3.22 ± 0.02
Experimental results (liquid-gas transition)	1.8 ± 0.2	1.88 ± 0.12	1.95 ± 0.15			2.06 ± 0.2	1.7 ± 0.3	1.87 ± 0.14	1.57 ± 0.03	3.12 ± 0.1

a. The scaling laws predict that, for a given transition, all the numbers indicated in the table (except for y and 2x/y) should be the same.

* Concept of the table and theoretical and experimental values obtained from reference 2.

From equation (2-29) one gets, in the limit h = 0, that

$$\frac{1}{y} = \nu = \nu' = \frac{2-\alpha}{d} \tag{2-30}$$

When $\varepsilon = 0$, $h = 0$ we have as well that

$$g(R, \varepsilon = 0, h = 0) = \frac{1}{R^{d-2+\eta}}$$

which defines η and further that

$$\frac{d\gamma}{(2-\eta)} = 2 - \alpha \tag{2-31}$$

Table IV summarizes the above results and compares the scaling law predictions with the results of theoretical calculations on two-dimensional and three-dimensional Ising models and with experimental results.

2.2 Dynamical Theory

2.2.1 Introduction

As with the equilibrium properties of critical systems, certain dynamical parameters show anomalous values near the critical point[17]. For instance in a liquid-gas system there are anomalous changes in the thermal conductivity, the sound attenuation and the shear viscosity. In a liquid-liquid system we observe large increases in the sound attenuation coefficient, a somewhat smaller increase in the coefficient of shear viscosity while the inverse of the chemical diffusion coefficient (the diffusive resistance) goes to infinity as T_c is approached[17]. Similar

effects are found to occur in other critical systems. It therefore appears that at critical points certain hydrodynamical transport modes become critical and this is manifested in the anomalous properties of the corresponding transport coefficients.

Unfortunately, a theoretical treatment of these dynamical effects is not as simple nor as universal as is the theoretical description of equilibrium properties. Apart from the complication of having another variable, i.e., the time, lack of universality seems to be associated with the fact that in dynamical studies the exact nature of the molecular forces still matters[41]. By comparison, in the equilibrium case, once a system becomes critical this feature of a system ceases to have any theoretical importance.

The next section deals with a classical description of hydrodynamical transport modes and in particular with a description of the cause of sound attenuation in fluid systems when critical effects are absent. Following that is a section dealing with various attempts to describe anomalous attenuation of sound in liquid-liquid and liquid-gas critical systems. The general tactic has been to use some of the results derived from the equilibrium theory of critical points together with the application of frequency dependent transport coefficients.

2.2.2 Hydrodynamic Equations for Non-Critical Sound Propagation

For a fluid system, the attenuation of ultrasonic waves of small amplitudes, such as occur in ultrasonic pulse experiments, is most directly and simply calculated by the use of the linearized equations of hydrodynamics[18].

For a viscous fluid the linearized equation of motion is written as

$$\rho_o \frac{\partial u}{\partial t} = - \frac{\partial p}{\partial x} + \frac{4}{3} \eta \frac{\partial^2 u}{\partial x^2} - \zeta \frac{\partial^2 u}{\partial x^2} \tag{2-32}$$

for unidimensional compressional flow (such as a plane longitudinal sound wave travelling in the x-direction). In the above equation

ρ_o = density of the fluid in the absence of a sound wave

u = fluid velocity in the x-direction

p = hydrostatic pressure

η = shear viscosity

ζ = bulk viscosity, which is related to the time rate of change of the density

Following Stokes setting $\zeta = 0$ in equation (2-32) one obtains the Stokes-Navier equation

$$\rho_o \frac{\partial u}{\partial t} = - \frac{\partial p}{\partial x} + \frac{4}{3} \eta \frac{\partial^2 u}{\partial x^2} \tag{2-33}$$

The above takes account only of losses due to shear viscosity. A more complete description of sound absorption must also include a heat transfer equation to correct for the assumption of adiabatic compression. This equation, known also as the Fourier heat law, is written as

$$C_p \rho_o \frac{\partial T}{\partial t} - T\beta \frac{\partial p}{\partial t} = \lambda \frac{\partial^2 T}{\partial x^2} \tag{2-34}$$

where C_p = specific heat at constant pressure

T = temperature

β = coefficient of thermal expansion $\frac{1}{\rho} \left(\frac{\partial \rho}{\partial T} \right)_p$

λ = heat conductivity

To completely solve the problem of a propagating sound wave in a fluid one also needs the continuity equation

$$\frac{\partial s}{\partial t} = \frac{\partial u}{\partial x} \tag{2-35}$$

where s is a quantity known as the condensation. The particular form of this equation was derived by assuming that for small amplitude ultrasonic waves the changes in density are small and hence one can define the condensation s by the relation

$$\rho = \rho_0 (1 + s) \tag{2-36}$$

where s is small. Equation (2-36) is then substituted into the mass continuity equation

$$\frac{1}{\rho} \frac{D\rho}{Dt} + \text{div } \bar{w} = 0 \tag{2-37}$$

where $\bar{w}$ is the fluid velocity (in vector notation). This equation is linearized. It is then assumed that the solution of the above equations for quantities such as s, u, $p-p_0$, $T-T_0$, etc. is proportional to

$$e^{-\alpha x + i\omega (t - \frac{x}{c_0})} \tag{2-38}$$

Here α is the absorption coefficient, usually written in units of cm^{-1} or nepers/cm and c_0 is the adiabatic velocity of sound. Equation (2-38) describes the amplitude of the sound wave. The absorption coefficient for the intensity, which is the usual quantity measured in an ultrasonic pulse-echo experiment, is 2α. Another quantity which is sometimes used is the absorption coefficient per wave-length defined as

$$\alpha_\lambda = \alpha\lambda = 2\pi \frac{c_o}{\omega} \alpha \tag{2-39}$$

Substituting the waveform given by equation (2-38) into equations (2-33), (2-34) and (2-35) and assuming that the absorption is small (i.e., specifically that $\alpha\, c_o/\omega = \alpha_\lambda/2\pi < 1$) and neglecting third and higher order terms in small quantities such as s, one can obtain the "classical" expression for the sound absorption coefficient

$$\alpha_{class}(\omega) = \frac{\omega^2}{2\, c_o^3 \rho_o} \left[\frac{4}{3} \eta + (\gamma_T - 1) \frac{\lambda}{C_p} \right] \tag{2-40}$$

where ω = frequency in radians/sec and $\gamma_T = C_p/C_v$. There is also a dispersion relation for velocity (i.e., the velocity is frequency dependent) but this effect is, in general, quite small and can be ignored here.

It is evident from equation (2-40) that for systems obeying the classical absorption relation, the quantity α/f^2 (where $f = \omega/2\pi$) is a constant as a function of frequency. Experimentally, except for some monatomic metallic systems[19], it is found that α is always larger than the α_{class} obtained by substituting data for η, γ_T, λ, C_p into equation (2-40). Two types of deviations from the classical behaviour are found[18]:

(1) The graph of α/f^2 versus f is a horizontal line of a magnitude higher than given by equation (2-40).

(2) The graph of α/f^2 versus f shows a frequency dependence in a certain frequency range. A system showing this latter behaviour is said to undergo "relaxation".

Tisza[20] was the first to point out that the excess absorption could be formally accounted for by inserting a volume viscosity into the equation of motion. It is usually further assumed that ζ is a constant similar to η and λ. Equation (2-33) then becomes

$$\rho_o \frac{\partial u}{\partial t} = -\frac{\partial p}{\partial x} - \frac{\partial}{\partial x}\left[2\eta \frac{\partial u}{\partial x} - \frac{2}{3}\eta \frac{\partial u}{\partial x} + \rho \frac{\partial u}{\partial x}\right]$$

$$= -\frac{\partial p}{\partial x} - \frac{4}{3}\left[\eta + \frac{3}{4}\zeta\right]\frac{\partial^2 u}{\partial x^2} \qquad (2\text{-}41)$$

This equation is similar to equation (2-33), the constant η being replaced by the constant $\eta + 3/4\ \zeta$. Substituting this new constant into the sound attenuation expression gives

$$\alpha(\omega) = \frac{\omega^2}{2\, c_o^3\, \rho_o}\left[\frac{4}{3}\eta + \zeta + (\gamma_T - 1)\frac{\lambda}{C_p}\right] \qquad (2\text{-}42)$$

and this new expression takes care of the deviation described as case 1 above. However, it does not deal with case 2 concerning frequency dependent deviations from α_{class}. For the simplest cases, these are of the form[21]

$$\alpha - \alpha_{class} \sim \frac{\omega^2}{(1 + \omega^2\tau^2)} \qquad (2\text{-}43)$$

where τ is a relaxation time. The question arises as to whether to correct by making the above transport coefficient frequency dependent or by adding new frequency dependent transport coefficients. Originally there was considerable criticism of the former approach[21] and so the latter was usually attempted by assuming some relaxation model and

calculating an expression for the absorption due to this model and adding this onto the expression for the classical sound absorption.

Recently it has been found that it is possible to quantitatively account for the excess sound absorption by assuming the coefficients η, ζ and λ to be frequency dependent. This was made possible by advances in the statistical mechanical theory of irreversible processes which led to explicit and rigorous formulas for frequency dependent transport coefficients[22].

In many cases the frequency dependent excess absorption can be accounted for by a frequency dependent bulk viscosity. The bulk viscosity is the transport coefficient which indexes losses associated with uniform density changes that occur in a fluid. If the relaxation time or times for this process are of the order of the reciprocal frequency of the sound wave, then significant losses will occur in that frequency range. For instance, there may be a slow energy exchange between external and internal degrees of freedom of the molecules comprising the substance, or there may be slow structural changes occuring in the fluid[18]. In either case the system is unable to sustain local equilibrium and so is continually subject to energy dissipation. If the relaxation times for the fluid, however, are fast enough to keep pace with the rapid density changes, then the restoration of equilibrium follows the density changes almost immediately and no losses occur[23].

2.2.3 Fixman's Theory of Critical Sound Absorption

One of the more plausible and successful theories of the anomalous absorption of sound in a binary mixture is that due to Fixman[24]. His

explanation of the cause of the excess absorption is based upon a relaxation mechanism.

After a first abortive attempt to explain the anomalous absorption[25], Fixman decided that the critical fluctuations enter into the sound absorption mainly through the strong functional dependence of the O-Z long-range correlation length κ^{-1} upon the temperature changes produced by the sound wave. That is, the varying pressure and density of the adiabatic sound wave produces an oscillating temperature. Near T_c changes in T cause strong structural changes in the fluid corresponding to this changing value of κ^{-1}. It is the lag in response of the fluid to the rapidly changing values of κ^{-1} and the concomitant oscillating diffusion currents which Fixman considered to be the principal cause of the excess sound absorption.

Fixman's method consists of calculating, in terms of κ, a frequency dependent (complex) excess heat capacity and coupling this into the expression for the amplitude of the propagating sound wave via the thermodynamic equation which relates the adiabatic sound velocity to the isothermal one and to γ_T, the ratio of C_p to C_v. By the use of appropriate series expansions of excess thermodynamic quantities an expression for the excess frequency dependent specific heat is obtained and this expression is substituted into the exponential function which is used to describe the propagating sound wave. The imaginary part of the calculated complex velocity of sound in this expression is then identified with the excess absorption. As usual, the assumption that the absorption is small has been made in the derivation.

Specifically, the sound wave can be described by

$$e^{i(\omega c_c^{-1} x - \omega t)} \tag{2-44}$$

where c_c is the adiabatic sound velocity which turns out later to be complex. Now

$$c_c = c_T \gamma_T^{\frac{1}{2}} \tag{2-45}$$

is the well-known expression relating the adiabatic and isothermal velocities of sound. We write

$$\begin{aligned} C_p &= C_p^o + \Delta_M \\ C_v &= C_v^o + \Delta_M \end{aligned} \tag{2-46}$$

where C_p^o, C_v^o are non-critical specific heats and Δ_M is the excess frequency dependent specific heat in cal/mole deg. The assumption has been made that both C_p and C_v get equal increments from the critical fluctuations (small compressibility). Using relations (2-46) in relation (2-45) and expanding by the binomial theorem (assuming $\Delta_M << C_p^o, C_v^o$) yields

$$c_c = c_o \left[1 - \left(\frac{\Delta_M}{2 C_p^o}\right) (\gamma_{To} - 1) \right] \tag{2-47}$$

where $c_o = c_T \gamma_{To}^{\frac{1}{2}}$ and $\gamma_{To} = C_p^o/C_v^o$. Now the coefficient for excess absorption α_e is given by

$$\alpha_e = \mathrm{Im}\,(\omega c_c^{-1}) \tag{2-48}$$

Inverting equation (2-47), again expanding by the binomial theorem and taking the imaginary part gives

$$\alpha_e = \pi f \frac{(\gamma_{To} - 1)}{(C_p^o \; c_o)} \; Im(\Delta_M) \tag{2-49}$$

Fixman also obtains an expression for the dispersion in the velocity of sound, but since this effect turns out to be small for our case it will be omitted.

It now remains to calculate the frequency dependent excess specific heat Δ. Fixman employs the following procedure. The local entropy is expanded up to quadratic terms in the composition fluctuations. By local is meant a region of the system which is small compared to the overall volume yet large enough to contain a sufficient number of particles that the entropy can be defined in the usual thermodynamic sense. It is then found that the entropy increment associated with critical fluctuations (using volume fractions as the composition variables) is given by[39]

$$\langle \delta s \rangle_{av} = \frac{\phi_2}{2V_1} \left(\frac{\partial^2 \mu_1}{\partial \phi_2 \partial T} \right)_p \int_o^{k_{max}} \hat{G}_k dk \tag{2-50}$$

The time dependence of these entropy fluctuations is then written as

$$\langle \delta s \rangle_{av} = \frac{\phi_2}{2V_1} \left(\frac{\partial^2 \mu_1}{\partial \phi_2 \partial T} \right)_p \int_o^{k_{max}} \hat{G}_k(t) dk \tag{2-51}$$

where $\hat{G}_k(t)$ is the Fourier transformed expression of the O-Z correlation function

$$G(r) = \frac{a}{r} \; e^{-\kappa r} \tag{2-52}$$

at time t.

Using the well-known thermodynamic expression[26]

$$\left(\frac{\partial \pi}{\partial n_2}\right)_{\mu_1,T} = k_B T \left[1 + n_2 \int G(r)dr\right]^{-1} \tag{2-53}$$

relating the derivative of the osmotic pressure with respect to composition (in number density) to the integral of the pair correlation function, performing some thermodynamic manipulations[27] to simplify this expression and to change it into volume fraction composition variables, yields the equation

$$\frac{4\pi a}{\kappa^2} = -\frac{V_1}{\phi_2}\left[\frac{k_B T}{\left(\frac{\partial \mu_1}{\partial \phi_2}\right)_{p,T}} + \frac{V_2}{V_1}\right] \tag{2-54}$$

In this expression use has been made of the O-Z expression (2-52) to evaluate the integral over G(r).

Equation (2-54) can now be used (assuming $\partial\mu_1/\partial\phi_2$ to be small near T_c and ϕ^c) to give

$$\frac{\partial^2 \mu_1}{\partial \phi_2 \partial T} \simeq -\frac{V_1 k_B T_c}{4\pi a \phi_2}\left(\frac{\partial \kappa^2}{\partial T}\right) \tag{2-55}$$

which, when substituted in equation (2-51), yields

$$\langle \delta s \rangle_{av} = -\frac{k_B T_c}{8\pi a}\left(\frac{\partial \kappa^2}{\partial T}\right)\int_0^{k_{max}} \hat{G}_k(t)d\bar{k} \tag{2-56}$$

The task is now to calculate $\hat{G}_k(t)$.

In an earlier paper[27] on the anomalous shear viscosity in a binary mixture Fixman had already derived a diffusion equation (for

constant p and T and no external forces) involving an expression for G(r) which included the effect of high gradient composition fluctuations near T_c, viz.,

$$\frac{dG}{dt} = h\,(\kappa^2 \nabla_r^2 G - \nabla_r^2 \nabla_r^2 G) \tag{2-57}$$

where

$$h = \frac{k_B T_c \phi_1 V_1^2\,(n_1 + n_2)}{m_1 2\pi a\beta\, C_2} \tag{2-58}$$

and m_1 = molecular mass of particle 1

n_1, n_2 = number densities of 1, 2 respectively

C_2 = mass fraction of particle 2

β = friction constant (in sec^{-1}) = $k_B T_c / m_2 D_{id}$

D_{id} = ideal mixture (non-critical) chemical diffusion coefficient

Fixman assumes that the above diffusion equation is properly modified to take account of the disturbances created by the sound wave through the dependence of κ on local temperature. Hence κ^2 in equation (2-57) is replaced by $\kappa^2 + (\partial\kappa^2/\partial T)\,\delta T$. Introducing the transformations

$$\begin{aligned} \delta T &= T_\omega e^{-i\omega t} \\ G(r) &= \int \hat{G}_k(t) e^{i\bar{k}\bar{r}}\, d\bar{k} \\ \hat{G}_k(t) &= \hat{G}_k e^{-i\omega t} \end{aligned} \tag{2-59}$$

and assuming that $k << \kappa^{-1}$ (i.e., the sound wavelengths are much longer than the long-range correlation length) the following equation is obtained from equation (2-57):

$$-i\omega\hat{G}_k = -\,h\,k^2(k^2+\kappa^2)\hat{G}_k - h\,k^2\,\frac{\partial\kappa^2}{\partial T}\,\hat{G}_k^o\,T_\omega \tag{2-60}$$

where $\hat{G}_k(t)$ has been replaced by the equilibrium value

$$\hat{G}_k(0) = \frac{a}{2\pi^2}\,\frac{1}{k^2+\kappa^2} \tag{2-61}$$

Solving for $\hat{G}_k$, substituting it in equation (2-56) and dividing by δT gives the excess specific heat

$$\Delta = T\,\frac{\langle\delta s\rangle_{av}}{\delta T} = \frac{k_B h}{16\pi^3}\left(T_c\,\frac{\partial\kappa^2}{\partial T}\right)^2\int_0^\infty \frac{k^2}{k^2+\kappa^2}\,\frac{dk}{-i\omega+hk^2(k^2+\kappa^2)} \tag{2-62}$$

This can be written more simply as

$$\Delta = \frac{k_B}{4\pi^2}\left(T_c\,\frac{\partial\kappa^2}{\partial T}\right)^2\left(\frac{h}{2\pi f}\right)^{1/4} f(d) \tag{2-63}$$

where f(d) is a complex integral that can be solved numerically in terms of the dimensionless parameter

$$d = \kappa^2\left(\frac{h}{2\pi f}\right)^{1/2} \tag{2-64}$$

Fig. 36 shows the variation of Im[f(d)] with d.

Finally transforming Δ into units of cal/mole deg via

$$\Delta_M = \Delta\,\frac{N_o}{(n_1+n_2)} \tag{2-65}$$

where N_o is Avogadro's number, we obtain (near the critical composition and temperature)

$$\alpha_e = \frac{\gamma_{To}-1}{4\pi}\left(\frac{R}{C_p^o c_o}\right)\left(\frac{f^{3/4}}{(n_1+n_2)}\right)\left(\frac{h}{2\pi}\right)^{1/4}\left(T_c\,\frac{\partial\kappa^2}{\partial T}\right)^2 \mathrm{Im}[f(d)] \tag{2-66}$$

and

$$\frac{\alpha_e}{f^2} = \frac{\gamma_{To}-1}{4\pi c_o}\left(\frac{R}{C_p^o}\right)\left(\frac{f^{-5/4}}{n_1+n_2}\right)\left(\frac{h}{2\pi}\right)^{\frac{1}{4}}\left(T_c\,\frac{\partial\kappa^2}{\partial T}\right)^2 \quad \mathrm{Im}[f(d)] \qquad (2\text{-}67)$$

As shown in Fig. 36, Im[f(d)] increases with decreasing d. However, to see how this function, and α_e varies with $(T - T_c)$, it is necessary to substitute into equations (2-64) and (2-66) an expression for κ^2. For a system at the critical composition the most suitable result for κ^2 which is consistent with Fixman's derivation is that given by the O-Z-Debye theory. Hence, substituting

$$\kappa^2 = \frac{6}{\ell^2}\,\frac{|T-T_c|}{T_c} \qquad (2\text{-}68)$$

into equations (2-64) and (2-66), we obtain

$$\alpha_e = \frac{36(\gamma_{To}-1)}{4\pi c_o \ell^4}\left(\frac{R}{C_p^o}\right)\left(\frac{f^{3/4}}{n_1+n_2}\right)\left(\frac{h}{2\pi}\right)^{\frac{1}{4}} \quad \mathrm{Im}[f(d)] \qquad (2\text{-}69)$$

where

$$d = \frac{6}{\ell^2 T_c}\left(\frac{h}{2\pi}\right)^{\frac{1}{2}} f^{-\frac{1}{2}}\,|T-T_c| \qquad (2\text{-}70)$$

For constant f, these equations show that as one gets closer to T_c, d decreases, causing an increase in Im[f(d)] and consequently an increase in α_e. For $T = T_c$, $d = 0$, giving Im[f(d)] = 0.425 which defines the maximum value of α_e. Thus α_e increases with decreasing $(T - T_c)$ but remains finite for $T = T_c$ for any non-zero value of f. Equations (2-69) and (2-70) show that the frequency dependence of α_e is not a simple power law as might be expected for a relaxation mechanism de-

pending on a single relaxation frequency. A plot of the quantity $\alpha_{e\lambda} = \alpha_e c_o/f$ versus f shows that $\alpha_{e\lambda}$ has a rather broad maximum at a particular value of $(T - T_c)$ and this peak moves to lower and lower ranges of f values with decreasing $(T - T_c)$ at the same time steadily increasing in magnitude. At the limiting value of $f = 0$, $\alpha_{e\lambda} \to \infty$.

A further piece of information which can be obtained from equations (2-64) and (2-66) is the variation of α_e/f^2 with composition. This can be achieved through the composition dependence of κ which can be obtained either experimentally or theoretically. To derive the dependence of α_e/f^2 on the composition variables it is necessary to go back to equations (2-64) and (2-51) (thus omitting the approximation which led to equation (2-66)), since one is now interested in the derivative of $\partial^2\mu_1/\partial\phi_2\partial T$ (where $\partial\mu_1/\partial\phi_2$ is <u>not</u> small) away from the critical point. Thus, combining (2-51) and (2-60), one has

$$\Delta = -\frac{a\phi_2 hT_c}{4\pi^2 V_1}\left(\frac{\partial^2\mu_1}{\partial\phi_2\partial T}\right)\left(\frac{\partial\kappa^2}{\partial T}\right)\int_0^\infty \frac{k^2}{k^2+\kappa^2}\,\frac{dk}{-i\omega+hk^2(k^2+\kappa^2)} \qquad (2\text{-}71)$$

which by the same substitution of variables as before becomes

$$\Delta_M = -\frac{a\phi_2 T_c}{\pi V_1}\left(\frac{N_o}{n_1+n_2}\right)\left(\frac{\partial^2\mu_1}{\partial\phi_2\partial T}\right)\left(\frac{\partial\kappa^2}{\partial T}\right)\left(\frac{h}{2\pi f}\right)^{1/4} f(d) \qquad (2\text{-}72)$$

and hence

$$\frac{\alpha_e}{f^2} = -\frac{\gamma_{To}-1}{C_p^o c_o}\left(\frac{a\phi_2 T_c}{V_1}\right)\left(\frac{N_o}{n_1+n_2}\right)\left(\frac{\partial^2\mu_1}{\partial\phi_2\partial T}\right)\left(\frac{\partial\kappa^2}{\partial T}\right)\left(\frac{h}{2\pi}\right)^{1/4} f^{-5/4}\,\mathrm{Im}[f(d)] \qquad (2\text{-}73)$$

with $d = \kappa^2 (h/2\pi f)^{\frac{1}{2}}$ unchanged.

This expression, in combination with equation (2-54) giving κ^2 as a function of $\partial\mu_1/\partial\phi_2$, can be used to study the composition dependence of α_e/f^2. In the absence of experimental information on $\partial\mu_1/\partial\phi_2$ and $\partial^2\mu_1/\partial\phi_2\partial T$, we can use the Flory-Huggins solution model to give the composition dependence of μ_1. Since this model has proven useful for systems where the two constituent molecules show vastly different molecular sizes (as in polymer solutions)[28] it is expected that for a system such as Ga-Bi where the molecular sizes aren't too dissimilar this model should be reasonably reliable. The results of the Flory-Huggins solution theory are that[28]

$$\mu_1 = k_B T \left[\ell n\ \phi_1 + (1 - m^{-1})\phi_2 + \left(\frac{\mu_o}{T}\right)\phi_2^2\right]$$

$$\mu_o = \left(\frac{T_c}{2}\right)\left(1 + m^{-\frac{1}{2}}\right)^2 \quad \text{(independent of } \phi_2 \text{ and } T\text{)} \qquad (2\text{-}74)$$

$$m = \frac{V_2}{V_1}$$

and the critical composition is given by

$$\phi_2^c = \left(1 + m^{\frac{1}{2}}\right)^{-1} \qquad (2\text{-}75)$$

In Chapter 7 we will present a numerical analysis of the Fixman equations and their relation to the experimental data on the system Ga-Bi. However, a few general remarks concerning Fixman's derivation of α_e are in order. To begin with, there is an underlying assumption in the calculation of the excess absorption to the effect that it is a separate phenomenon over and above the effects of attenuation caused

by the shear and bulk viscosities. Now Fixman[27] has shown, as have other workers[29,30], that the shear viscosity diverges near the critical point of a binary liquid mixture and this has been demonstrated experimentally[31,32]. For a system at and near the critical composition, Fixman[27] obtains a divergence for the shear viscosity which goes as $(T - T_c)^{-\frac{1}{2}}$. Notwithstanding the infinity, the effect is quite small if T isn't too near T_c and the expectation is that a similar result holds for that part of the sound absorption which is associated with the shear viscosity. Fixman appears to have believed that the anomalous sound absorption effect which he describes is over and above the effects caused by both the shear and bulk viscosities[33]. In actual fact, without realizing it, his equation gives the excess absorption due to the anomalous bulk viscosity. This was demonstrated by Kawasaki[34] whose theory is presented in the following section.

There is a widely held view, shared by Fixman himself[33], that the theory is not a consistent treatment within the framework of the theories of hydrodynamics and thermodynamics, representing instead an ad hoc addition to both of these. Consequently it is difficult to codify and assess the assumptions and approximations in the theory. Explanations for discrepancies between the Fixman theory, other theories and experiments can be found in the fact that it is a molecular field theory which, as has been pointed out earlier, is not a very good approximation for real systems close to T_c.

The discussion of the limitations of the theory is more appropriately presented in Chapter 7 after some of the other theories have been presented.

As it will turn out, these other theories help to clarify the overall status of the Fixman theory and to assess its ability to predict quantitatively the excess sound absorption near the critical point of a liquid binary mixture.

2.2.4 Kawasaki's Theory of Critical Sound Absorption

Kawasaki[34] has followed the lead of other workers in supposing that the reason for an anomalous absorption of sound (i.e., when α/f^2 is not a constant for different frequencies) is to be found in an investigation of the frequency dependent transport coefficients which enter into the sound absorption expression coefficients, for which generally accepted and well-defined formulas exist[21]. Kawasaki works on the expectation that for a critical mixture the major contribution to the anomalous sound absorption comes from the frequency dependent bulk viscosity.

In reference 35 Kawasaki outlines in general form the procedure that is to be followed in the calculation of anomalous transport coefficients. Briefly, we have an equation for the transport coefficient of the form

$$\Theta = \frac{w}{V} \int_0^\infty \langle J(t)J \rangle dt \qquad (2\text{-}76)$$

where the J is the flux corresponding to Θ and w is a known function of temperature. The total volume of the system is given by V and the brackets $\langle\ \rangle$ represent an equilibrium ensemble average. The assumption is then made that the flux can, to a good approximation, be expanded in a power series of the Fourier components of those local macroscopic

variables which are supposed to contribute to the anomaly in Θ. This expansion usually consists only of quadratic terms, the linear terms cancelling out in the time correlation function expression and the higher order terms being omitted. It is entered into the time correlation function expression with the time correlation of the terms in the power series being evaluated by the use of the (local, if necessary) macroscopic equations of motion.

The truncation of the series at the quadratic term makes the derivation of Θ from this point analogous in spirit to the power series expansions in the theory of equilibrium critical systems. The series expansion can generally be written as

$$J = \sum_{\alpha\beta} \sum_{k} S^{k}_{\alpha\beta} A^{\alpha}_{k} A^{\beta}_{-k} + \ldots \tag{2-77}$$

where the k-th Fourier component of the α-th macroscopic variable is denoted by A^{α}_{k}. These A^{α}_{k} represent deviations from equilibrium values, since they are chosen such that $\langle A^{\alpha}_{k} \rangle = 0$. The linear terms, as stated earlier, are excluded because of the orthogonality condition $\langle J A^{\alpha *}_{k} \rangle = 0$.

The macroscopic equations of motion are written (in Fourier components) as

$$\frac{d}{dt} \langle A^{\alpha}_{k}(t) \rangle_{1} = - \sum_{\beta} M^{\alpha\beta}_{k} \langle A^{\beta}_{k}(t) \rangle_{1} \tag{2-78}$$

To simplify the resulting expression for the anomalous transport coefficient the random phase approximation is often used which is a reasonable approximation for macroscopic variables that follow a Gaussian distribution[35]. The only difficulty with this approximation appears

when the system is extremely close to T_c.

The simplest form for the time correlation function expression is that for which the bulk viscosity is combined with the shear viscosity, viz.[34],

$$\Theta = \zeta + \frac{4}{3}\eta = \frac{1}{Vk_BT} \int_0^\infty \langle J^{xx}(t) J^{xx} \rangle dt \tag{2-79}$$

where Θ is often called the "longitudinal" viscosity. In the above expression

$$J^{xx} \equiv I^{xx} - \langle I^{xx} \rangle - V\Delta p \tag{2-80}$$

where

$$I^{xx} \equiv \sum_i \frac{\left(p_i^x\right)^2}{m_i} - \sum_{i<j} r_{ij}^x \frac{\partial u_{ij}}{\partial r_{ij}^x} \tag{2-81}$$

m_i = mass of i-th particle

p_i = momentum of i-th particle

r_{ij}^x = relative co-ordinate of particles i and j (x-component)

u_{ij} = intermolecular potential

The brackets < > denote an ensemble average of the local quantities in their (assumed) slowly varying non-equilibrium states. Δp represents the molecular expression for the fluctuations of pressure, which for a multi-component system is given in the grand canonical ensemble by

$$\Delta p = \left(\frac{\partial p}{\partial e}\right)_{n^\alpha, V} \Delta e + \sum_\alpha \left(\frac{\partial p}{\partial n^\alpha}\right)_{e, V, n^\beta (\beta \neq \alpha)} \Delta n^\alpha \tag{2-82}$$

where e = total energy divided by the volume, and

n^α = number density of particles of type α

The inclusion of this term is important in later extracting the dominant contribution to $\Delta\Theta$ out of the expansion of J^{xx} with respect to composition. To make the problem tractable, the assumption is now made that the anomaly in Θ arises solely from the critical concentration fluctuations.

The flux J^{xx} is then expanded to quadratic terms (with the linear terms excluded for the previously mentioned reasons) in the concentration fluctuations (using, as usual, Fourier components)

$$J^{xx} = \sum_k S_k (1 - P) \Delta|C_k|^2 + \ldots \tag{2-83}$$

Use has been made of the Mori projection operator P which projects the fluctuations of a quantity onto the thermodynamic subspace[36,37]. Making use of the random phase approximation (i.e., assuming that $\langle P\Delta|C_k|^2\rangle$ is zero) Kawasaki[34] obtains the result that

$$\Delta\Theta = \frac{1}{k_B T V} \sum_k S_k^2 \frac{(\langle|C_k|^2\rangle)^2}{M_k} \tag{2-84}$$

The equation of motion for C_k is written, following Fixman[24], as

$$\frac{\partial C_k}{\partial t} = - M_k C_k \tag{2-85}$$

where $M_k = \gamma^o k^2 (k^2 + \kappa^2)$, γ^o being equivalent to 2h in Fixman's terminology. If it is further assumed that the O-Z form for $\langle|C_k|^2\rangle$ can be used, then

$$\langle|C_k|^2\rangle = V \frac{\xi^o}{\kappa^2 + k^2} \tag{2-86}$$

where ξ^0 is a constant. Kawasaki thus obtains

$$\Delta\Theta = \frac{1}{4k_B T W_Y^0} \sum_k \frac{1}{k^2(k^2 + \kappa^2)} \left(\frac{j_k}{\langle |C_k|^2 \rangle} \right)^2 \tag{2-87}$$

where

$$j_k = \langle [(1 - P)\, \Delta I^{xx}]\, [(1 - P)\, \Delta |C_k|^2] \rangle \tag{2-88}$$

The task now is to evaluate the above expression for j_k.

Now j_k can be expanded (making use of some mathematical properties of the projection operator P) to read

$$j_k = \langle \Delta I^{xx}\, \Delta |C_k|^2 \rangle - \langle (P \Delta I^{xx})\, \Delta |C_k|^2 \rangle \tag{2-89}$$

where each term is investigated separately. The first term gives

$$\langle \Delta I^{xx}\, \Delta |C_k^2| \rangle = - k_B T\, k_x \frac{\partial}{\partial k_x} \langle |C_k|^2 \rangle \tag{2-90}$$

It would be tempting to apply the random phase approximation again, which would make the second term vanish. This would be unwise, however, since it turns out that the term is necessary to the anomaly in $\Delta\Theta$. The alternative procedure is to recognize that

$$V^{-1}\, P\, \Delta I^{xx} = \Delta p \tag{2-91}$$

and that

$$\langle \Delta p \Delta |C_k|^2 \rangle = \frac{k_B T^2}{V C_v} \left(\frac{\partial p}{\partial T} \right)_{V,C} \left(\frac{\partial \langle |C_k|^2 \rangle}{\partial T} \right)_{S,C} \tag{2-92}$$

making use of various equations relating fluctuating quantities[38]. In the above, C_v is the specific heat at constant volume per unit volume of the system.

Substituting equations (2-91) and (2-92) into equations (2-87) and (2-88) and changing the sum over k to an integral over k with limits from zero to infinity (since the integral converges) and taking only the dominant contribution, Kawasaki obtains the result that

$$\frac{j_k}{\langle |C_k|^2 \rangle} \cong \frac{k_B T^2}{C_v} \left(\frac{\partial p}{\partial T}\right)_{V,C} \left(\frac{\partial \kappa^2}{\partial T}\right)_{S,C} \frac{1}{\kappa^2 + k^2} \tag{2-93}$$

and

$$\Delta\Theta \cong \frac{3k_B T}{2^7 \pi \gamma^0} \left[\frac{T}{C_v} \left(\frac{\partial p}{\partial T}\right)_{V,C} \left(\frac{\partial \kappa^2}{\partial T}\right)_{S,C} \right]^2 \frac{1}{\kappa^5} \tag{2-94}$$

From the complete calculation and Kawasaki's earlier paper[35] it can be shown that the above represents the contribution of the bulk viscosity to $\Delta\Theta$ alone, the shear viscosity contribution having been left out, since it diverges much less rapidly as $T \to T_c$.

With the O-Z-Debye value for κ, equation (2-94) indicates that the bulk viscosity goes as $\varepsilon^{-5/2}$ near T_c (ignoring the weaker temperature dependence of the terms multiplying $1/\kappa^5$).

To calculate the frequency dependent sound absorption coefficient, the usual equation for the sound losses is used with the modification that constant transport coefficients have been replaced by frequency dependent ones, viz.,

$$\alpha(\omega) = \frac{\omega^2}{2\rho c_o^3} \left[\Theta(\omega) + \left(\frac{1}{C_v} - \frac{1}{C_p}\right) \lambda(\omega)\right] \tag{2-95}$$

Now it is necessary to calculate the frequency dependent bulk viscosity $\Theta(\omega)$. Since it is known that $\lambda(\omega)$ does not become anomalously large

near a critical point[17] while C_v and $C_p \to \infty$[1], the second term in the equation for $\alpha(\omega)$ can be neglected. The assumption is once more made that the sound wavelength is much longer than the correlation length κ^{-1} so that no correction to the hydrodynamics due to the finite wavelength is necessary. Using equation (2-87) for $\Delta\Theta$ and equation (2-93) for $j_k/\langle|C_k|^2\rangle$, substituting $e^{-i\omega t}$ into the time integral and once more changing $\sum_k$ to $\int_0^\infty dk$, we obtain

$$\Delta\Theta = \frac{T}{4C_v V\gamma^o}\left(\frac{\partial p}{\partial T}\right)^2_{V,C}\left(\frac{\partial \kappa^2}{\partial T}\right)^2_{S,C}\int_0^\infty\int_0^\infty \frac{e^{-i\omega t}dt}{k^2(k^2+\kappa^2)}\,\frac{dk}{(k^2+\kappa^2)} \tag{2-96}$$

This equation, when substituted into equation (2-95) and integrated over the time, becomes

$$\alpha_e(\omega) = \frac{k_B T^3}{2^5\pi^3\rho c_o^3 C_v^2}\left(\frac{\partial p}{\partial T}\right)^2_{V,C}\left(\frac{\partial \kappa^2}{\partial T}\right)^2_{S,C} \int_0^\infty \frac{\omega^2 dk}{2\gamma^o k^2(\kappa^2+k^2)+i\omega}\left(\frac{1}{\kappa^2+k^2}\right)^2 \tag{2-97}$$

With two minor qualifications, this result can be shown to be identical to the excess absorption coefficient calculated by Fixman. The first one, put forward by Kawasaki, is that we must identify Kawasaki's $(\partial\kappa^2/\partial T)_{S,C}$ with Fixman's $(\partial\kappa^2/\partial T)$. The second qualification, put forward by us, is that in Kawasaki's expression his heat capacities are allowed to vary with temperature as $T \to T_c$ while Fixman's heat capacities can only have fixed non-critical values. The associated discrepancy should be relatively mild, however, since the divergences in C_v and C_p

are weak[1,39] and would only be significant very close to T_c where the theory is probably invalid. The similarity between Fixman's and Kawasaki's results is not too surprising, since the approximations in both theories are similar. It appears that the status of these calculations is equivalent to the status of a molecular field calculation in the theory of equilibrium critical points[35]. This means that the theories may be expected to represent only the gross features of the behaviour of $\alpha_e(\omega)$ and fail very close to T_c.

2.2.5 Other Theories of Critical Sound Absorption

Some of the more recent theories deal mainly with the application of the ideas and results drawn from the scaling laws to the solution of the dynamical problem of divergent transport coefficients. Kadanoff and Swift[40] have used a perturbation theory approach based on the Liouville equation, where it is assumed that one transport mode breaks up into several low wave-number modes. This allows the calculation of transport coefficients (different in various frequency domains) for a critical liquid-gas system. Information drawn from the scaling laws, such as the values of critical indices and some symmetry relations among them, were used to estimate the order of magnitudes of transport coefficients and their divergence character.

For instance, a perturbation calculation for $\zeta + 4/3\ \eta$, where it is assumed that the initial sound wave of wave vector $\bar{q}$ breaks up into two waves of wave vectors $\bar{q}$ and $\bar{q} - \bar{q}'$, yields the result that (on the critical isochore and near T_c)

$$\zeta(\bar{q},s) + \frac{4}{3}\eta(\bar{q},s) \sim \frac{1}{C_v c}(\xi^{-2}k_B)\left[T\left(\frac{\partial c}{\partial T}\right)_{S/N}\right]^2 \qquad (2\text{-}98)$$

where N is the total number of particles in the system and S is the total entropy. This relation becomes, on making use of scaling law results:

$$\zeta(\bar{q},s) \sim \rho c_0 \xi \qquad (2\text{-}99)$$

where $\bar{q}$ is the wave vector, s is a frequency and ρ, c_0, ξ have their usual meaning as used in this thesis. From the full expression and the scaling laws the above result becomes

$$\zeta \sim \varepsilon^{2\nu - 2 + \alpha/2} \sim \varepsilon^{-2/3} \qquad (2\text{-}100)$$

on the critical isochore and this result is expected to hold for frequencies $s \geq (\lambda/\rho C_p)\xi^{-2}$ and $s \leq c_0\xi^{-1}$. It has been assumed throughout that $q \leq \xi^{-1}$.

Assuming slowly relaxing modes of the solution of the Liouville equation of the form e^{-st}, the sound waves (for the usual case of $\alpha\lambda << 1$) obey a dispersion relation where

$$s = \pm i q_x c(\bar{q}) + \tfrac{1}{2}(q^2) D_s(\bar{q},s) \qquad (2\text{-}101)$$

with the second term representing the losses and given by

$$D_s(\bar{q},s) = \frac{\frac{4}{3}\eta(\bar{q},s) + \zeta(\bar{q},s)}{\rho} + \frac{\lambda(\bar{q},s)}{\rho}\left(\frac{1}{C_v(\bar{q})} - \frac{1}{C_p(\bar{q})}\right) \qquad (2\text{-}102)$$

Equations (2-101) and (2-102) have the usual form for the equation of sound losses as given in the section on classical hydrodynamics, except that the equation formally takes into account the $\bar{q}$ and s dependence of the losses. It should be noted that for the frequency range given, $\lambda(\bar{q},s)$ is expected to contribute to the losses incorporated in $D_s(\bar{q},s)$

with roughly the same temperature dependence as ζ. The effect of the divergence of η is, as usual, much less. Hence the final result is that (noting that on the critical isochore $\xi \sim \varepsilon^{-\nu}$)

$$D_s = A\xi c_o \tag{2-103}$$

where A is a constant of order unity. Thus the dispersion relation takes the form

$$s = c_o q \left[\pm i + Aq\xi\right] \tag{2-104}$$

for the frequency range given above. Halperin and Hohenberg[41], using slightly different methods but still basing their theory on scaling law ideas, derived a similar result for D_s for a critical liquid-gas system.

To solve the problem of the sound wave damping constant in a critical liquid-liquid mixture, Swift[42] has drawn upon the close analogy between the liquid-liquid and the liquid-gas problem. Eschewing a direct approach to solving the problem, he has assumed certain correspondences between the various thermodynamic variables as well as transport coefficients. Since experiments seem to indicate that the thermal diffusivity in a liquid-liquid system does not exhibit anomalous effects due to critical fluctuations, while the mass diffusion coefficient does, he identifies the mass diffusion coefficient D with the thermal diffusivity $\lambda/\rho C_p$ wherever it appears in the liquid-gas problem. Hence, the relaxation frequency s_T^* associated with processes contributing to $\lambda/\rho C_p$, which is $s_T^* \sim \lambda^* \xi^{-2}/\rho C_p$, is now given for D as $s_{D^*} \sim D^* \xi^{-2}$ where λ^* and D^* are the thermal conductivity and diffusion coefficient, respectively, evaluated at wavenumber $q \sim \xi^{-1}$.

Swift obtains the result that the singular parts of D* and $(\zeta + 4/3\ \eta)(\bar{q},s)$ are related by

$$D^* \left[(\zeta+\frac{4}{3}\eta)(\bar{q},s)\right]_{sing} \sim \xi^{-1} k_B c_o \left(\frac{1}{C_v} - \frac{1}{C_p}\right)\left[T\left(\frac{\partial \mu_{12}}{\partial c_1}\right)_{p,T} \frac{\partial}{\partial T}\left(\frac{\partial c_1}{\partial \mu_{12}}\right)_{p,T,C_2,\frac{S}{N}}\right]^2 \tag{2-105}$$

as long as $s \leq s_{D^*}$ and $q \leq \xi^{-1}$. To obtain the singular part of $(\zeta+4/3\eta)(\bar{q},s)$ from the above equations, the value for $D^* \sim \xi^{-1}$ is used. This makes $s_{D^*} \sim \xi^{-3}$. Solving for $(\zeta+4/3\eta)(\bar{q},s)$ gives

$$(\zeta + \frac{4}{3}\eta) \sim - \gamma k_B c_o^2 T^2 \left(\frac{1}{C_v} - \frac{1}{C_p}\right) \frac{1}{|T - T_c|^2} \tag{2-106}$$

This equation is put into equations (2-101) and (2-102) (with $\lambda(\bar{q},s)$ omitted from equation (2-102)) thus giving the equation for the sound losses.

At this point it isn't clear how the above results fit in with the more complicated, yet more explicit expressions for $\alpha_e(\omega)$ derived by Fixman and Kawasaki. More will be said about this in Chapter 7.

Kadanoff and Swift have pointed out that the calculations of Fixman and Kawasaki are similar in spirit to theirs since in both cases the non-linear couplings among hydrodynamic modes cause one mode to break up into several other different wavenumber modes, which are then lost to the sound wave. Nonetheless, Kadanoff and Swift felt that their calculations are significantly different because of their use of the scaling laws to estimate correlation functions and critical indices in contradistinction to Fixman and Kawasaki who take recourse to critical indices

and correlation functions that are based on the O-Z-Debye theory. It seems to us that the discussion this far is incomplete, since, as the two calculations stand, they are only consistent if O-Z-Debye results are used. This is particularly evident when considering the derivative $\partial\kappa^2/\partial T$ which appears as a factor in the sound absorption expression. Noting that $\kappa \sim |T - T_c|^{\nu}$, it is clear that only when $\nu = \frac{1}{2}$ (classical or O-Z-Debye value) will the derivative $\partial\kappa^2/\partial T$ loose its dependence on $|T - T_c|$. Thus $\nu > \frac{1}{2}$ (non-classical value) would leave a factor $|T - T_c|$ in the sound absorption expression causing the absorption maximum to occur <u>above</u> T_c, while at T_c the anomalous absorption would be zero, a result which is in disagreement with all the experimental findings. In contrast to Fixman's approach, however, Kawasaki's formalism frees him in a straightforward way from the above restriction. He could achieve this by keeping higher order terms in the expansion of the conserved fluxes.

CHAPTER 3

EXPERIMENTAL APPARATUS

3.1 Introduction

This chapter describes the experimental apparatus which was designed to measure the velocity and attenuation of ultrasound as a function of composition, temperature and frequency in the system Ga-Bi above its miscibility gap.

Briefly, and very generally, the experimental arrangement needed for this experiment consisted of electronic equipment to produce and measure the ultrasonic signals, an ultrasonic delay line for the production and insertion of the signal into the liquid metal sample, high temperature equipment for holding and moving the delay line and for containing the sample at the required temperatures, and a stirred, constant temperature oil bath, plus temperature control and measurement equipment.

For measurement of the attenuation and velocity of ultrasound, the standard and well-documented pulse-echo, single-ended method was used[44,47]. In particular, a single transducer produces high frequency, longitudinal sound waves which propogate down a long, cylindrical fused silica delay line immersed in the liquid sample. Most of the sound passes from the bottom face of the delay line into the melt. At the bottom of the melt is situated a reflector which causes the sound to reverse direction and travel up the sample into the rod and to the transducer

again. Here it is reconverted into an electrical signal and after some amplification, is observed on the oscilloscope.

In the following sections a more detailed description of all of the above mentioned features is given.

3.2 Electronics

A schematic diagram of the electronic equipment is given in Fig. 3. High power, high frequency pulses were produced by the Arenberg PG-650-C pulsed oscillator. At the oscillator, these pulses were typically of 2 μs duration and had a peak-to-peak amplitude of about 550 v into 93 Ω. The pulses were triggered by a Tektronix 184 Time-Mark generator which also triggers the horizontal sweep on the oscilloscope (CRO). The pulse repetition frequency was 1000 Hz. This proved to be a convenient frequency, both for a reasonably bright display of the waveform on the CRO, as well as for proper modulation of the comparison oscillator for generating the comparison pulses. The high power pulses were passed into an Arenberg 93 Ω attenuator and from there via a BNC-Tee connector they could travel both to the ultrasonic delay line, where they were converted into high frequency sound pulses and into an Arenberg PA-620 tuned preamplifier which amplifies the low level ultrasonic echoes coming from the delay line. The high power pulses initially overloaded the preamplifier. Since however the ultrasonic echoes arrived much delayed in time (about 70 μs) with respect to the high power pulse and the recovery time from severe overload for the preamplifier was 10 μs or less, the effects of the high power pulse could be ignored. The low level echoes were amplified by the preamplifier, two of which were used on various occasions -- one

for the low frequency range from 4.5 MHz to 13.5 MHz, the other for the high frequency range from 16.6 MHz to 49.7 MHz. Nevertheless, at the highest frequencies some loss in gain was experienced. Usually (after passing through the preamplifier) the signals were sufficiently amplified to be passed into the oscilloscope for final amplification and visualization. At higher frequencies, however, they could be further amplified by passing them through an Arenberg WA-600-E wideband amplifier. Unfortunately, the useful gain of this arrangement was very small for rf signals, since the amplifier was a wideband one and the signal to noise ratio became very poor if a large amount of amplication was required. On the other hand, when the signals were highly attenuated and signal levels were low, another stage of amplification could be obtained by using the video stage of the wideband amplifier. Notwithstanding, measurements of both attenuation and velocity were more difficult using this type of display and hence it was never actually used in this experiment. The power supply of the wideband amplifier conveniently served to power the PA-620's.

For display of the signals, a high frequency (85 MHz) Tektronix 585A oscilloscope was used having two time bases and a delay time generator. This CRO was used in conjunction with a type 82-dual-trace plug-in unit which had a maximum amplification of 10 mv/cm. The delay time generator on the CRO was a necessary feature, since it allowed the rf signal to be viewed on any time scale (mostly 5 μs/cm or shorter) no matter what temporal position it had occupied originally with respect to the triggering pulse from the Time-Mark generator. This feature was most important for accurate velocity measurements.

The high power oscillator, apart from generating the necessary power to excite the transducer, also had another function as it had available a delayed trigger output. This trigger could be continuously delayed from 0 to 11,000 μs with respect to the initial trigger (coming from the Time-Mark generator) that generates the high power pulses. This trigger pulse was fed into a Tektronix 163 pulse generator which was set to generate a 700 μs long pulse of about 8 v amplitude when fed into the 600 Ω external modulation input of the hp606A (hp standing for Hewlett-Packard) signal generator. The hp606A could, in turn, generate a low level 700 μs rf pulse that was then used as the comparison pulse. The comparison pulse was passed directly into the first stage of the preamplifier although at a slightly different input than the ultrasonic signals (i.e., the cathode rather than the grid of the first stage). The comparison pulse could be tuned (up to 65 MHz) to the same frequency as the high power pulse. The trigger generating the comparison pulse could be delayed with respect to the initial, main triggering pulse, thus enabling the comparison pulse to be positioned anywhere along the sweep and hence conveniently either beside or overlapping the first echo. Changes in ultrasonic signal levels were determined by adjusting the comparison pulse height to be always the same as that of the echo. The height of the comparison pulse was then determined by the hp606A output attenuator which had a total range of 140 db.

To measure velocity, time markers from the Time-Mark generator were fed into the other input of the CRO dual-trace plug-in unit and simultaneously displayed with the ultrasonic echoes using the CRO's

"alternate" mode. The smallest time interval available here was 0.1 μs.

3.3 Delay Line

3.3.1 Introduction

By "delay line" is meant the combination of sound delay medium (rod) and piezioelectric crystal (transducer) including the bond material between them, plus the electrode for passing electrical signals to this assembly.

There were a number of reasons for making use of a delay line rather than passing the sound from the transducer straight into the liquid metal sample. One reason was that in the melt only relatively short ultrasonic path lengths were feasible. For such short pathlengths, the ultrasonic echo would arrive at the preamplifier typically within 4 μs to 15 μs and would then find the preamplifier still in the cut-off region caused by overload from the high power pulse. The delay line served to delay the arrival of the echoes at the preamplifier until well after it had recovered from severe overload.

Another reason for using a delay line was that, given a sufficient length of it, the transducer could be kept cool and this aided in improving the quality of the signals and enabling construction of a mechanically simpler and more readily dismountable electrode holder for the transducer. Unfortunately, the inclusion of a delay line led to other problems:

1) Difficulty was experienced in bonding the transducer to the rod so as to achieve a good band width (BW).

2) Due to the smallness of the rod diameter, diffraction and mode interference effects gave rise to signal losses and spurious echoes which interfered with measurements at the lower frequencies[45,46].

3) There was a signal loss at the rod-sample interface, the amount of which depended on the ratio of acoustic impedances (the acoustic impedance is denoted by $Z = \rho_{mixt} c_o^{mixt}$) between the two media and the excellence of the bond achieved between them[44].

Items 1 and 2 led to considerable difficulties initially. In the case of 2, this was because cost and size considerations required the fused silica rod to be about 1¼" outside diameter (OD) which wasn't large enough to eliminate diffraction and mode interference effects at the lower frequencies used.

Nevertheless, all of the problems were eventually successfully overcome. A detailed description of the complete delay line and the solutions to these problems is given below.

3.3.2 Transducer and Bond

The piezoelectric material which was used to convert the electrical signals into ultrasonic ones was a 1.5 MHz fundamental X-cut quartz crystal of 1.146" diameter (for the meaning of these terms see reference 44), which had been coaxially plated with chrome and gold such that it had an 0.85" diameter active center. Although a coaxially plated crystal has many disadvantages it has considerable advantages from

the point-of-view of ease of mountability of the electrode holder to the transducer and for this reason was used[47].

A very early guess for the frequency range to be covered in this experiment was 4.5 MHz to 16.5 MHz, covering all the odd harmonics in between. Hence a transducer with a fundamental frequency of 1.5 MHz was chosen to generate the ultrasound. However, a more knowledgeable assessment later put the frequency range for this experiment at 16.6 to 49.7 MHz, which explains why a transducer with such a low fundamental frequency was chosen to cover a frequency range starting so far above its own fundamental frequency.

After first using various viscosity grades of silicone oils, as well as Nonaq stopcock grease for a bond between the crystal and the rod[44], it was decided, instead, to use a metal bond[48].

One of the disadvantages of the oils and the stopcock grease was the difficulty of getting a thin enough and even enough layer between the two faces. This necessitated "wringing in" the transducer with the coupling media in between to squeeze out any excess material. The effect of this "wringing in" was difficult to control and often resulted in severe scratching and wearing of the gold plating on the bottom transducer face. Also, scratches appeared on the fused silica rod face (due, probably, to the presence of dust particles in the sealant). Even after repeated trials of this procedure, the best BW achieved was never as good as for the metal bond. The reason for this was the large difference in acoustic impedance between the coupling media and the transducer and rod, which meant that a very thin bond was required in order that the final BW of

the combination could approach the theoretical value, i.e., assuming that one had an air-backed X-cut quartz transducer radiating directly into a fused silica rod[44].

The material finally used as a bonding medium was pure Gallium which has a freezing temperature around 30°C and which adheres well upon freezing to both the gold plating of the transducer and the fused silica rod. The method of bonding was as follows. The Ga was melted and then smeared evenly as a thin layer on both the rod and transducer faces. Since the Ga used was of high purity (99.999%) it supercooled considerably and remained liquid during the above operation. The transducer was then pressed onto the rod face and any excess Gallium squeezed out and removed at the sides. The rod and transducer were then left overnight to allow the Gallium to freeze. If quicker freezing was desired, liquid nitrogen was poured over the transducer and rod. No attempt was made to control the thickness of the bond other than to squeeze out as much of the bond material as possible by pressing the transducer onto the rod face by hand. A seal like this was made many times in the initial setting up stages of the experiment and was found always to have approximately the same transmission properties.

There were three main improvements achieved by the above bond as compared to previous attempts using oil or Nonaq stopcock grease:

1) The ultrasonic signal level was increased by 15 - 20 db.
2) Minimum pulse length required for maximum signal build-up for the first harmonic frequency was about 3½ - 4 μs. This was about the same as had been achieved with the oil bonds, but with far less effort.

3) Minimum pulse length remained almost the same up to the 33rd harmonic (49.7 MHz) of the fundamental frequency of the transducer. In the case of the oil bonds, the minimum pulse length quickly increased with increasing harmonic frequencies. This meant an improvement in the BW[44].

It should be noted that a good BW is important because it determines the minimum pulse length of the ultrasonic pulse that can be generated[44,49]. The larger the BW of the electrode-transducer-bond-rod combination, the shorter the ultrasonic pulses that can be generated. On the whole, a short pulse was desirable, since it enabled one to observe the melt echo after short melt path lengths and this was useful when the sample caused large attenuation or when only small amounts of it were available. This was because the earliest time that one could observe a signal from the melt was of the order of the pulse length of the signal itself since the signal had to get clear of the echo which had reflected from the rod-melt interface before it could be seen without interference.

The good BW and large signal levels achieved with the Gallium bond were mainly due to the small difference in acoustic impedance between the Gallium and the fused silica. Figs. 5, 6 and 7 show some typical pulse shapes obtained at three frequencies, 4.5 MHz, 16.6 MHz and 49.7 MHz with the 12" long fused silica rod.

3.3.3 Delay Medium

The delay medium as shown in Fig. 8 was a cylindrical rod made

out of optical grade fused silica (Amersil II) whose ends had been polished and were flat to within ¼ λNa light. The rod was almost 12" long, 1¼" in diameter with an NF 12 thread along its entire length. The two faces of the rod were made parallel to within 6 sec of arc. This rod and others used in trials were supplied by the Valpey-Fisher Co. of Massachusetts.

The property that made fused silica eminently useful for a delay line was its extremely low coefficient of sound attenuation[44]. Other features which made it suitable for this experiment were its superior mechanical qualities as determined by its hardness, low thermal conductivity and low coefficient of thermal expansion[44]. As an added advantage its acoustic impedance matched well with that of the melt. This fact, plus its wettability by both Ga and Bi allowed for excellent sound transmission into the sample. Indispensable also, was the rod's good corrosion resistance to alloying attacks by Ga or Bi[50].

The threading of the rod served two purposes. It reduced the height of the spurious signals caused by mode conversion at the cylindrical boundaries to a workable level[51], and it served as a means for attaching the electrode holder (which doubled as the rod holder) to the rod. Figs. 9 and 10 show the difference in the level of the spurious echoes between two fused silica rods of roughly the same diameter -- the first one with a smooth face, the other with an NF 12 thread along its entire length. The effect of the threading was to scatter the sound and to spread it over a larger time interval. An irregularly rough surface would probably have done the job even better, except that the threading, as mentioned above, served another purpose. Despite the reduction in the spurious

sound level, the amount of spurious signals still present, particularly at 4.5 MHz would still interfere with any melt echo were it not for the fact that a further reduction of about 20 db occurred in the spurious level upon reflection from the rod-melt interface. Most of the spurious echoes were then found behind the first melt echo.

3.3.4 Electrode and Electrode Holder

The final item needed for the delay line was the electrode and electrode holder that allowed the electrical signals to pass to and from the transducer in a convenient and efficient way. A complete description of this electrode holder is given below with the description of the high temperature apparatus.

3.4 High Temperature Apparatus

3.4.1 Introduction

As was stated earlier, the object of the experiment was to measure the attenuation and velocity of sound as a function of frequency and temperature in a mixture of Ga-Bi. This was to be done at various compositions using a variable path length and at temperatures above the critical temperature of Ga-Bi, i.e., above 263^{o}C. Hence a number of requirements associated with the above objective had to be achieved. These were:

1) The sample chamber holding the liquid metal mixture would have to be made of a material which was fairly resistant to the

corrosion attacks of Ga and Bi and in such a way as to ensure very small thermal deviations in the liquid metal sample and still give, with relatively small amounts of the mixture available, a maximum path length for the sound waves.

2) The metal mixture would have to be melted while kept in an inert or relatively oxygen free atmosphere to reduce the amount of oxidation.

3) The rod and reflector would have to be inserted into the liquid mixture in such a way as to prevent any oxide layer, which was always present in a thin layer at the surface of the melt, from adhering to either surface, since this would eliminate almost completely, or seriously reduce, any sound transmission into the melt.

4) The fused silica rod would have to be accurately aligned with respect to the reflector face and this alignment would have to be kept while the rod was being moved relative to the reflector.

5) The entire arrangement would have to be made so that it could be easily put together and taken apart to change the composition of the melt.

6) Some means would have to be provided to stir the metal after it had melted since the Bi is considerably heavier than the Ga and sinks to the bottom when unstirred.

The sections below describe an apparatus which was able to fulfill all of the above requirements in an acceptable manner.

Briefly, as shown in Fig. 11, the following apparatus was devised. A metal beaker which contained the sample was mounted on a platform which was about 2-3" above the bottom of the oil bath. Mounted on top of the beaker was another platform. This held all the necessary equipment for holding and moving the reflector and rod. This support platform was made long enough so that it would protrude considerably out of the oil bath. It had a narrow cylindrical section between the bottom and the top flanges to cut down on thermal conduction. The idea was to keep the top flange quite a way out of the oil so that it could be kept cool. This was done in order that all 'O'-ring seals on moving parts were at room temperature. On the top flange were mounted three hardened stainless steel rods that served to guide a moveable platform. A sufficient number of guide bearings were used so that any free play between rod and bearing was reduced to a minimum and the platform could move accurately up and down parallel to the cylindrical axis of the guide rods. Either the rod or the reflector holder could be mounted, respectively, on top of and below the guide platform. The brackets which held the reflector holder to the can were made of such a length as to ensure that the top part of the rod holder would be clear of the guide platform and the entire assembly -- reflector holder and rod -- could be lowered into and out of the melt with the bottom face of the rod resting flat on the reflector. Lowering the assembly into the melt this way ensured that no oxide layer from the liquid metal surface would come between the rod and reflector faces.

Once in the melt, the reflector holder was fastened onto three

pods mounted on top of the main platform and the brackets disconnected from the guide platform. The guide platform could then be raised, catching the flared-out section of the rod holder, which was then fastened to it. Further raising of the guide platform caused the rod to move relative to the reflector.

Up and down motion of the guide platform was achieved by attaching the platform to a series of gears and connecting rods which were conveniently brought out at hand level beside the electronic equipment. To measure the distance the rod had moved, a vernier micrometer was mounted above it at the point where the guide rods stopped.

The following sections will give a more detailed account of the various parts of the apparatus.

3.4.2 Sample Container

The liquid metal beaker is shown in Fig. 12. It was made of stainless steel type 304 and had a narrow and a wide section. The narrow section was just wide enough to fit the reflector holder, reflector and fused silica rod and it had two thermocouple wells located 120^{o} apart. The wider section was to allow for sample spill-over when a large amount of sample was used and with the rod resting right on the reflector. Wall thickness of the stainless steel beaker was roughly 1/16" all around. A thin wall was desired to ensure good thermal contact between the liquid metal and the oil bath in which the beaker was immersed. The beaker had a flange at the top where a platform could be attached to it. The beaker was sealed off from the surroundings at the flange by means of a Viton 'O'-ring. This 'O'-ring was quite suitable for the temperature

range used, although it flattened to the size of the groove within a day at 265°C. However, it still maintained some of its flexibility and all of its sealing capability. Stainless steel was considered a good material for holding the Ga and Bi at the temperature used, as our own tests and references in the literature had shown that it was impervious to alloying attacks by the above metals[50].

Copper inlet and outlet tubes for Argon were fed into the beaker at opposite ends. The incoming Argon was first fed through many turns of coils of copper tubing immersed in the oil bath before entering the sample chamber. The Argon passed into the sample chamber via a copper ring which had a series of small, evenly spaced holes placed along its inside circumference, so arranged that the Argon jets would hit the fused silica rod and reflector holder assembly first so as to keep both of them as close to the liquid metal temperature as possible. This was done in an effort to cut down temperature variations in the liquid sample since it was assumed that the rod and reflector holder would cause significant gradients in the melt if they were considerably colder than the liquid. Ultimately, as mentioned in more detail in a later section, temperature differences in the melt were found to be negligible over the measurement interval of 1".

3.4.3 Support Platform

Mounted on top of the stainless steel container was the support platform. As shown in Fig. 13, it consisted of a narrow cylindrical section with a flange at either end. The bottom flange rested on the

beaker and sealed against the Viton 'O'-ring, while the top flange had mounted on it three hardened stainless steel guide rods and three support pods for the reflector can. There was an 'O'-ring groove and screw holes for an 'O'-ring lid at the opening of the flange to the cylindrical section. The reflector can fitted into this cylindrical section with a small amount of clearance between it and the cylindrical walls and was sealed off to the outside by means of an 'O'-ring which fitted into the above groove.

The top part of the cylindrical section and the bottom part of the top flange had lead cooling coils wrapped around them. These helped to keep everything on top of the platform cool and greatly simplified the design of gas tight seals on the moveable components.

3.4.4 Reflector Can

The purpose of the reflector can was to provide a moveable structure for holding the reflector which could be sealed off to the outside by means of an 'O'-ring seal. To this end the reflector can had a wide cylindrical section which fitted inside the cylindrical section of the support platform. The bottom end, which fitted just inside the narrow section of the melt beaker was much narrower and had three thin support rods, 120^{o} apart, ending in a thin ring on which was mounted a stainless steel reflector. The reflector's top face was polished to a mirror finish using, as a final polish, a 6 μ diameter diamond paste. The bottom face had a series of concentric grooves cut into it to reduce possible internal sound reflections[19]. The reflector was mounted onto

the ring via three flat-headed screws. It was thus possible to lower the reflector right to the bottom of the melt beaker and push any melt material up into the ultrasonic path area. This was important since if the heavier Bi between the bottom of the reflector and the beaker were to stay there throughout the measurement period, the composition of the melt upon which measurements were made would not be the same as the composition originally prepared.

The top of the reflector can had a flared-in section which ended in an 'O'-ring groove and screw holes for an 'O'-ring seal lid similar to the one on the support platform. This provided a sealable opening for the fused silica rod holder. The top part of the can also had openings for two 1/8" OD stainless steel bubbler tubes. The thermocouples as well as the bubbler tubes extended down into the melt. The holes through which they passed were sealed off by means of liquid silicone rubber.

The can also had a flared out section, or ring, slightly below its top end which served as a means for resting it on the three support pods mounted on top of the support platform. This ring also served for holding three brackets. These could be connected to the guide platform for moving the can up and down.

A photograph of the bottom part of the reflector can is shown in Fig. 14 while Fig. 15 shows a drawing of the entire can.

3.4.5 Thermocouples

Two stainless steel sheathed, 1/8" diameter iron-constantan thermocouples supplied by the Thermo-Electric Co. were used to measure the

temperature of the melt. The two thermocouples were mounted about 120° apart -- one was immersed at a depth of about 3/8" above the reflector, while the other was mounted 1 1/8" above it. Since they were attached to the reflector can, they could move with the can, but remained fixed in position while the rod was being moved. They fitted into the two thermocouple grooves (wells) cut into the beaker and were therefore to the side of the reflector. The thermocouples were bent at right angles immediately upon coming out of the can. They each terminated in a male connector, made of the same material as the thermocouples themselves, which was connected to a corresponding female connector and thermocouple extension wire that led to the cold junction.

They were calibrated and certified accurate to ±0.04°C in the above form, including the extension jacks and wires, by the National Research Council of Canada in the temperature range from 0 -320.0°C. The five calibration points were found to lie very close to a straight line which was constructed from them using the method of least squares. A table was constructed giving values of emf readings versus °C for every 0.1°C for each thermocouple.

3.4.6 Argon Atmosphere Supply Lines

High purity Argon supplied by Matheson of Canada Ltd. was used as the inert atmosphere in the sample chamber. A needle valve controlled the flow of Argon out of the regulator. The Argon could then flow via copper tubing either:

1) Directly into the sample chamber.
2) Through two separate bubbler tubes into the melt for stirring.

Each line had a separate valve. The sample chamber line had an on-off toggle valve while each bubbler line made use of a needle valve. All inlet lines were fed into the oil bath first so that the Argon would be preheated. There was one outlet line and the amount of overpressure inside the chamber could be controlled by a needle valve positioned on this line. From this valve the Argon passed into an empty overflow beaker and then into a beaker filled with oil where the Argon flow rate could be observed. When Argon was being bubbled through the melt, the toggle valve was closed so that the bubble rate through the melt could be viewed directly by observing the oil bubbler.

Connected to all of the above lines and hence also to the sample chamber was a mechanical vacuum pump. This pump was used to flush out the system for a run about four times before the actual flow of Argon was started, and initially, to check it for leaks. A pressure-vacuum gauge was also installed along the main Argon supply line which helped to roughly monitor the overpressure or vacuum in the system. Fig. 16 shows the schematic diagram of the above set-up.

3.4.7 Guide Platform

The guide platform shown in Fig. 17 consisted of a solid 3/16" thick plate. At the periphery of the plate, mounted 120^{0} apart, were three sets of guide bearings. Each complete set of guide bearings was 3" long. In this way the effective free play between bearing and guide rods was reduced to a minimum enabling the guide platform to move up and down in a rigid fashion. The center of the plate was cut out to allow

the fused silica rod and rod holder to pass through it. The diameter of the cut-out was, however, small enough so that the flared-out section of the rod holder (described below) would be caught by the guide platform when the guide platform was raised. Various screw holes were put into the platform plate to allow either the reflector can brackets, or the rod holder to be attached to it via Allen screws.

3.4.8 Rod Holder

The rod holder had a number of functions. It served as a means for containing the electrode arrangement to the transducer. It was used for fastening the rod to the guide platform. As well as this, it provided a convenient means for sealing the rod off from the outside. Fig. 18 gives a cross-sectional drawing of the holder with the fused silica rod threaded into it.

The electrode was simply a cylindrical, hollow brass spacer, open on the side which fitted onto the outside ground ring of the transducer. It had a BNC connector mounted on the other, closed end. A thin, spring-mounted brass rod passed from the center wire of the BNC connector to the center electrode of the transducer -- this was the "live" part of the connection. The size of the electrode was determined by the size of the transducer electrode plating as well as the length of the BNC center connector and spring.

Wrapped around the outside of the holder just below the top plate was some lead tubing which was used to run water through it and keep the transducer cool so that the Gallium bond would stay solid during a run.

On the top and wide part of the holder were mounted three levelling screws. Also mounted on it was a small platform which came above the BNC connector and which provided a flat surface from which the Vernier micrometer, mounted above the rod, could measure the rod's position relative to that of the reflector. The micrometer used had a 2" travel. It was made by the Starrett Co. of Massachusetts and could measure distances to maximum possible error of ±0.0001".

The rod holder had an NF 12 thread along its length, except for the last inch of its length which was made slightly wider to give clearance to the electrode. The NF 12 thread mated with the threading of the fused silica rod. To accomplish this the rod holder was threaded first and then the fused silica rod was threaded (by the Valpey-Fisher Co.) to fit this particular thread, as small variations were possible and a loose fit was desired. Rigidity of the fused silica rod in the rod holder and parallelism of both their cylindrical axes was achieved by threading the rod and transducer tightly against the electrode. The brass electrode fitted flush against the top inside of the rod holder and thus lined up the rod, assuming that the transducer was properly mounted. The assembly was sealed there to the outside by means of liquid silicone rubber. Similarly the BNC connector screwed into the brass electrode and was sealed there by means of an 'O'-ring mount.

3.4.9 Gears and Connectors

Fastened to the guide platform and mounted each on the same bolt circle and beside the guide bearings were three stainless steel support rods. These were about 12" long and fitted into a brass plate at the

top. This plate, in turn, was firmly attached to a screw threaded through a gear mounted on the top of a housing which had been built around the oil bath. A series of gears and shafts were connected to this arrangement and ended up in a wheel and handle conveniently placed in such a position that a person seated in front of the electronics could easily turn it. Turning this handle, then, caused the main gear to turn which had the effect of causing the guide platform to either rise or fall depending on the direction of turning motion. In this way the rod, which was attached to the guide platform, or alternately the reflector can and rod together, could be slowly, surely and easily moved while one was at the same time watching the ultrasonic signals on the CRO.

3.5 Testing for Alignment

One of the more important requirements of the equipment was that the alignment between rod and reflector be sufficiently accurate that an ultrasonic pulse which was at the highest frequency to be used in this experiment (49.7 MHz) could pass into the liquid sample, be reflected at the reflector and come back up the rod again without losing too much of its amplitude due to misalignment. Thus great care was taken in machining all the parts that could affect this alignment.

After it had been built, the equipment was tested for alignment using water in the sample chamber rather than Ga-Bi. Using water, the testing could be done at room temperature and with minimal effort. Initially, it was found that with the rod holder just resting flat on the guide platform, the alignment was very poor. As a first attempt at alignment,

levelling screws were put into the top of the rod holder so that now the rod holder would rest on the guide platform via these levelling screws. However, when an attempt was made to line up the rod using these screws, it was discovered that before the signal could build up to a satisfactory size, the rod holder hit the insides of the 'O'-ring groove of the reflector can holder. Thus the misalignment was too large for this method to work. It became very clear that very little misalignment between rod and reflector down in the sample chamber was needed to cause a very large shift in the position of the rod holder at the 'O'-ring seal which was about 12" higher up. Hence an obvious and simple adjustment to make was to adjust the position of the reflector with respect to the reflector can holder by using different thicknesses of spacers (a few thousandths of an inch difference), such as washers, around the three screws which held the reflector against the reflector can holder. By trial and error, a combination of spacers of various thicknesses were finally found which required only a very small adjustment of the levelling screws at the top to achieve a suitably large ultrasonic echo from the water even at 49.7 MHz. It was further observed that when the rod was fully aligned like this it was also well centered going into the reflector can holder and had sufficient clearance. This situation prevailed over at least 1½" of vertical travel of the rod away from the reflector.

3.6 Oil Bath

An oil bath was used to heat the sample, the reason being that this gives a more gradient-free heat source and is more readily controllable

than, for instance, a furnace with resistance heating. Dow Corning F-1-0173 fluid was used as the heat exchange oil. This was a very stable oil which could easily be taken up to 288°C in an open system with only moderate evaporation rates and no cracking. The oil was heated by two 750 watt heating coils which were wound around and placed at the bottom of the oil bath. The oil was stirred by two mechanical stirrers. The level of the oil in the system was such that at around 260°C it was about 2" above the bottom flange of the support platform. An appropriately cut out lid covered the oil bath to contain some of the evaporating oil and to prevent condensation from the cooling coils dripping into it on humid days. The oil was contained in a stainless steel beaker that was insulated otherwise from the surroundings by some finely ground alumina. There was a large outlet valve near the bottom of the oil bath container which allowed oil to be siphoned out. This was done after every run for ease of dismantling and assembling the equipment.

3.7 Temperature Controller

The temperature of the oil bath was controlled to within ±0.1°C over short periods (2-3 hours) by a Thermo-Electric Type 400 stepless proportional controller using as a sensing element an iron-constantan thermocouple that was mounted in the oil very close to the two heating coils. The maximum output of the controller was slightly more than 1500 watts. The iron-constantan thermocouple used as a sensing element for the temperature controller was 6" long and mounted in a stainless steel sheath.

3.8 Temperature Measurement Devices

Two pieces of equipment were used for measuring the temperature of the liquid metal sample:

1) A potentiometer for accurate spot measurements.

2) A double pen recorder for continuous indication.

Both of these were connected to the two iron-constantan thermocouples mentioned in the previous section. The potentiometer was an accurate Pye potentiometer which had dial readings down to 1 μv and had inputs for a maximum of three thermocouples. It was used in conjunction with an Eppley Lab. Inc. unsaturated standard cell which was occasionally checked against a saturated Weston standard cell that was used only for these purposes.

For indications, the potentiometer was connected to a Cambridge Instruments Ltd. dc suspended spot galvanometer with a maximum sensitivity of 0.6 mm scale deflection per μv. This was sufficient sensitivity to measure changes in temperature of $0.02^{o}C$ when the sensing elements were iron-constantan thermocouples which have an output of roughly 5.5 μv per $0.1^{o}C$ near $260^{o}C$.

The thermocouples were also connected to a Honeywell Elecktronik 19 dual-pen recorder which continuously monitored the temperature and which proved useful in watching the temperature fluctuations while equilibrating the melt or moving the rod during attenuation measurements.

The reference junctions of the thermocouples were held at $0^{o}C$ accurate to $\pm 0.01^{o}C$ by a Thermo-Electric Ice-Cell reference junction controller.

3.9 Temperature Inhomogeneities

Considerable effort was put into assuring that the temperature differences in the liquid metal in the container were small over the ultrasonic measurement interval of 1" and would not be a factor in the results of attenuation measurements. Thus two thermocouples were used to measure the temperature in the liquid and, as mentioned in an earlier section, they were mounted 120° apart and at differing heights. Unfortunately, this situation was not completely ideal for a number of reasons. One difficulty was that the difference in height between the two thermocouples was large and in many cases one thermocouple was so high that its tip was situated close to the surface of the melt, the level of which rose and fell with the motion of the rod, and near the surface the temperature of the melt had a steep gradient causing the temperature to drop by about 1°C in an 1/8" interval. Another difficulty was that, by necessity, both thermocouples had to be placed outside the region of travel of the ultrasonic pulses and hence the temperature could never be directly measured in this important region.

Nevertheless, a reliable estimate of the the temperature profile in the liquid was inferred by the following procedure. First, from one run to the next, the longer (and hence lower) thermocouple was switched from its own well to the well of the other thermocouple. This was to assure that there was no difference in the temperature readings between the two locations which were located 120° apart along the circumference of the beaker. The controller set-point was set at the same set-point for each of the two runs (this could be done to better than ±0.2°C).

It was found that there was no difference in the measured temperature in the melt between the two runs for the identical controller set-points. Secondly, after all the measurements had been made during a run, the can, with the rod resting on the reflector, was slowly raised and then left for awhile at positions such as 1/8, 3/8, 5/8" etc. above its original resting position and the value of the thermocouple reading noted. It was found repeatedly that the temperature indicated by the thermocouple remained the same within the accuracy of the temperature measurements until one got very close to the surface of the melt, where, as was mentioned above, the presence of a very steep temperature gradient was detected.

Further indications of the lack of significant temperature differences was obtained from the ultrasonic signal which remained steady over long periods of time and did not behave differently from the test case when water at room temperature was the sample. If there had been a large temperature gradient present there would have been convection currents set up and this would have caused the signal to drift[52]. At the same time, plots of attenuation versus height always gave a straight line with an even scatter of data points about it. Particularly for measurements near T_c and C_{Bi}^c a shift of temperature with height would have caused the attenuation versus height graphs to become curved.

Since there appeared to be no change in temperature in a vertical direction at the point where the thermocouple was situated, it was assumed as well, that no gradient existed across the center section of the melt. This appeared reasonable since the beaker was completely surrounded by

stirred oil which was at a uniform temperature and represented a large heat reservoir so that the most likely change in temperature was to be expected in a vertical direction.

It was finally concluded that the temperature differences over the entire measuring height were no worse than the accuracy to which the temperature in the melt could be measured. They were thus considered to be negligible.

CHAPTER 4

EXPERIMENTAL TECHNIQUE

4.1 Introduction

To perform attenuation and velocity measurements on the Ga-Bi alloy system at the desired temperatures a great many preparations first had to be made. These preparations were essentially always the same for each run -- a run consisting of the measurement of the attenuation and velocity of ultrasound as a function of frequency and temperature at a particular composition of the melt.

To change the composition, the equipment had to be taken apart after each run and subsequently put together again for the next one. This aspect of the experiment and the general procedures for performing attenuation and velocity measurements will now be described in detail below.

4.2 Preparations Before a Run

Since Ga is very expensive, the same material was used for successive runs. To change the composition, only Bi was added. The stainless steel container, with the melt from the previous run in it, was weighed, accurate to 0.1 g. This gave the weight of sample lost at the end of the previous run when the rod and reflector were taken out of the melt, taking some of the material with them. To change the composition, more Bi was added to the melt beaker, which was then weighed

again. The composition could be calculated for each run by knowing the amounts of Ga and Bi in the melt. This was obtained by assuming that the sample lost on taking the rod and reflector out, after measurements at the last temperature were taken, had been uniformly mixed. This seemed reasonable as long as the last temperature used was above the miscibility gap, and hence the mixture was still uniform throughout. An additional check on the composition of the melt was made by chemically analysing all of the melt removed from the beaker. The agreement between the weighed mixture and chemical determinations was reasonably good, vindicating the above assumptions. More will be said about this in Chapter 6 when discussing errors.

After a sample of the desired composition had been prepared, the equipment was assembled. Before the support platform was attached to the melt beaker, however, a quick visual check was made that the alignment screws on the fused silica rod holder were set properly, so that the rod when lowered onto the reflector by means of the guide platform would rest with its face flush with the reflector face.

Having done so, the equipment was put together, the reflector can resting on 2" long pods mounted on top of the regular pods. This arrangement ensured that the bottom of the reflector would be well above the frozen melt surface. All 'O'-rings were sealed, making sure first that the rod holder was properly centered going into the reflector can, the Argon and water lines were attached and the thermocouple connected. The system was then pumped upon until the evening when the warm-up period for the run was started. Just before pouring oil into the oil

bath, however, the cooling water was turned on and the system was flushed four times with Argon to aid in producing an oxygen free atmosphere. The set-point of the controller was set for a temperature of around 230°C. After flushing, with the Argon finally flowing through the system and the oil in the oil bath, the heaters were turned on.

Early the next morning, the controller was raised to a set-point of 273.0°C, which was the first and highest temperature at which most of the velocity and attenuation measurements were made. The next step was to attach the reflector can to the guide platform. The reflector can was then raised slightly, the 2" long pods were removed and the can lowered to a position just above the top melt surface. It was kept there until the indicating controller and the thermocouples showed that the melt had completely liquified. The can was then lowered all the way into the melt until it pushed against the bottom of the beaker. Argon bubbling into the melt was started at a moderate rate. Mixing usually took less than an hour but a whole hour was used nevertheless to ensure equilibration and a steady set-point temperature. The equilibration of the system could be observed by watching as the two thermocouple traces approached one another. While bubbling Argon through the melt, the main Argon inlet to the beaker was kept closed. After mixing was complete and the Argon bubbling through the melt was stopped, the can was raised very slightly and 1/8" spacers were put on the short pods. After first disconnecting from the guide platform, the can was then lowered onto this arrangement and securely fastened to it.

A few minutes were allowed to let the system stabilize. After

this the guide platform was raised slowly, catching the rod holder from underneath and raising the rod off the reflector. The rod was moved up until the melt echo was well separated from the internally reflected (rod face) echo. The signal was then lined up to maximize it at the highest frequency (49.7 MHz). When this was completed the rod holder was fastened securely to the guide platform. It was important to raise the rod slowly off the reflector, since this helped to ensure a good bond between rod face and melt. A rapid raising could create turbulence and gas bubbles.

The velocity was measured first; data points were taken at 0.1000" intervals and a quick check of the data over six to eight points enabled one to determine whether the system was indeed uniformly mixed. This was usually the case and the velocity of sound calculated from these points was recorded for this highest temperature. Attenuation measurements were started, after letting the system stabilize for another hour.

4.3 Preparations after a Run

After all the measurements had been made, the reflector can, with the rod resting on the reflector, was slowly raised from the melt. The 2" long pods were once more put into place and the can was left resting on them. The guide platform was then loosened from the reflector can brackets and moved up to move the rod and rod face off the reflectors. This was done to prevent the possibility that melt left on the reflector might freeze the rod to the reflector while the system was left to cool down overnight.

The heaters were turned off as soon as the reflector can was out of the melt. The Argon and water flows were left on for the overnight cooldown, although the Argon flow rate was considerably reduced.

The next day the oil had cooled down enough that it could be conveniently drained from its container. While this was being done the superstructure of the apparatus, including all the Argon bubbler tubes, water and thermocouple connections as well as 'O'-ring seals, connections to gears and coaxial cables were removed.

First the rod and then the reflector holder were taken out of the support platform. Once the level of the oil was below the level of the melt beaker platform, the main Argon supply and exit lines were disconnected and the beaker, with support platform still connected to it, was taken out of the oil bath.

Once out of the oil bath container, the platform was separated from the melt beaker. This had to be done using a jack device, since the Viton 'O'-ring was usually badly deformed and caked to the guide platform flange. This 'O'-ring was discarded and a new one used for the next run. The melt container was then covered and left to cool for a while so that all of the melt in it was frozen, after which it was cleaned of the oil on the outside and weighed as indicated in an earlier section.

In the meantime, the reflector was removed from the reflector holder, enabling the now frozen ring of melt left behind on the reflector to be removed. All parts of the apparatus which had been immersed in the melt were cleaned with hot water, with particular attention being paid to the rod and rod face and the reflector face, which was polished

after each run. It was important that no melt material get between rod face and reflector face while putting the equipment together for the next run and hence all melt material here was carefully removed. Traces of melt usually remained on the other submersible parts but the amount was negligible.

4.4 Attenuation Measurements

Attenuation measurements of the ultrasonic signal in the melt were made by altering the distance that the signal had to travel in the melt and comparing the height of the signal at each position with the height of a comparison pulse which was conveniently positioned close to the ultrasonic echo. Specifically, the height of the melt signal was first measured at the shortest path length as shown in Fig. 19. This value could be a non-integral db value read off the meter of the hp606A oscillator output attenuator which had provision for a continuous signal height variation over a 10 db range and a 10 db variation switch independent of this, the combination covering a total range of 140 db. The rod position for this reading was measured by means of the Vernier micrometer. The height of the comparison pulse was then lowered to the nearest convenient integral db value and the rod moved further away from the reflector until the ultrasonic signal level had dropped and was once more even with that of the comparison pulse. This procedure was repeated until sufficient data points had been collected. The comparison pulse height, except for the first point, was usually dropped or raised by 1 or 2 db steps, the precise value depending on the amount of attenuation

present. When the attenuation was very small, however, smaller intervals were sometimes used.

The total distance over which measurements were made was kept as uniform as possible, usually starting with a position when the rod face was about 0.25" above the reflector and ending up with a final position of between 0.65 to 0.85" above the reflector. The final height to which the rod was taken depended on the magnitude of the attenuation.

When a large amount of attenuation was present (such as at f = 49.7 MHz and near the critical temperature and composition) 2 db intervals were used and sufficient data points were found to be collected over the shorter total measuring distance. Usually anywhere from 5 to 10 points were collected at a particular frequency and temperature while raising the rod. The same number of measurements were then taken on lowering the rod again. Doing this helped in checking the consistency of the data and ensured that no alignment shifts or large thermal drifts had affected the measurements.

To get a set of measurements as described above took about 15 - 20 minutes per frequency setting, since care was taken not to move the rod too fast to disturb the system as little as possible. Nonetheless, temperature drifts did occur while raising and lowering the rod, amounting to temperature uncertainties of $\pm 0.1^{o}C$. If one had moved the rod very slowly to a new position and left it there for a sufficiently long time, the temperature value could have been held to its original value. Thus, in principle, the temperature drift could have been avoided. However, the procedure would have been extremely tedious and the measurements would then have taken so long that long term drifts in the

controller could have started to become a factor in the temperature control.

After each change of the controller set-point to a new temperature, 2 - 4 hours were allowed for temperature equilibration (from the time that the temperature of the melt was first at the new temperature) before any new measurements were started. The shorter time period was accepted for situations when the melt was far off critical conditions, both in terms of composition and temperature. A check was made to determine whether the equilibration time stated above was long enough. Measurements of attenuation were performed at f = 49.7 MHz after a 4 hour equilibration period for the mixture at the critical composition and at T = 263.8^{o}C. The measurements were repeated an hour later. It was found that no significant change in the attenuation coefficient had occurred.

With this method of measuring attenuation, great care had to be taken to use the same top part of the melt echo and the comparison pulse while lining them up. To this end, the horizontal graticule markings on the CRO were used as fiducial markers and a characteristic feature near the top of the ultrasonic echo (since on an expanded sweep of 5 μs/cm or more, none were perfectly smooth) was used to line up with the horizontal line which simultaneously lined up with the top part of the comparison pulse. Further, to aid the experimenter to make a consistent and objective decision as to when the echo had risen or fallen to the next level which had been set by the comparison pulse, the gain control on the CRO was always adjusted to compensate for this change and to keep the comparison pulse height always at the same level

(and hence always lined up with the same graticule line).

The frequency of the ultrasonic signals was always set at the same value, conveniently an optimum value around each particular harmonic frequency, the major criteria for this optimum being a clean and large signal. This optimum value for each frequency had been determined in earlier tests, before starting any of the runs. To measure the frequency of the signal, the video display mode was used and the comparison pulse moved over to overlap the ultrasonic echo[53]. The frequency of the comparison pulse was then tuned to the same frequency as that of the echo by observing that the beating between the two phase incoherent signals was at a minimum. Figs. 20 and 21, respectively, show the case when the comparison pulse frequency is different from and the same as that of the ultrasonic signal. As can be seen from the photographs, the on-frequency case is characterized by the beat in the echo envelope lines being parallel to one another. The frequency was read off the hp606A oscillator dial, the calibration of which was occasionally checked by means of an hp frequency counter.

4.5 Velocity Measurements

Velocity measurements were performed at 25.5 MHz and at each temperature at which attenuation measurements were made. Since the velocity effects are small, it was decided that there was no point in making these measurements at all frequencies. The signals were displayed in their true form; i.e., with their rf content still present and on an expanded sweep. Fed into the other CRO input were time-markers from the

Tektronix 184 Time-Mark generator. The CRO was set on "alternate" sweep to display both cycles simultaneously. The sweep of the CRO was expanded until one cycle of the signal was spread sufficiently to cover a distance of about 0.4 cm. The melt echo was then moved as close as possible to the internally reflected echo (the "main" echo) without the trailing edge of the "main" echo interfering with the leading edge of the melt echo. For fixing the position in time of the leading edge, both signals were separately adjusted (i.e., first one and then the other), using the continuously variable gain control of the CRO to achieve the same height on the oscilloscope display face -- usually exactly 3 cm peak-to-peak. The following procedure was then adopted.

After setting its height at 3 cm peak-to-peak, the leading edge of the "main" echo was moved, using the CRO sweep delay feature, until a cycle covering exactly 0.4 cm of vertical distance (height) was at the vertical center line. This temporal position was then noted using the time-markers, two of which were simultaneously displayed -- 1 μs and 0.1 μs. The height of the melt echo was then adjusted in the same way and, using the CRO sweep delay, its leading edge was similarly lined up and this position noted. The difference between the two readings was noted as Δt representing the time taken for an echo to travel from the rod face into the melt and, after reflection at the bottom, back into the rod again.

The rod was then moved up until it reached a height indicated by the micrometer as a multiple of an even tenth of an inch, say 0.3000, 0.4000, 0.5000" etc. The same procedure as described above was repeated,

except that it was only necessary now to repeat the measurements for the melt echo -- the temporal position of the "main" echo remaining constant over the measurement period of 10 - 15 minutes. Of course the melt echo height had to be readjusted to be 3 cm peak-to-peak on the CRO face each time after moving the rod, since the attenuation in the melt would alter its height with the distance it had travelled in the melt.

Fig. 22 shows a photograph of the leading edge of the melt echo with the time-markers superimposed upon it.

CHAPTER 5

EXPERIMENTAL RESULTS

5.1 Attenuation Measurements

Using the method described in Chapter 4, values of the attenuation (in db) were obtained versus distance of the fused silica rod moved (in inches). These values were recorded and a least squares straight line was fitted to the points, the slope of the line giving α'. For demonstrative purposes, and to illustrate the quality of the fit, some typical graphs showing attenuation versus distance have been given in Figs. 23, 24, 25 and 26. The value obtained for the slope of the line was divided by 5.08 cm/inch to convert the slope to the proper units of db/cm. In this respect, it should be noted that in the graphs shown, the values of attenuation are plotted against only half the actual distance travelled by the sound pulse (since this is what was measured) and this accounts for the division by 5.08 cm/inch rather than 2.54 cm/inch. The value of α' for the attenuation of the sound intensity thus calculated was then converted to a form which would make the anomalous absorption effects immediately apparent -- i.e., α' was divided by 8.686 and f^2 where f was in cycles/sec and 8.686 is the conversion factor which changes α' from a quantity expressed in db/cm to one which is dimensionless per unit length (often written as nepers/cm or simply cm^{-1}). This quantity is denoted by α and represents the attenuation of the sound wave amplitude, which is the quantity usually calculated in a theoretical treatment. The above

conversion from α' to α follows simply from the derivation given below.

Assume that at a position, ℓ_1, the amplitude of the sound wave is proportional to $e^{-\alpha\ell_1}$ while at a position $\ell_2 > \ell_1$ it is proportional to $e^{-\alpha\ell_2}$. Now, power loss in decibels is defined as

$$\text{Power Loss} = \text{P.L.(db)} = 10 \log_{10} \frac{I_o}{I_i} \tag{5-1}$$

where I_i = power into system and I_o = power out of system.

Now for the sound wave, its intensity or power is found to be proportional to the square of its amplitude. Hence one has (calling position ℓ_1 as the position where power is put into the system and position ℓ_2 as the position where power is taken out) simply

$$\text{P.L.} = 20 \log_{10} \frac{e^{-\alpha\ell_2}}{e^{-\alpha\ell_1}} = 20 \log_{10} e^{-\alpha(\ell_2 - \ell_1)} \tag{5-2}$$

and converting to natural logarithms this becomes

$$\text{P.L.} = 20 \times 0.4343 \ln e^{-\alpha(\ell_2 - \ell_1)} = -8.686\, \alpha(\ell_2 - \ell_1) \tag{5-3}$$

Hence

$$\alpha \text{ (in nepers/length)} = - \frac{\text{P.L.}}{\ell_2 - \ell_1} \frac{1}{8.686} \tag{5-4}$$

where $\text{P.L.}/(\ell_2 - \ell_1)$ is in units of db/length -- the required conversion formula given earlier.

The values of α/f^2 calculated as described above were then recorded as a function of temperature, composition and frequency. No corrections for diffraction effects were made to these figures, since a relatively high velocity of sound and frequency, combined with reasonably short path

lengths aided in keeping the sound pulses within the Fresnel diffraction region where no divergence of the sound beam occurs[52,44]. In this region possible oscillations of the sound beam with distance could occur due to the rapid pressure oscillations along the axis of transmission. However, this can be minimized to a negligible level by making the reflector larger than the source as was the case in this experiment. The source here was the fused silica rod face.

As can be seen from the graphs of Figs. 23 - 26, the actual magnitude of the attenuation that is measured on the CRO (i.e., the actual change in height of the amplitude of the signal) is largest for the largest frequencies used while the opposite is true of the calculated α/f^2. Since the attenuation in liquid metals is considerably smaller than for organic materials (even near the critical point) the lowest frequency that could reasonably be used with any accuracy (i.e., sufficient attenuation over a given path length) was 16.6 MHz. This was unfortunate, since as can be seen from Table V, lower frequencies show a more spectacular α/f^2 versus temperature variation. Our choice of cut-off for the highest frequency studied was more arbitrary, although some limitation was imposed by the equipment's ability to line up the rod face parallel to the reflector face to achieve sufficient signal strength, and by the ability of the tuned amplifier to amplify the signal sufficiently at the higher frequencies.

The reliability of the method and the accuracy of the hp606A output attenuator were also checked in a number of ways before any of the critical region measurements were made on the sample. First, a study was made of the attenuation of sound for compositions far off

the critical composition. Here the attenuation is unaffected by critical fluctuations and thus should be low and with a value very close to the classical α/f^2 value. This was indeed found to be the case. Further confirmation of the accuracy of the method was found in comparing attenuation results on pure Ga with values in the literature[54,55]. Here too a very satisfactory agreement was found. In addition to this, before any of the above measurements were even started on the system Ga-Bi, the equipment was used to study the attenuation of sound in water. A detailed account of this method has already been given in Section 3.5 in connection with the initial alignment of the equipment. Here it is sufficient to say that the value of α/f^2 obtained at 37.6 and 49.7 MHz were, within experimental error, in agreement with each other and also with the value of α/f^2 for water as given in the literature[18,*].

Table V shows the values obtained for the attenuation of sound divided by the square of the frequency (in nepers sec^2/cm). These results were obtained from measurements on two different cumulative mixtures (henceforth labelled batches). It was found necessary to use two batches because the Ga-Bi phase diagram given by Predel[56] (shown in Fig. 27) was sufficiently uncertain that an accurate reading of C^c_{Bi} and T_c was not possible. Our own attenuation and velocity measurements on the first batch and on an exploratory batch helped to better establish the values of C^c_{Bi} and T_c. After changing the composition using the first batch and an exploratory batch right across the most important section of the phase diagram, the location of C^c_{Bi} and T_c was determined from the data. A second batch was prepared to fill in gaps in the α/f^2

---

* See Table V Supplement 2 for the values.

versus composition diagram and to repeat some of the data from runs made on the first batch. Measurements at the estimated critical composition were carried out twice, each time with a different batch, and the results at T = 273.0, 265.9 and 263.8°C averaged. The repeated measurements were within the experimental error of the first measurements, indicating good reproducibility of the results. Additional attenuation measurements were made at lower $(T - T_c)$ values once a reliable value of T_c had been obtained. On one of the last runs, measurements were also made a considerable distance away from the critical temperature, while still at the critical composition, to see how much of the critical absorption remained at large $(T - T_c)$ values.

Although attenuation measurements very near T_c and C_{Bi}^c on the first batch and on an initial exploratory batch gave a good approximation to the true value of T_c, final evaluation of the critical temperature was more effectively and more simply made using the velocity data, as will be described in the following section. The method described in that section gains further significance in that it gives an independent check on T_c. The best values of the critical constants found from these experiments are $C_{Bi}^c = 0.60 \pm 0.01$ weight-fraction, and $T_c = 263.1 \pm 0.2°C$, where the value of C_{Bi}^c was inferred from the maxima in the sound absorption peaks of α/f^2. The error quoted for C_{Bi}^c is a probable error determined by combining the estimated error due to the finite intervals between compositions for which the attenuation was measured with the overall accuracy of the composition determination. The quoted error in T_c is also a probable error and is calculated in a similar manner as the error for C_{Bi}^c (see Sections 5.2 and 6.1).

The values of α/f^2 versus composition are also plotted for the three main temperatures used as shown in Figs. 28, 29 and 30. Attenuation values for the four frequencies used are plotted on one graph as an aid to comparison of the data. As is evident from Table V, since the values of α/f^2 for the compositions C_{Bi} = 0.20, 0.30, 0.35 and 0.40 weight-fraction show no increase with increasing f or with $T \rightarrow T_c$, they were assumed to contain no effects due to the critical fluctuations and hence the four numbers obtained for each composition at the two frequencies and temperatures used were averaged for each composition. This average value was then used in the graphs of Figs. 28, 29 and 30. As can be seen from these graphs a baseline has been drawn representing the normal non-critical sound losses in the liquid metal mixture due to the usual dissipative effects of thermal conduction and shear viscosity. There is a small excess absorption in the pure materials for both Ga and Bi[54], but there are no anomalous relaxation effects, since α/f^2 remains a constant for different values of f[57]. Hence, for the calculation of the non-critical sound attenuation which follows it is assumed that the bulk viscosity ζ is independent of frequency. This behaviour is expected for the mixture well away from the critical point as well as for each of the pure components, and therefore the effects due to this bulk viscosity should be easily separable. The assumption is made that the non-critical contribution to α/f^2 for the mixture can be calculated by assuming that[58]

$$\alpha_{mixt}/f^2 = \alpha_{Ga}/f^2\,(1-C_{Bi}) + \alpha_{Bi}/f^2\,(C_{Bi}) \qquad (5\text{-}5)$$

i.e., that there is a linear relationship with respect to weight-fraction

between the absorption for the pure substances and the mixture. The values of α/f^2 for the pure components have been quoted as [54]

$$\alpha_{Ga}/f^2 = 3.0 \times 10^{-17} \text{ nepers cm}^{-1} \text{ sec}^2 \text{ (around 250°C)}$$

and

$$\alpha_{Bi}/f^2 = 8.1 \times 10^{-17} \text{ nepers cm}^{-1} \text{ sec}^2 \text{ (around 280°C)}.$$

Hence at the critical composition of $C^c_{Bi} = 0.60$ weight-fraction the value for the non-critical background attenuation is calculated to be 6.0×10^{-17} nepers cm^{-1} sec^2. The increase with temperature of this non-critical background attenuation is assumed to be negligible over the temperature changes considered in this experiment and this should be a reasonable approximation in view of the low temperature dependence quoted in the literature for the pure components[54].

It can be seen from Table V that at f = 16.6 MHz and T = 263.4°C for which the highest α/f^2 values were obtained, the value of α/f^2 is roughly 15 times that of the assumed non-critical value. Even at 290.3°C, which is 27°C away from T_c, α/f^2 is still more than 4 times the assumed non-critical value. A graph showing the temperature dependence of the α/f^2 values at the critical composition is given in Fig. 31, while the frequency dependence is shown in Fig. 32.

It should be noted that all of the attenuation measurements given in Table V were made in the region <u>above</u> the phase separation boundary (in the one-phase region) since it was felt that values below the phase separation boundary (i.e., in the two-phase region) would not be transparently related to any of the theories that have been derived to explain the anomalous sound absorption effect, for in this two-phase region the equilibrium compositions would change continuously with changing temperature. (For an illustration of curves of α/f^2 versus T <u>below</u> T_c see Ref. 65).

However, several efforts were made at compositions off the critical composition to approach the phase separation boundary as close as possible, and the results in Table V show two runs (at C_{Bi} = 0.47 and at C_{Bi} = 0.52 weight-fraction) where the lowest temperature to which the system was taken was below T_c but still above T_p, the phase separation temperature. It is not known how far these temperatures are above T_p although an estimate can be obtained from Predel's data[56,*]. (See Fig. 27 for a reproduction of his Ga-Bi phase diagram.) Unfortunately, the temperature accuracy from his phase diagram is no better than $\pm 1^{o}C$. At any rate, the results show that the attenuation continues to increase as T approaches T_p. A more graphic illustration of this tendency was found in a run at C_{Bi} = 0.68 weight-fraction where the temperature was taken up to and (accidentally) below T_p. From the data on the velocity of sound it is very probable that the lowest temperature at which attenuation measurements were made, as indicated in Table V, was just below T_p. Hence from this data it appears that the attenuation of sound increases until the temperature is at $T_p \leq T_c$. Of course the overall level of the attenuation will be lower, the further the composition of the mixture gets away from the critical composition.

Graphs were also plotted for the values of α/f^2 at a particular frequency as a function of temperature using data with different values of C_{Bi} plotted on the same graph. These are shown in Figs. 33 and 34. From these graphs it can be seen that the form of the functional dependence of α/f^2 with temperature is maintained even for mixtures fairly far off

---

* Predel has been the only investigator so far who has mapped the miscibility gap for Ga-Bi. For an indirect confirmation of the validity of Predel's results see the critical neutron scattering data of Wignall and Egelstaff (Refs. 74 and 70) on Ga-Bi.

the critical composition. This implies that the exponent governing the temperature dependence of κ in the Fixman expression is not very strongly composition dependent near C^c_{Bi}. A similar result was found by Chu and Schoenes[59] from light-scattering data on the isobutyric-acid-water system which yields information on $\partial \mu_{12}/\partial C_1$, thus giving the diffusion coefficient. The exponent giving the temperature dependence of this coefficient was found to be nearly independent of composition near C^c. Hence the results of Figs. 33 and 34 lend further credence to the reliability and consistency of the data.

5.2 Velocity Measurements

The velocity of sound was measured at 25.5 MHz and at each of the temperatures at which the attenuation of sound was measured. The method for doing this has already been outlined in an earlier section. A frequency of 25.5 MHz was chosen to measure the velocity of sound because at this frequency we obtained a good, clean signal with a uniformly rising leading edge. Furthermore, since a reasonable expansion of the signal was desired so that each cycle covered about 0.4 cm horizontal distance on the CRO screen, the frequency could not be so high that the low frequency bright display of the waveform on the CRO screen deteriorated. On the other hand, too low a frequency meant that one cycle covered a longer time interval and hence an occasional choice of an incorrect cycle of the leading edge from which to measure time intervals would introduce a considerable error (about ± 0.05 μs or more) into the overall measurement of the transmission time.

It was found that, within the experimental accuracy, at a particular composition there was no change in the velocity of sound in going from T = 273.0 to 263.8°C no matter whether the composition was at the critical composition or far away from it. Hence no large critical effects on the velocity of sound were evident. Fig. 35 shows a graph of the velocity of sound as a function of the composition in weight-fractions. The velocity of sound in pure Ga (c_o^{Ga}) was measured in this experiment also, and this result compares well, within experimental error, to the most reliable value of c_o^{Ga} quoted in the literature[54]. As can be seen from the graph the variation of sound with composition in weight-fraction does not follow a linear relationship as has been found in another metallic system[58], but deviates positively from it. Since there is an appreciable difference between the velocity of sound for the two pure components and no temperature effects, the velocity serves as a good measure of the composition of the melt. This circumstance was made use of to signal the onset of phase separation. Indeed, it was the only way that a phase separation could be detected in this system since even when there were two layered phases present and the rod was moved so high in the melt that the sound pulse had to go through the interface between the two layers, no reflection from this interface was observed. This is probably because the acoustic impedances of the two phases are always very close.

Phase separation could be detected by the change in the velocity of sound in two ways; one, from observation of the change in the value of the sound velocity when going from the one-phase region to the lower phase in the two-phase region; two, from the observation of the difference

in value obtained for the velocity of sound in each of the two phases. The first method was, of course, the easier one and was used to get our best measure of T_c. This was done starting with a mixture at C^c_{Bi} and about at 1°C above the preliminary value of T_c and by lowering the temperature by 0.3°C increments. The method was quite tedious as sufficient time had to be allowed to let the system equilibrate after a temperature change. For the system so close to the critical temperature, this equilibration time is much slower than normal and so initially about two hours was allowed. The velocity was then measured and another hour was allowed for further equilibration, whereupon the velocity was measured again. If there was no change in velocity the system was then assumed to be still in the one-phase region and the temperature lowered a further 0.3°C. In contrast to the normal attenuation measurements, care was taken here, when measuring the velocity, that temperature drifts due to the motion of the rod were kept to a negligible level. The above procedure was repeated twice, each time with a different starting point, so that different temperatures were covered each time. The procedure indicated quite a large change (around 0.08×10^5 cm/sec) in the velocity of sound even when the melt was only an estimated 0.2°C below T_c. Since the phase boundary[56] goes as $|C_{Bi} - C^c_{Bi}| \sim |T - T_c|^{1/3}$ and also has a flat top near T_c, there is a large change in composition for a very small temperature deviation from the critical temperature*. The limit of accuracy of T_c obtained considering the limitations of the above method is estimated to be ±0.1°C. This accuracy (probable error) is combined with the accuracy of a temperature measurement (Section 6.1) to give the overall accuracy on T_c as it is stated in Section 5.1.

---

* See Table V Supplement 1 for the velocity data below and above T_c.

After measurements on the first batch had been completed and the velocity of sound results obtained, they were plotted on a graph of velocity versus composition. This graph served as a check on compositions prepared with the second batch. It was found that the values of velocity of sound measured on this second batch, when plotted on this graph, were all within experimental error of the line that had been drawn to points from the first batch. The good agreement shows that the method outlined earlier for calculating the composition of the mixture was reliable.

Another way by which phase separation and the location of the critical temperature was observed was by the decrease in the values of the sound attenuation below the phase separation temperature. However, these values were not recorded in this thesis because of the reasons mentioned earlier in this chapter (Sec. 5.1).

Table V. Experimental values of α/f^2.

$A = \alpha/f^2$ in units of 10^{-17} nepers $cm^{-1}sec^2$				$T(^oC)$ $\pm 0.2^oC$	$c_o(10^5$ cm/sec)	C_{Bi} weight-fraction
f = 16.6 MHz	f = 25.5 MHz	f = 37.6 MHz	f = 49.7 MHz			
		2.73	4.54	273.0	2.66	0.20
		4.66	4.23	265.9	2.66	
		5.72	4.58	273.0	2.61	0.30
		6.05	5.74	265.9	2.61	
		8.00 ± 0.70	7.11 ± 0.57	273.0	2.56	0.35
		6.36 ± 0.66	6.20 ± 0.52	265.8	2.56	
		7.75	7.53	272.9	2.50	0.40
		7.02	7.34	265.7	2.50	
	12.3	10.7	9.77	272.9	2.41	
	19.8	14.5	12.2	265.7	2.41	0.45
	21.6	16.5	12.5	262.9	2.41	
	14.5	12.2	10.4	272.9	2.40	
	20.5	16.6	13.3	265.8	2.40	0.47
	24.3	17.4	14.3	263.8	2.40	
	28.2	21.7	20.4	261.7	2.40	
	20.9	17.7	17.0	272.9	2.35	
	32.2	23.1	21.8	265.7	2.35	0.52
	37.4	27.6	22.2	263.8	2.35	
	41.0	29.2	26.3	262.0	2.35	
31.7	24.9	21.4	17.6	273.0	2.31	
49.0	39.3	29.0	21.2	265.8	2.31	0.53
58.7	45.2	34.2	27.6	263.9	2.31	
37.1	30.6	24.2	21.2	273.1	2.26	
55.6	45.4	33.9	26.0	265.7	2.26	0.56
66.3	53.9	40.4	31.1	263.8	2.26	
40.4	35.2	27.4	24.5	272.9	2.23	
65.9	52.1	40.9	32.9	265.9	2.23	0.58
77.8	61.4	50.1	39.7	263.8	2.23	
27.0 ± 1.7	24.1 ± 1.6	21.7 ± 1.4	19.9 ± 1.5	290.3	2.20	
45.7 ± 2.0	38.3 ± 2.0	32.0 ± 1.5	29.2 ± 1.7	273.0	2.21	
68.5 ± 3.1	57.2 ± 3.2	44.2 ± 1.6	35.5 ± 2.4	265.8	2.21	0.60
83.8 ± 7.3	66.7 ± 3.5	55.2 ± 2.9	42.7 ± 3.1	263.8	2.21	
90.3 ± 5.8	71.2 ± 3.7	57.0 ± 3.1	45.8 ± 2.7	263.4	2.21	
40.3	35.2	30.8	28.2	272.9	2.20	
66.2	55.1	43.1	34.3	265.8	2.20	0.61
75.9	62.3	52.9	40.4	263.9	2.20	
38.0	33.3	27.8	24.0	273.0	2.18	
62.4	47.7	39.5	32.3	265.8	2.18	0.63
71.3	55.6	45.2	38.1	264.0	2.18	

Table V (continued).

$A = \alpha/f^2$ in units of 10^{-17} nepers $cm^{-1}sec^2$				T(°C) ± 0.2°C	$c_o(10^5$ cm/sec)	C_{Bi} weight-fraction
f = 16.6 MHz	f = 25.5 MHz	f = 37.6 MHz	f = 49.7 MHz			
33.5	32.4	25.1	22.2	272.9	2.14	
55.4	46.8	34.1	30.1	265.8	2.14	0.64
69.2	51.5	43.1	36.8	264.0	2.14	
27.7	24.6	21.2	18.1	273.0	2.09	
43.3	34.9	25.9	22.9	265.8	2.09	
45.0	37.1	30.2	23.8	263.8	2.09	0.68
50.7	39.2	30.5	24.7	261.9	2.09	
46.0	38.1	28.1	23.4	259.9	2.06*	
	12.0	11.0	9.17	272.9	2.01	
	14.8	13.0	12.5	265.8	2.01	0.75
	16.0	14.2	13.3	263.9	2.01	

* Velocity measured in lower phase after phase separation has occurred.

Table V.Supplement.

1. Values of velocity of sound near T_c.

C_o (10^5 cm/sec)	T (°C)
2.21	263.9
2.21	263.6
2.21	263.5
2.21	263.3
2.21	263.2
2.13	263.0
2.12	262.9

2. Calibration data: Values of α/f^2 for distilled water.

α/f^2 (10^{-17} nepers cm^{-1} sec^2)		T (°C)
f = 37.6 MHz	f = 49.7 MHz	
24.2	23.5	21.5

CHAPTER 6

DISCUSSIONS OF ERRORS

6.1 Temperature Measurements

As mentioned in Chapter 3, the sensing elements used to measure the temperature of the melt were stainless steel sheathed iron-constantan thermocouples that had been calibrated by the National Research Council of Canada to ±0.04°C at the five temperature points of 150, 200, 250, 300 and 320°C. The temperatures quoted were based on the IPTS-68 scale. From this data a table was constructed giving emf versus temperature values at 0.1°C temperature intervals. The values in this table were calculated from a straight line fitted to the above points using the method of least squares*. It was found that the points for all the three thermocouples closely fitted a straight line with a correlation coefficient of 0.9999997. From 250 to 300°C the deviation between the value of temperature calculated from the straight line fitted to the data and the actual experimental values for the two points is less than 0.1°C. Hence the error in emf versus temperature readings resulting from the use of the straight line fitted to the five calibration points is only slightly worse than the stated accuracy of the temperature measurements for these calibration points. The accuracy (in this chapter accuracy refers to a maximum possible error) of a temperature point in the table is therefore considered to be ±0.1°C.

Considering that the thermocouples were never taken higher than 270°C it is assumed that the reproducibility of the emf versus temperature

---

* See Appendix A for the complete calculation and data.

values is $\pm 0.1^{o}C$[60].

The emf was measured with a Pye potentiometer and a Cambridge Instruments Ltd. dc suspended spot galvanometer with a maximum sensitivity of 0.6 mm scale deflection per μv. This equipment allowed one to measure the absolute emf to an accuracy of approximately 5 μv, the main limitation being the standardization circuit of the potentiometer. For an iron-constantan thermocouple in the 250 - 300°C range this corresponds to an accuracy of $\pm 0.1^{o}C$. Combining all of the above effects, the absolute temperature accuracy of an individual measurement can be considered to be about $\pm 0.3^{o}C$.

A further error in the temperature arises as a result of the drift which occurred while moving the rod up and down in the melt. This drift could be controlled by the rate of motion of the rod and was kept within the limits of $\pm 0.1^{o}C$ about the set-point temperature.

Summing up it is estimated that all the uncertainties produce a maximum possible error entering into each measurement of α corresponding to less than $\pm 0.4^{o}C$. However, this error represents a conservative outer limit. A careful estimate of the true "probable error" places the actual error in the temperature more within $\pm 0.2^{o}C$.

6.2 Composition Determination

For the first run of a batch, to prepare a sample of Ga-Bi at a particular composition, predetermined amounts of the metals were weighed and combined in the stainless steel beaker. The composition C_{Bi}

was then calculated by taking the ratio (by weights) of the amount of Bi over the total amount of metal in the mixture. This calculation was done to a high precision since the amounts of Ga and Bi used were weighed accurate to ±0.1 g. Since the initial amounts of Ga and Bi used for the first run were 190.1 g and 48.0 g, respectively, the accuracy for this first value of C_{Bi} was considerably better than 0.01%. As was stated, however, in Chapter 4 the same materials were used over and over for subsequent runs in order to conserve material. Composition changes were thus brought about by merely adding more Bi. This in itself was acceptable, but after each run, in the neighbourhood of 3 g of the mixture was lost on taking the rod, reflector and reflector holder out of the liquid metal mixture. Now the temperature of the mixture was always kept above the miscibility gap, which means that it was homogeneous before the removal of the equipment. Moreover, the amounts of Ga and Bi that were contained in the sample that was removed were the same as those in the mixture left behind. Hence the amount of each constituent in the lost sample could be calculated along with the amounts remaining for the subsequent runs.

In order to check on the above suppositions, most of the sample that was lost from the melt was recovered from the rod, reflector and reflector holder (after waiting for all of it to freeze) and it was chemically analysed for Bi. Although the accuracy of the method used was no better than 3%, judging from the scatter of the data, it showed that most of the sample removed was close to the composition of the melt and that the above method of calculating compositions could be accepted as reliable. It should be pointed out that not all of the samples analysed

were within the 3% limit of the calculated composition. In no case, however, was this deviation more than 10%. This would still cause only a negligible error in calculating the next composition, as the overall sample weight was much larger than the sample weight that was lost.

Another check on the reliability of the composition determination method was obtained via a measurement of the velocity of sound. This point was previously mentioned in Chapter 5. Now the velocity of sound was measured at each new composition of the melt. For the first batch about 14 different compositions were prepared ranging from C_{Bi} = 0.20 to C_{Bi} = 0.75 weight-fraction. These points, then, gave a calibration curve of velocity versus composition. From the graph of the velocity of sound of the mixture versus the composition as given in Fig. 35 it can be seen that for a change of 0.01 X 10^5 cm/sec in the velocity of sound the composition changes by 1%. Hence a velocity measurement is a sensitive check on the changes in composition.

It was found that once the second batch had been prepared for a certain composition C_{Bi} and the velocity of sound was measured, the velocity of sound was always with ±0.01 X 10^5 cm/sec of the expected velocity of sound taken from the graph assuming the mixture value of C_{Bi} to have been correct. In fact, the velocity measured on the second batch for the mixture at the composition C_{Bi} = 0.60 weight-fraction (critical composition) was found to be identical to the velocity measured on the first batch at this same composition.

Using the results of the velocity measurements and the chemical analysis as a guide it is estimated that in all cases the probable error in the quoted values of C_{Bi} is ±0.01 weight-fraction.

6.3 Velocity Measurements

The velocity of sound was usually measured by taking the total distance the rod had moved, this representing the change in path length that the ultrasonic pulse had to traverse in the melt, and dividing it by the difference in time elapsed between the initial and final positions of the ultrasonic echo. A detailed description of how this was done is given in Chapter 4. The total distance travelled by the rod was usually 0.5000". The time interval for this distance varied, depending on the composition of the melt, from Δt = 9.60 to 12.64 μs. The increase in path length that the ultrasonic pulse had to traverse was measured by a Vernier micrometer which was mounted above the rod. The smallest scale division on the micrometer was 0.0001". Thus a difference in position of the rod could be measured accurate to ±0.0001". Over a total measuring distance of 0.5000" the percent maximum possible error in $\Delta \ell$ was ±0.02%. The time difference was measured by means of the time markers from the Tektronix Time-Mark generator. The smallest interval available from the Time-Mark generator was 0.1 μs. Making use of the scale markings on the CRO and taking sufficient care, this interval could be extended to allow one to read changes in time accurate to ±0.02 μs. Consequently the percent maximum possible error in the time measurements ranges from ±0.22 to ±0.16%. Combining the two errors it is found that the maximum possible error in velocity is ±0.005 X 10^5 cm/sec.

When shorter length intervals of 0.1000" were used the determination of the velocity of sound was less accurate. Taking an average case, the accuracy in the length came to only ±0.1% while the corresponding time

interval was determined to an accuracy of ±1%. Hence for a velocity of sound of 2.31×10^5 cm/sec we have an accuracy of $\pm 0.02 \times 10^5$ cm/sec. The velocity of sound was determined using these shorter intervals when studying phase separation or the homogeneity of the sample. Because of the large (approximately 1%) maximum possible error in such measurements, if a change in velocity of sound with height of the rod was detected, the measurements were always validated by repetition.

6.4 Attenuation Measurements

All values of attenuation per unit distance, denoted initially by α', were obtained by a least squares straight line fitted to the intensity versus distance data. The variance of this slope was calculated from the scatter in the data in relation to this least squares line. To get the error in α/f^2 the % error for α (call this the nominal error representing one standard deviation limit) which is identical to that for α' was added to twice the % maximum possible error in f; both errors were treated as though they were maximum possible errors. The appropriate value of α/f^2 was then multiplied by this overall % error, thus yielding the total error in α/f^2. Due to the method employed of combining the errors in α and f, the above error represents a small overestimate of the total nominal error in α/f^2.

It should be noted in relation to the above that the implicit assumption in this experiment has been that the absorption measured is for monochromatic, continuous waves. Considerable errors might arise because we are actually using pulses. However Nozdrev[49] has shown that

for the conditions of our experiment (pulse length ~4 μs and $f \geq 16.6$MHz) this gives rise to a negligible error in the value of the absorption.

Errors were for the most part calculated only for the α/f^2 data at the critical composition, since these figures were the ones later used to test the validity of theoretical treatment. However, for some representative extreme values of α/f^2, errors were also calculated to give an impression of the overall accuracy of the data. The results of all the error calculations are appended to Table V and incorporated into graphs where appropriate. For those measurements which were repeated, the error quoted in Table V is the average of the error of the averaged measurement.

With respect to the graphs of attenuation versus distance given in Figs. 23, 24, 25 and 26, the error flags drawn on the points represent the maximum possible error of an individual echo height determination. The accuracy to which this could be done was estimated to be ±0.25 db. The error in measuring the distance was assumed to be negligible compared to the other errors.

CHAPTER 7

DISCUSSION OF THEORY AND RESULTS

7.1 Discussion of Results

7.1.1 Temperature and Frequency Dependence of Data at the Critical Composition

In Chapter 2, three theories of sound absorption near the critical point of a liquid-liquid system were introduced. It was shown that the theoretical methods of Fixman and Kawasaki, although different in approach, give almost identical final results. Because of this identity, when the data is analysed below, mention will only be made to the Fixman equations.

We use his equations in the form

$$\frac{\alpha}{f^2} = Af^{-5/4}\ \mathrm{Im}[f(d)] + B \qquad (7\text{-}1)$$

and

$$d = Cf^{-\frac{1}{2}}\ |T-T_c| \qquad (7\text{-}2)$$

In (7-1) the excess absorption is given by the first term, while the second term (B) represents the temperature and frequency independent classical absorption background. The integral f(d) can be calculated using a computer which has complex arithmetic capabilities.

The Fixman equation was put in the above form to determine whether values of the constants A and C could be found that would make the theoretical expressions conform to the data in both its temperature and frequency dependence. Anantaraman et al[53] and Singh and Verma[62] have both given accounts

of how one goes about fitting the data. In our particular case the situation is fairly simple since B can be assumed to be temperature independent. This was indicated in Chapter 5. Using equation (5-5) to calculate B we first obtained $B = 6.0 \times 10^{-17}$ nepers cm^{-1} sec^2. Values of A and C for a "best fit" to the data were then determined by using a computer program to generate different pairs of values of A and C and calculating the corresponding values of α/f^2 for each set. "Best fit" pairs of A and C were then picked at each frequency. The results of these "best fit" values are given in Table VI below and presented in Figs. 37 - 40 by the solid line. The "best fit" values were picked by comparing our data points with the α/f^2 points generated by equations (7-1) and (7-2).

Table VI. "Best fit" values of constants A and C.

Frequency (MHz)	$A \times 10^6$ (nepers cm^{-1} $sec^{3/4}$)	$C \times 10^{-2}$ ($sec^{\frac{1}{2}}$ deg^{-1})
49.7	3.84	2.0
37.6	3.42	2.0
25.5	2.80	2.0
16.6	2.20	2.0

As can be seen from Table VI and Figs. 37 - 40, at each particular frequency a pair of values for the constants A and C was found that made the temperature dependence of equation (7-1) conform to the temperature dependence of the data. To accomplish this however, A is found to vary slightly with frequency while C remains the same for all four frequencies. This shows that the Fixman equation cannot be made to conform to the data simultaneously as a function of both the temperature and the frequency.

Indeed it was found impossible to find values for A and C that would make equation (7-1) fit the data as a function of frequency at constant temperature. Hence we conclude that the temperature dependence of the Fixman equation shows good agreement with the experimental temperature dependence while the frequency dependence of the Fixman equation is only roughly followed by our data.

The above was strictly a test to see if the Fixman equation could generate the functional dependence of the data with temperature and frequency. Thus, the constants A and C were considered to be freely adjustable parameters and no consideration was given as to whether the values of A and C were reasonable in terms of the thermodynamic parameters given in Fixman's equations (2-69) and (2-70). Hence we will now examine the values of A and C theoretically by comparing Fixman's equation (2-69) and (2-70) with the empirical equations (7-1) and (7-2). The correspondence is to be checked through

$$A = (\gamma_{To} - 1)\left(\frac{R}{C_p^o}\right)\left(\frac{36}{\ell^4}\right)\left(\frac{1}{n_1 + n_2}\right)\left(\frac{1}{4\pi}\right)\left(\frac{h}{2\pi}\right)^{\frac{1}{4}}\frac{1}{c_o^{mixt}} \qquad (7\text{-}3)$$

$$C = \frac{6h^{\frac{1}{2}}}{(2\pi)^{\frac{1}{2}}\ell^2 T_c} \qquad (7\text{-}4)$$

Assuming that Ga is component 1 and evaluating the coefficients at the experimental critical composition, the following data can be substituted into equations (7-3) and (7-4):

$T_c = 536.1^{\circ}K$

$m_{Bi} = 3.47 \times 10^{-22} g$

$m_{Ga} = 1.16 \times 10^{-22} g$

$C_{Bi}^c = 0.60$ weight-fraction

$\phi_{Ga}^c = 0.53$ volume-fraction

$V_{Ga} = 19.6 \times 10^{-24}$ cm^3/atom

$V_{Bi} = 34.6 \times 10^{-24}$ cm^3/atom

$D_{id} = 1.0 \times 10^{-5}$ cm^2/sec

$c_o^{mixt} = 2.21 \times 10^5$ cm/sec

along with the equations

$$n_1^c = n_{Ga}^c = \frac{\phi_{Ga}^c}{V_{Ga}}$$

and

$$n_2^c = n_{Bi}^c = \frac{\phi_{Bi}^c}{V_{Bi}}$$

The following two equations were used to evaluate the other constants:

$$a = \frac{3\ V_{Bi}}{2\pi \ell^2}$$

and

$$\beta = \frac{k_B T_c}{m_{Bi} D_{id}}$$

which were needed in turn to calculate h in equation (7-3). The remaining unknown parameter is ℓ, the Debye short-range correlation length, and we may, for the moment, regard this as adjustable. We have chosen it so as to make the value of C calculated by using equation (7-4) come closest to the "best fit" C value (Table VI). Hence with ℓ = 4.5 Å we find that

$C = 1.98 \times 10^{2}$ sec$^{\frac{1}{4}}$ deg^{-1} and $A = 14.32 \times 10^{-6}$ nepers cm^{-1} sec$^{3/4}$. A larger value of ℓ would give both smaller A and C values, but the smaller C would destroy the fit of the Fixman equation to the data as a function of the temperature. The above value of ℓ compares well with other ℓ values obtained from light-scattering experiments on monatomic liquid-gas systems and organic liquid-liquid systems[63] (the ℓ values measured near T_c covering a range from 5 to 15 Å with the organic liquid-liquid systems being mostly represented by the large ℓ value).

The above theoretical value of A, which is based on the assumption that our experimental results give us a good approximation to the theoretical C, is 6.5 times greater than the "best fit" value of A obtained at 16.6 MHz. This correspondence between the "best fit" and theoretical A is perhaps not too bad when one considers that the Fixman equation was derived from a crude molecular field theory. In a companion paper to that on the anomalous sound absorption, Fixman[39] calculated the temperature dependence of the specific heat of a binary mixture and obtained a specific heat divergence with a value for the exponent α of $\frac{1}{2}$. This answer and the method whereby Fixman obtains it, have now been recognized to have been erroneous[64] -- the method largely overestimating the effect of the critical fluctuations and thus getting too strong a divergence in the specific heat. Since Fixman's calculations on the anomalous absorption follows directly from his results on the specific heat, it might be expected that the method predicts also too large an anomalous absorption effect. Furthermore, it should be pointed out that some discrepancy between Fixman's expression (the theoretical A) and the "best fit" A's is to be expected purely on the

basis that the thermodynamic data used was inaccurate. Very little reliable thermodynamic information exists for the pure components Ga and Bi and none at all for the mixture. As an example, one of the sensitive constants used here is γ_{To}, and a change in γ_{To} from 1.1 to 1.05 would cause a change in the value of A by a factor of two.

Comparing the data of this experiment with the few results on organic mixtures which are available in the literature we obtain the following. Anantaraman et al[53] find for the nitrobenzene-iso-octane system at f = 16.6 MHz, $(T - T_c) = 0.3^oC$ and at the critical composition an α/f^2 value which is 17 times the expected non-critical background α/f^2 value. This compares with our experiment at f = 16.6 MHz, $(T - T_c) = 0.3^oC$ and at the critical composition, where we find a 15 times anomalous increase in α/f^2. The results of the other papers are more difficult to compare since different values of f and $(T - T_c)$ were used. However, rough extrapolations indicate that the results of D'Arrigo and Sette[65] are comparable to the results of this experiment. Somewhat different results were obtained by Singh and Verma[62] on methyl alcohol-cyclohexane. They obtained a much slower increase of α/f^2 with T and consequently found a rather poor agreement of their results with the Fixman theory.

In view of the good agreement of the data of this experiment with the predictions of the Fixman theory in respect to the temperature dependence at constant frequency, it is perhaps surprising to find a rather poorer agreement for the frequency dependence of the data at constant temperature. However, as the functional discrepancy is only within a factor of two in our frequency range, we might dismiss it as being due to the limitations of molecular field theory and inaccurate thermodynamic

data. It is nonetheless instructive to attempt a specific explanation for this discrepancy, since it will give us an opportunity to examine the results of past workers in their efforts to understand the anomalous sound absorption near a critical point.

One approach is to assume that the previously assumed constant B in equation (7-1) is frequency dependent. This means that there are possible additional losses operative in the mixture other than those which were assumed by Fixman. Suppose as a start, that the Fixman equations only account for all the losses at the lowest frequency measured, f = 16.6 MHz. Thus the constants A = 2.20 X 10^{-6} nepers cm^{-1} $sec^{3/4}$ and C = 2.0 X 10^{2} $sec^{\frac{1}{2}}$ deg^{-1} apply to equations (7-1) and (7-2). Using these values of A and C, the Fixman equations predict α/f^2 values, as f increases, which deviate more and more from the actual experimental α/f^2 values. This is shown in Figs. 38 - 40 by the dotted lines. Hence the additional loss mechanism which must be added into equation (7-1) via a frequency dependent B to correct the theory must be one which gives increasing α/f^2 values with increasing f. This might suggest that losses through scattering from composition fluctuations is the mechanism needed to account for this additional frequency dependence of the data. However, use of the Rayleigh scattering equation, which has an f^4 dependence upon frequency for α, yields too sharp an increase in α/f^2 with frequency, while the overall magnitude of the effect is too small. Actually, the question of whether a scattering mechanism combined with a relaxation mechanism, or either one of these, can account for the total anomalous sound absorption losses in a liquid-gas or liquid-liquid system near a critical point, has been a source of conflict for some time[17]. It has long been clear that Rayleigh

scattering alone cannot properly account for all of the experimentally observed absorption, since it gives a strong increase in α/f^2 with frequency. An early effort was made to modify the Rayleigh scattering equation to account for the increase in size and correlation of the clusters as the critical point was approached[66]. Such an analysis gave a larger value for the overall magnitude of the effect, yet the strong dependency of the increase of α/f^2 on f remained.

The literature is full of conflicting reports. Anantaraman et al[53] were able to account for the results of their anomalous absorption completely on the basis of the Fixman relaxation theory alone. Brown and Richardson[67] purported to show that scattering was the important loss mechanism, yet weren't able to say that it contributed solely to their anomalous losses. Sliwinski and Brown[68] looked at the light diffraction pattern from both a liquid-gas and a liquid-liquid critical system in a Schlieren apparatus. Studying the effects of sound (as a function of time from the time of its initial passing) they concluded that the two systems behaved very differently. Their final conclusion was that a relaxation mechanism was probably the major cause of losses in a liquid-gas system. D'Arrigo and Sette[65] also indicated that scattering losses may contribute to the total absorption (in addition to the Fixman relaxation mechanism) but were unable to separate the two effects experimentally.

One might be inclined to follow D'Arrigo and Sette[65] and assume that both relaxation and scattering contribute to the anomalous losses were it not for one fact. For the system Ga-Bi, mixtures of different compositions have similar acoustic impedances so that even when phase sep-

aration has occurred no reflection is visible from the phase boundary. One would expect a similar situation to prevail with respect to clusters of different compositions that have formed near the critical phase transition. Thus the invocation of scattering losses to account either for all or for only some of the anomalous losses near the critical point is in our case untenable.

To check whether a simpler form for the excess absorption could be found, in line with what one might expect from the scaling law results of Swift, or from processes depending on a single relaxation time, it was assumed that α/f^2 depended on f and $|T-T_c|$ as

$$\frac{\alpha}{f^2} = Df^{-p} \, |T-T_c|^{-\tau}$$

The frequency and temperature dependence of the data were then checked by plotting, respectively, $\ell n\ \alpha/f^2$ versus ℓn f and $\ell n\ \alpha/f^2$ versus $\ell n\ |T-T_c|$. In the first case one was able to get an approximately straight line plot of the data. However a different value for p was found for each set of data at different values of $|T-T_c|$, p decreasing with increasing $|T-T_c|$. Similar results were obtained by Shakhparonov et al[73]. In the second case, however, it was not possible to connect the experimental points with a straight line at all. Hence no exponent was obtainable.

The above observations agree with what one expects if the data obeyed the Fixman equations (7-1) and (7-2). It appears, consequently, that neither the dynamic scaling laws nor processes depending on a single relaxation frequency give a proper description of the system in the temperature and frequency range explored by this experiment. This finding is also in agreement with those given in references 53 and 69.

7.1.2 Composition Dependence of Data

As was pointed out in Chapter 2, one could investigate the composition dependence of α_e/f^2 by examining the composition dependence of κ. To do this, one needs either experimental results on the chemical potential and its various derivatives, or a suitable theoretical model.

In the case of Ga-Bi no experimental results are available so that a theoretical model giving the chemical potential will have to be used. As a start, the Flory-Huggins solution model can be tried[27]. This model was designed to take rough account of the size difference between the two constituents in a polymer solution and thus should be a fair approximation for a liquid metal mixture such as Ga-Bi where the size disparity between the two components is 1.7 to 1. The validity of this proposition is borne out by a calculation of the critical composition using the results of the theory (equation (2-75)). The Flory-Huggins theory predicts $C_{Bi}^c = 0.56$ weight-fraction which is in agreement with Predel's[56] phase diagram and close to the $C_{Bi}^c = 0.60$ weight-fraction value obtained from the peak of our α/f^2 versus composition results.

The simplest way to compare the composition dependence of the data with the Fixman expression is to take all the composition independent terms and those terms only weakly dependent upon composition in the Fixman equation and group them together as one constant. One then has the following form for the Fixman equations

$$\frac{\alpha_e}{f^2} = A' \phi_2 \left(\frac{\partial^2 \mu_1}{\partial \phi_2 \partial T} \right) \left(\frac{\partial \kappa^2}{\partial T} \right) \mathrm{Im}[f(d)] \qquad (7\text{-}8)$$

and

$$d = B' \kappa^2 \tag{7-9}$$

which holds at constant frequency. The composition and temperature dependence of $\partial^2 \mu_1 / \partial \phi_2 \partial T$ and $\partial \kappa^2 / \partial T$ now has to be substituted into equations (7-8) and (7-9) above. Doing this using the method outlined in reference 65, one obtains that

$$\frac{\alpha_e}{f^2} = A'' \left[\frac{\phi_2^3}{T^2} \left(\Psi + \frac{2\mu_o}{T} \phi_2 \right) \frac{1}{[1-m\Psi]^2} \right] \mathrm{Im}[f(d)] \tag{7-10}$$

$$d = B'' \left[\frac{\phi_2 \Psi}{1-m\Psi} \right] \tag{7-11}$$

where Ψ is a known function of composition and temperature and A'' and B'' are constants independent of composition and temperature, but dependent on frequency.

The constants A'' and B'' are now calculated by assuming that the values of α_e/f^2 and d given by equations (7-10) and (7-11) (and thus $\mathrm{Im}[f(d)]$) are equal to the "best fit" α_e/f^2 and d values obtained earlier for the mixture at the experimental critical composition and at the various frequencies (equations (7-1) and (7-2) and Table VI). In doing this, the composition dependent equations (7-10) and (7-11) above are calculated at the critical composition given by the Flory-Huggins model and at the same temperature at which the "best fit" α_e/f^2 value is obtained. Thus all the quantities in equations (7-10) and (7-11) are known except A'' and B'', which are then solvable. Once A'' and B'' are obtained a check on the correspondence of the "best fit" α_e/f^2 values versus the Flory-

Huggins α_e/f^2 values is made over a larger temperature range. When the agreement is good, the temperature and frequency independent but composition dependent constant B is added to equation (7-10) giving

$$\frac{\alpha}{f^2} = \frac{\alpha_e}{f^2} + B \qquad (7\text{-}12)$$

The above equation (7-12) is now used to calculate the composition dependence of α/f^2 at various frequencies and temperatures.

The approach given above essentially follows that of D'Arrigo and Sette[65] except that they made a small error in using Fixman's final expression in the form

$$\frac{\alpha_e}{f^2} = A'' \left(\frac{\partial \kappa^2}{\partial T}\right)^2 \mathrm{Im}[f(d)] \qquad (7\text{-}13)$$

an equation which carries within it an approximation which makes it strictly valid only near the critical composition. This was pointed out in Chapter 2. However, when comparing the α/f^2 versus composition results using either equations (7-12) or (7-13) for Ga-Bi it turns out that there is very little difference in the final outcome except that our equation (7-12) gives a slightly broader top and a narrower bottom of the α/f^2 versus composition curve.

Comparing the theoretical composition dependence with the experimental one, we find that the theoretical profile of α/f^2 versus composition is appreciably narrower than the experimental one. This result was also found by D'Arrigo and Sette[65]. This result was to be expected, since the actual phase diagram for Ga-Bi shows a cubic phase boundary in the vicinity

of C_{Bi}^{c} while the Flory-Huggins solution model, being a molecular field model, generates a quadratic coexistence curve. Thus the derivatives of the chemical potential show a much more rapid change with composition for the Flory-Huggins solution model than they do for the real system. Supporting experimental evidence for the above results are to be obtained from the small-angle neutron scattering results of Wignall and Egelstaff[70] who obtained the composition dependence of $\partial\mu_{12}/\partial C_1$ and found that it varied near C^c and T_c with a value of the exponent $\delta = 4.5 \pm 0.5$ (see Tables II and III). A classical variation of α/f^2 with composition such as the one given by the Flory-Huggins solution model would require that $\delta = 3.0$.

A somewhat unexpected result arising from equation (7-12) and (7-11) is that the peak of α/f^2 versus composition is <u>not</u> at the Flory-Huggins critical composition but slightly higher. Moreover, this peak shifts to higher composition values, the higher the frequency. D'Arrigo and Sette[65] obtained a similar result. A consequence of the above effect is that the peak values of the theoretical plots of α/f^2 are now also slightly higher than the experimental ones. That is, the equations had been fitted to the "best fit" results at a composition slightly below the composition giving the highest theoretical α/f^2 values.

One is tempted to infer that the shift of the peak of the α/f^2 values to higher compositions is real rather than introduced by the use of the Flory-Huggins solution model, since the results of this experiment also show peak α/f^2 values at a higher composition than predicted by either the phase diagram or equation (2-76). However, the same shift in the peak α/f^2 value was observed by D'Arrigo and Sette[65] who also made an independent

determination of the phase diagram of their system. They found the critical composition obtained from the experimental peak of α/f^2 and their phase diagram to be identical. Hence it appears that the shift in the theoretical α/f^2 peaks to higher composition than the true critical composition is a consequence of the theoretical method used to generate the composition dependence of the Fixman equation. This is further supported by using a different approach in the calculation of α/f^2 versus composition than that of D'Arrigo and Sette mentioned above. The new method which was carried out required the insertion of all necessary thermodynamic data into the full composition dependent Fixman equation (equation (2-73). The composition dependence of variables such as specific heat or velocity was accounted for in this equation by assuming these variables to be a linear function of weight-fraction composition variables. The results of this method are that the α/f^2 values peaked at C_{Bi} = 0.56 weight-fraction, in agreement with C_{Bi}^c = 0.56 weight-fraction obtained from the Flory-Huggins model. This condition prevailed for all f and $(T - T_c)$ for which α/f^2 was calculated (from $(T - T_c)$ = 0.0 to 20°C and f from 4.5 to 49.7 MHz). Unfortunately, it is difficult to use this approach to compare the theoretical composition dependencies with our experimental ones since, as was indicated in Section 7.1.1, the magnitude of the theoretical α/f^2 values as calculated with this method is 6.5 times larger than the experimental one at f = 16.6 MHz. Hence, even though the approach used by D'Arrigo and Sette is incorrect, we have used it here since it allows us to simply compare the functional form of the composition dependence of α/f^2 predicted by the Fixman and Flory-Huggins theories to our experimental one.

Fig. 41 gives a plot of the theoretical α/f^2 values versus composition (obtained using the method of D'Arrigo and Sette) superimposed on the experimental α/f^2 composition dependence. The graph shown is for f = 25.5 MHz and T = 265.8^{o}C, but similar results hold at all other temperatures and frequencies at which measurements were made.

7.2 Discussion of Theory

7.2.1 Fixman's and Kawasaki's Critical Sound Absorption Theories

We give first of all a detailed verbal account of the main features of the Fixman sound absorption theory. We do this because we feel that this has not been done properly before in the literature and because it will help us understand Fixman's derivation and the major results of his theory in relation to experiment.

Consider first an adiabatic sound wave fed into the fluid. The sound wave causes pressure and density changes in the fluid and consequently temperature changes. Under non-critical conditions this has a negligible effect on the normal homogeneous composition distribution in the mixture. Near a critical point, however, the concentration distribution is subject to fluctuations (clusters) and is a very sensitive and strong function of the temperature through κ, the inverse long-range correlation length. A change in the temperature will cause the system to relax to new equilibrium concentration distributions corresponding to this temperature (new distribution of clusters). This is a diffusional process, hence it is dissipative, causing losses. The speed at which this diffusion process occurs is determined

by the diffusion coefficient, which varies strongly with $|T-T_c|$ ($D \sim |T-T_c|^{\nu} \sim \kappa$ where $\nu \approx 2/3$ and $\kappa \sim |T-T_c|^{\nu}$). Hence, as $|T-T_c|$ becomes smaller and smaller, the relaxation times become slower and slower. It is well known from relaxation theory that if a periodic process occurs much faster than the time rate of relaxation to the new equilibrium state, then the non-equilibrium state appears "frozen in" with respect to the speed of the periodic process and the losses are small[18]. Conversely, if the periodic process occurs so slowly that the system relaxes relatively quickly to the new equilibrium condition, the losses will be small also, since the system is never far from an equilibrium state[23]. This qualitative picture can now be used to explain the frequency and temperature dependence of the sound absorption near the critical point of a binary fluid mixture.

For each $|T-T_c|$ there is a definite correlation length for concentration ordering. This correlation length (κ^{-1}) defines some average length for possible concentration fluctuations (cluster sizes) although smaller ones and larger ones are also possible. For each $|T-T_c|$ there is also a range of relaxation times connected with the correlation length and those hydrodynamic modes which couple to the sound wave damping coefficient in a binary mixture. The higher the temperature above the critical temperature, the lower would be this range of relaxation times and the smaller the correlation length for fluctuations. Hence, if one thinks of the relaxation process as corresponding roughly to one frequency, then a plot of α_λ versus f ($\alpha_\lambda = \alpha\lambda$) for increasing temperature will show the α_λ versus f peak drifting to higher and higher frequencies while the actual magnitude of absorption will decrease since the possible fluctuations are becoming smaller. Conversely, the closer the system gets to the

critical temperature the more the α_λ versus f peak will go towards lower f, while increasing in magnitude, until in the limiting case of $|T-T_c| = 0^oC$ ($\kappa = 0$) the peak will be at f = 0 MHz where its height will go to ∞. It should be noted that a process with a single relaxation frequency has a maximum absorption at that relaxation frequency when the quantity α_λ is plotted against f.

Of course the process being considered can only approximately be regarded as corresponding to a single relaxation frequency, since the correlation length at any $|T-T_c|$ corresponds to some average probable fluctuation size. Hence a broad maximum of the plot of α_λ versus f is to be expected.

Anantaraman et al[53] show experimental results which give the impression of following the above behaviour. Our own results for α_λ (which we have not shown since we have always plotted α/f^2) appear inconclusive, the peak of α_λ versus f being apparently at higher f values than the frequencies investigated for even the lowest $|T-T_c|$ value at which measurements were made.

A close examination of Fixman's derivation of the excess sound absorption expression reveals a point which has escaped notice. This matter lies in the fact that Fixman apparently expects the forced pressure oscillations caused by the sound wave to produce an oscillating temperature which will be the same no matter how close the system is to the critical point. The sound losses caused by the particle diffusion will thus be dependent only on the value of κ which indexes the range of correlations. That is, the number of particles that need to readjust themselves due to an oscillating value of κ caused by the oscillating

temperature is dependent only on how far the system is away from T_c. If however we consider the equation[18]

$$\left(\frac{\partial T}{\partial p}\right)_S = TV\frac{\beta}{C_p} \tag{7-14}$$

(where β is the coefficient of thermal expansion) which gives the rise in temperature due to an adiabatic change in pressure we can see that it is likely that the magnitude of the temperature oscillations may be considerably smaller closer to T_c than away from it due to the anomalous increase in C_p in equation (7-14). This means that κ will go through smaller and smaller oscillations the closer the system gets to T_c, the process having an effect on the sound attenuation which is opposite to that caused by the decrease of κ with $|T-T_c|$. We believe, however, that due to the relatively mild divergence of C_p the decrease of κ with $T \to T_c$ remains the primary cause of the anomalous losses, while the change in magnitude of the oscillating temperature with $T \to T_c$ is of secondary importance when the system is far enough away from T_c (1^oC or more). However, we have not found any way of tying equation (7-14) into Fixman's expression to validate this proposition.

The validity of the above ideas is supported by a closer look at Kawasaki's derivation of $\alpha_e(\omega)$. In his equation for $\alpha_e(\omega)$ (equation 2-97)) the expression $(\partial p/\partial T)_{V,C}$ appears as a multiplier. Such an expression is missing from Fixman's equation. Kawasaki is able to show a correspondence between his $\alpha_e(\omega)$ and Fixman's because he replaces $(\partial p/\partial T)_{V,C}$ in his equation using the relation

$$\gamma_T - 1 = \frac{K_T T}{C_V}\left(\frac{\partial p}{\partial T}\right)^2_{V,C} \tag{7-15}$$

However, a difference remains, since as was pointed out in Chapter 2, the heat capacities in Kawasaki's equation are free to vary as the system approaches the critical point while Fixman's heat capacities are supposed to maintain their constant non-critical values as $T \to T_c$. It appears therefore that Kawasaki's derivation automatically incorporates the possibility of a variable $(\partial T/\partial p)$ in the equation for the anomalous absorption of sound. Undoubtedly Kawasaki's results are the formally more correct ones for the calculation of frequency dependent transport coefficients.

There is one further controversial point about Fixman's derivation which has apparently been missed by Fixman and other workers. This lies in the fact that the oscillating pressure can cause not only the temperature of the mixture to rise and fall, but can also give a corresponding rise and fall in the critical temperature. This can be shown both analytically and experimentally. Usually a rise in pressure will lead to a rise in T_c, although the opposite is possible as well. Using equation (7-14) to calculate $(\partial T/\partial p)_S$ and some experimental results on $\partial T_c/\partial p$[71] it appears that $\partial T_c/\partial p$ can in some cases be larger than $(\partial T/\partial p)_S$. In such cases the change in κ will be determined, not by the oscillating fluid temperature, but by the oscillations of the critical temperature of the mixture. Since it is unlikely that $\partial T_c/\partial p$ will be equal to $(\partial T/\partial p)_S$ (so that a $|T-T_c|$ difference remains) and while it is expected that $\partial T_c/\partial p$ will stay roughly constant with changing T over the usual measurement span near T_c, it appears that the above results will not change the final outcome of Fixman's theory.

7.2.2 Swift's Critical Sound Absorption Theory

A third expression for the anomalous attenuation of sound, following Swift[42], was also presented in Chapter 2. This expression gives rather different results for the anomalous attenuation than the theory of Fixman and Kawasaki. An explanation for this difference might lie in different ranges of temperatures near T_c for which these theories are valid. However, the numerical analyses in Sections 7.1.1 and 7.1.2 show that the Fixman equation can be fitted to the data over the temperature range from $(T - T_c) = 0.3$ to $(T - T_c) = 9.9^{o}C$. This represents a range of $|\varepsilon| = |T-T_c|/T_c$ lying between approximately 6×10^{-4} to 2×10^{-2}. This is certainly a range in which the equilibrium scaling laws are expected to be valid. Alternatively, it is quite possible that some of the hypotheses entering into the development of the dynamical scaling laws are invalid. They have by no means been experimentally verified in all cases. In fact, Kawasaki[72] has cast doubt on their validity in a paper wherein he examines specifically the sound attenuation results of Kadanoff and Swift[40] on the liquid-gas system and the results of Swift[42] on the liquid-liquid system. He found that the dynamical scaling laws are valid for the sound attenuation calculations on the liquid-gas transition, but not when applied to the liquid-liquid critical transition. This procedure is reasonable for the equilibrium properties of systems but is questionable when applied to their dynamical properties. Swift's result for $(\zeta + 4/3\ \eta)(\bar{q},s)$ (equation (2-106)) shows another dubious property, for when the proper divergences of the various parameters are substituted into the equation we obtain

$$(\zeta + 4/3\ \eta) \sim - \gamma k_B c_o^2 T^2 \left(\frac{1}{C_v} - \frac{1}{C_p} \right) \frac{1}{|T-T_c|^2} \qquad (7\text{-}16)$$

which means that the divergence of $(\zeta + 4/3\ \eta)$ is independent of the exponent γ. This is in contradiction to the results of other calculations on $(\zeta + 4/3\ \eta)$ for binary critical mixtures[30,34].

CHAPTER 8

SUMMARY AND CONCLUSIONS

1. An apparatus was constructed which was capable of performing attenuation and velocity of sound measurements of good precision in a liquid metal mixture in the frequency range f = 4.5 to 49.7 MHz. The maximum temperature achievable in these measurements was near T = 290°C.
2. Measurements of the attenuation of sound in a Ga-Bi mixture in the one-phase region near the critical point as a function of frequency, temperature and composition were performed. The results of these measurements agreed substantially with those on organic mixtures near critical points.
3. The results of attenuation measurements made on the Ga-Bi system as a function of temperature and frequency at the critical composition were compared with the predictions of the Fixman-Kawasaki theories and substantial agreement was obtained within the limitations of the theories and the accuracy of the thermodynamic data. The theoretical predictions of a theory based upon the dynamical scaling laws or upon a model assuming only a single relaxation time were found to be in disagreement with our results.
4. A fit of the Fixman theory to our data at the critical composition established the value of ℓ, the Debye short-range correlation length. The value obtained for the Ga-Bi system was ℓ = 4.5 Å. This value is slightly smaller than ℓ values established by sound attenuation or light scattering measurements on organic mixtures near critical points

and is in agreement with qualitative theoretical expectations. Since the value of ℓ is largely governed by the size of the molecules, and the molecular sizes of Ga and Bi are smaller than most organic molecules we expect their value of ℓ to be smaller than that for a mixture containing organic molecules, and this is in fact the case.

5. It was established that losses due to a scattering mechanism are not operative in a Ga-Bi mixture and that within the limitations imposed by theory and experiment all losses can be accounted for by a relaxation mechanism such as the one proposed by Fixman and Kawasaki.
6. A comparison was made between the composition dependence of our attenuation results (at constant temperature and frequency) over a wide composition range on either side of the critical composition and the predictions of the Fixman theory when it is combined with the Flory-Huggins solution model. It was found that the experimental attenuation values showed a slower decrease with composition on either side of the critical composition than was obtained with the Fixman-Flory-Huggins theory. This result agrees with the expectation that the use of a classical theoretical solution model in conjunction with the Fixman theory will give a much sharper change in attenuation with respect to composition than is actually found. The results for Ga-Bi are in agreement with an identical analysis made on the results of attenuation studies of an organic mixture near a critical point.
7. The velocity of sound was measured at f = 25.5 MHz and at the same temperature and composition at which attenuation measurements were performed. It was found that no critical effects were evident in the velocity of sound, its value remaining constant within the accuracy

of our measurements over a 10°C temperature interval above T_c.

8. From the peak of the attenuation versus composition results and from phase separation measurements using the results for the velocity of sound, more reliable values for the critical composition and temperature were obtained than had previously been reported in the literature. These values are

$$C_{Bi}^{c} = 0.60 \pm 0.01 \text{ weight-fraction}$$

and $$T_c = 263.1 \pm 0.2^{\circ}C.$$

APPENDIX A

THERMOCOUPLE CALIBRATION DATA AND LEAST SQUARES FIT

The method of least squares was used to fit a straight line to the thermocouple calibration data reproduced below (by courtesy of the National Research Council of Canada). For this straight line fit the origin at $0^{o}C$ was ignored and the line fitted only for the points from $150^{o}C$ to $320^{o}C$ inclusive. A straight line of the form

$$Y = mX + b$$

was assumed where $Y \equiv T$ (temperature in ^{o}C) and $X \equiv$ emf (millivolts) and m and b are constants to be determined by means of the least squares fit. Given the above equation one can define a correlation coefficient τ which is a measure of the goodness of fit of the points to the least squares straight line. That is

$$-1 \leq \tau \leq 1$$

where the sign corresponds to the sign of the slope m. When $\tau = \pm 1$ it means there is a perfect fit between the least squares straight line and all points. The equation for the correlation coefficient is (assuming the above form for the straight line)

$$\tau = \frac{\sum_{i=1}^{n} (X_i - \bar{X})(Y_i - \bar{Y})}{\left(\sum_{i=1}^{n} (X_i - \bar{X})^2 (Y_i - \bar{Y})^2 \right)^{\frac{1}{2}}}$$

where

$$\bar{X} = \frac{\sum_{i=1}^{n} X_i}{n}$$

$$\bar{Y} = \frac{\sum_{i=1}^{n} Y_i}{n}$$

The least squares straight line equations for the three thermocouples were (only X1 and X2 were used in the experiment):

1) Thermocouple X1:

$$T = 18.0595 \text{ emf} + 4.71479$$

2) Thermocouple X2:

$$T = 18.0539 \text{ emf} + 4.80732$$

3) Thermocouple X3:

$$T = 18.0511 \text{ emf} + 4.88064$$

Below are presented the calibration points for the three thermocouples:

Temperature (IPTS - 68, in ^{o}C)	emf (millivolts)		
	X1	X2	X3
0	0.000	0.000	0.000
150	8.040	8.040	8.036
200	10.818	10.812	10.812
250	13.586	13.586	13.583
300	16.350	16.350	16.348
320	17.455	17.456	17.455

REFERENCES

1. M.S. Green and J.V. Sengers, eds., Proceedings of a Conference on the Phenomena Near the Critical Point, Washington, D.C., 1965, National Bureau of Standards, Misc. Publ. 273 (1966).
2. L.P. Kadanoff et al, Rev. Mod. Phys., 39, 395 (1966).
3. L.S. Ornstein and F. Zernicke, Proc. Acad. Sci. Amsterdam, 17, 793 (1914).
4. L.S. Ornstein and F. Zernicke, Physik. Z., 19, 134 (1918).
5. M.E. Fisher, Reports on Progress in Physics, 30, Part 2, 615 (1967).
6. P. Heller, Reports on Progress in Physics, 30, Part 2, 731 (1967).
7. M.E. Fisher, J. Math. Phys., 5, 944 (1964).
8. P. Debye, J. Chem. Phys., 31, 680 (1959).
9. A. Münster and C. Schneeweiss, Z. Physik Chem. (Frankfurt, N.F.), 37, 353 (1963).
10. F. J. Pearson, Proc. Phys. Soc., 75, 633 (1960).
11. B. Widom, J. Chem. Phys., 43, 3892 (1965).
12. B. Widom, J. Chem. Phys., 43, 3898 (1965).
13. L.P. Kadanoff, Physics, 2, 263 (1966).
14. V.L. Ginzburg, Sov. Phys. - Solid State, 2, 1824 (1960).
15. A.P. Levanyuk, Sov. Phys. - JETP, 9, 571 (1959).
16. R. Brout, Phase Transitions, W. A. Benjamin, Inc., N.Y. (1965).
17. J.V. Sengers and D. Sette, Proceedings of a Conference on the Phenomena Near the Critical Point, Washington, D.C., 1965, pp. 165 and 183, National Bureau of Standards Misc. Publ. 273 (1966).

18. K.F. Herzfeld and T.A. Litovitz, Absorption and Dispersion of Ultra-Sonic Waves, Academic Press, N.Y. and London (1959).

19. G. Abowitz and R.B. Gordon, Acta Met., 10, 671 (1962).

20. L. Tisza, Phys. Rev., 61, 531 (1942).

21. R. Zwanzig, J. Chem. Phys., 43, 714 (1965).

22. R. Zwanzig, Ann. Rev. Phys. Chem., 16, 67 (1965).

23. L.D. Landau and E.M. Lifshitz, Fluid Mechanics, Addison-Wesley Publishing Co. Inc., Reading, Mass. (1959).

24. M. Fixman, J. Chem. Phys., 36, 1961 (1962).

25. M. Fixman, J. Chem. Phys., 33, 1363 (1960).

26. J.G. Kirkwood and F.P. Buff, J. Chem. Phys., 19, 774 (1951).

27. M. Fixman, J. Chem. Phys., 36, 310 (1962).

28. J.H. Hildebrand and R.L. Scott, Solubility of Nonelectrolytes, Reinhold Publishing Corp., N.Y. (1950).

29. K. Kawasaki, Progr. Theor. Phys. (Japan), 41, 1190 (1969).

30. J.M. Deutch and R. Zwanzig, J. Chem. Phys., 46, 1612 (1967).

31. T.M. Reed and T.E. Taylor, J. Phys. Chem., 63, 58 (1959).

32. T.R. Barber and J.V. Champion, Phys. Letters, 29A, 622 (1969).

33. M. Fixman, Adv. Chem. Phys., 6, 175 (1964).

34. K. Kawasaki, Proc. Phys. Soc., 90, 791 (1967).

35. K. Kawasaki, Phys. Rev., 150, 291 (1966).

36. H. Mori, Progr. Theor. Phys. (Japan) 33, 423 (1965).

37. P. Schofield, Proc. Phys. Soc., 88, 149 (1966).

38. L.D. Landau and E.M. Lifshitz, Statistical Physics, Addison-Wesley Publishing Co. Inc., Reading, Mass. (1958).

39. M. Fixman, J. Chem. Phys., 36, 1957 (1962).

40. L.P. Kadanoff and J. Swift, Phys. Rev., 166, 89 (1968).

41. B.I. Halperin and P.C. Hohenberg, Phys. Rev., 177, 952 (1969).

42. J. Swift, Phys. Rev., 173, 257 (1968).

43. M.E. Fisher, Proceedings of a Conference on the Phenomena Near the Critical Point, Washington, D.C., 1965, p. 21, National Bureau of Standards, Misc. Publ. 273 (1966).

44. W.P. Mason, Physical Acoustics and the Properties of Solids, D. Van Nostrand Co. Inc., Princeton, N.J. (1958).

45. M. Redwood, Proc. Phys. Soc., 72, 841 (1958).

46. W.P. Mason and H.J. McSkimin, J. Ac. Soc. Am. 19, 464 (1947).

47. J.H. Andreae et al, Acoustica 8, 131 (1958).

48. H.J. McSkimin, J. Ac. Soc. Am., 27, 302 (1955).

49. J.F. Nozdrev, Application of Ultrasonics in Molecular Physics, Gordon and Breach, N.Y. (1963).

50. Liquids-Metals Handbook, U.S. Atomic Energy Commission, U.S. Government Printing Office, Wash., D.C. (1950).

51. H.J. McSkimin, J. Ac. Soc. Am., 31, 287 (1959).

52. J.M.M. Pinkerton, Proc. Phys. Soc., 62, 286 (1948).

53. A.V. Anantaraman et al, J. Chem. Phys., 44, 2651 (1966).

54. M.B. Gitis and I.G. Mikhailov, Sov. Phys.-Acoustica, 12, 131 (1966).

55. J.L. Hunter and K.S. Hovan, J. Chem. Phys., 41, 4013 (1964).

56. B. Predel, Z. Physik. Chem. (Frankfurt, N.F.), 24, 206 (1960).

57. J. Jarzynski, Proc. Phys. Soc., 81, 745 (1963).

58. K.G. Plass, Acoustica, 13, 240 (1963).

59. B. Chu and F.J. Schoenes, Phys. Rev. Letters, 21, 6 (1968).

60. R.K. Adams and E.G. Davisson, Oak Ridge National Laboratory -- 3649, 2, (1965).

61. H.D. Young, Statistical Treatment of Experimental Data, McGraw-Hill Book Co., Inc., Toronto (1962).

62. R.P. Singh and G.S. Verma, Proc. Phys. Soc., 1, 1476 (1968).

63. H. Brumberger, Proceedings of a Conference on the Phenomena Near the Critical Point, Wash., D.C., 1965, p. 116, National Bureau of Standards, Misc. Publ. 273,(1966).

64. M.E. Fisher, Proceedings of a Conference on the Phenomena Near the Critical Point, Wash., D.C., 1965, p. 108, National Bureau of Standards, Misc. Publ. 273 (1966).

65. G. D'Arrigo and D. Sette, J. Chem. Phys., 48, 691 (1968).

66. L. Liebermann, J. Ac. Soc. Am., 23, 563 (1951).

67. A.E. Brown and E.G. Richardson, Phys. Magazine, 4, 705 (1959).

68. A.S. Sliwinski and A.E. Brown, Acoustica, 14, 280 (1964).

69. R.P. Singh, G.S. Darbari and G.S. Verma, Phys. Rev. Letters, 16, 1150 (1966).

70. P.A. Egelstaff and G.D. Wignall, to be published.

71. J.S. Rowlinson, Liquids and Liquid Mixtures, Butterworths Scientific Publ., London (1959).

72. K. Kawasaki, Progr. Theor. Phys., 40, 930 (1968).

73. M.I. Shakhparonov et al, Sov. Phys. - JETP Letters, 7, 315 (1968).

74. G.D. Wignall and P.A. Egelstaff, Proc. Phys. Soc., 1C, 1088 (1968).

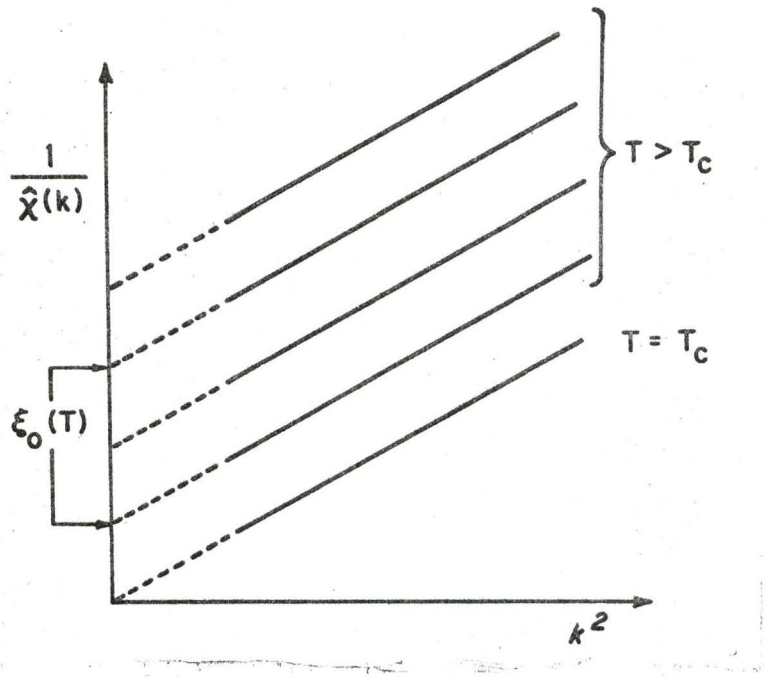

Fig. 1: Plot of inverse scattering intensity versus k^2 near the critical point to be expected on the basis of O-Z and equivalent theories. Ref. 64.

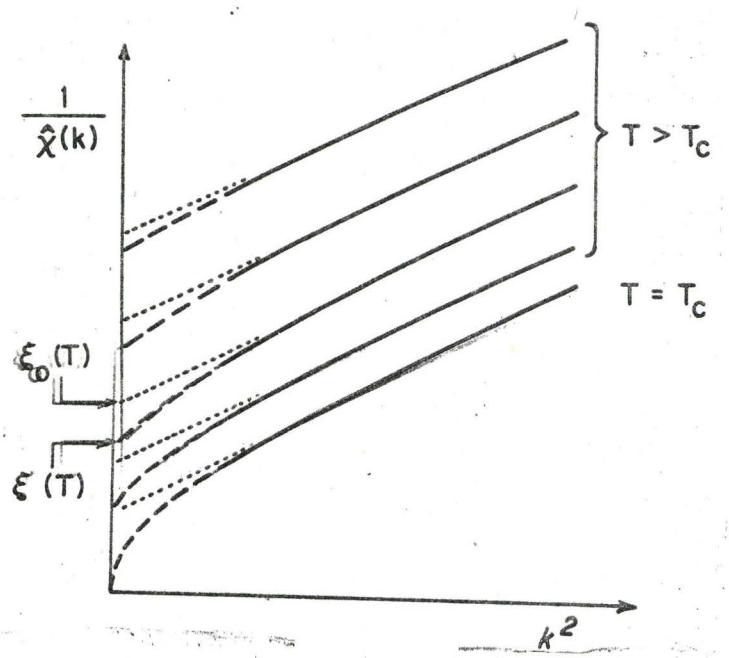

Fig. 2: Plot of inverse scattering to be expected with a positive η and $\gamma > 1$. Ref. 64.

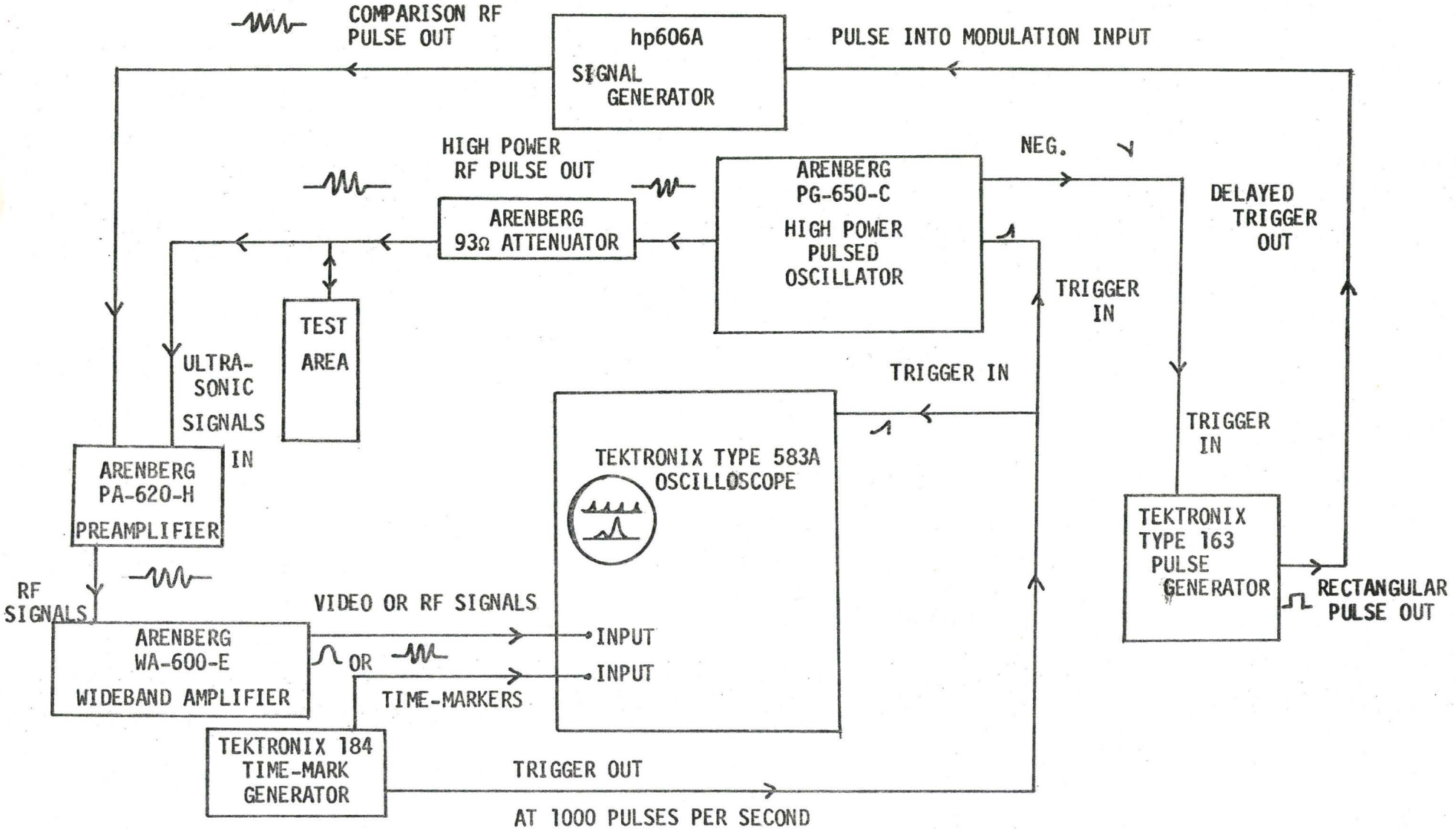

Fig. 3: Schematic of electronics.

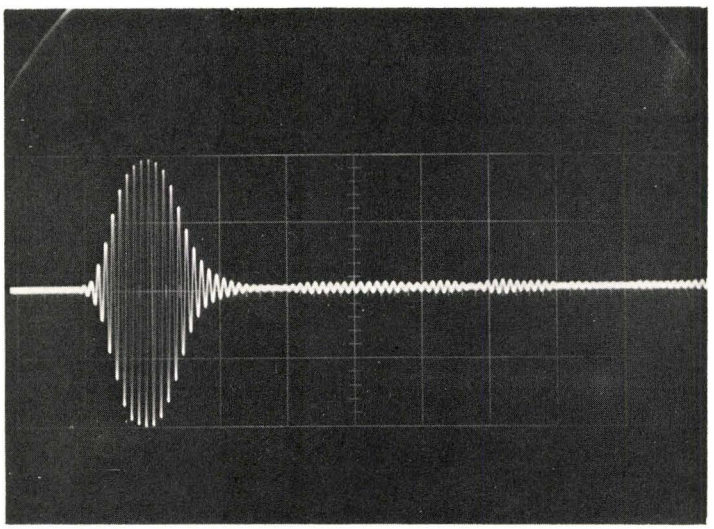

Fig. 5: Ultrasonic pulse at f = 4.5 MHz. Shown at the minimum pulse length at which the pulse still builds up to its maximum amplitude. Horizontal scale = 2 μs/cm.

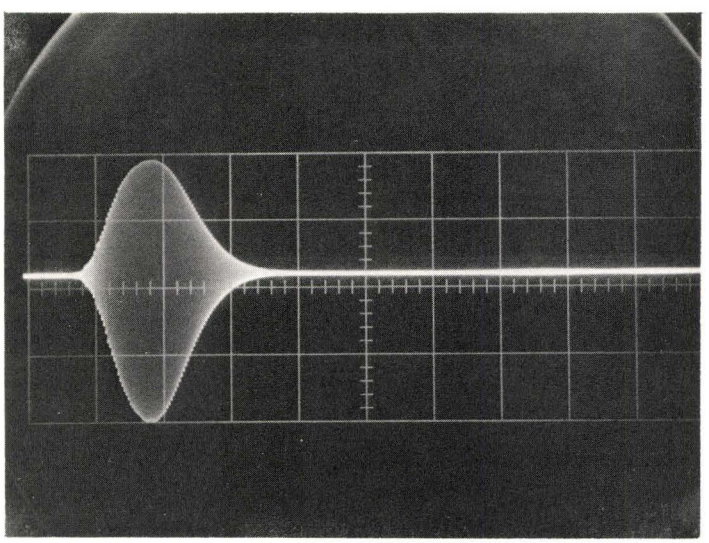

Fig. 6: Ultrasonic pulse at f = 16.6 MHz. Shown at the minimum pulse length at which the pulse still builds up to its maximum amplitude. Horizontal scale = 2 μs/cm.

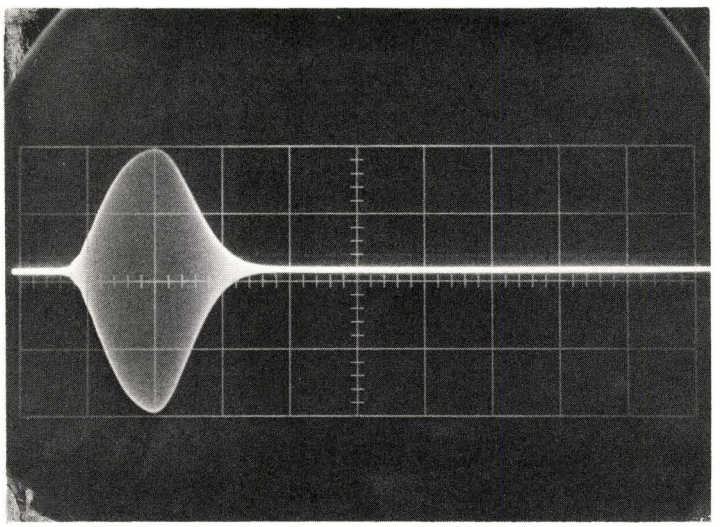

Fig. 7: Ultrasonic pulse at f = 49.7 MHz. Shown at the minimum pulse length at which the pulse still builds up to its maximum amplitude. Horizontal scale = 2 μs/cm.

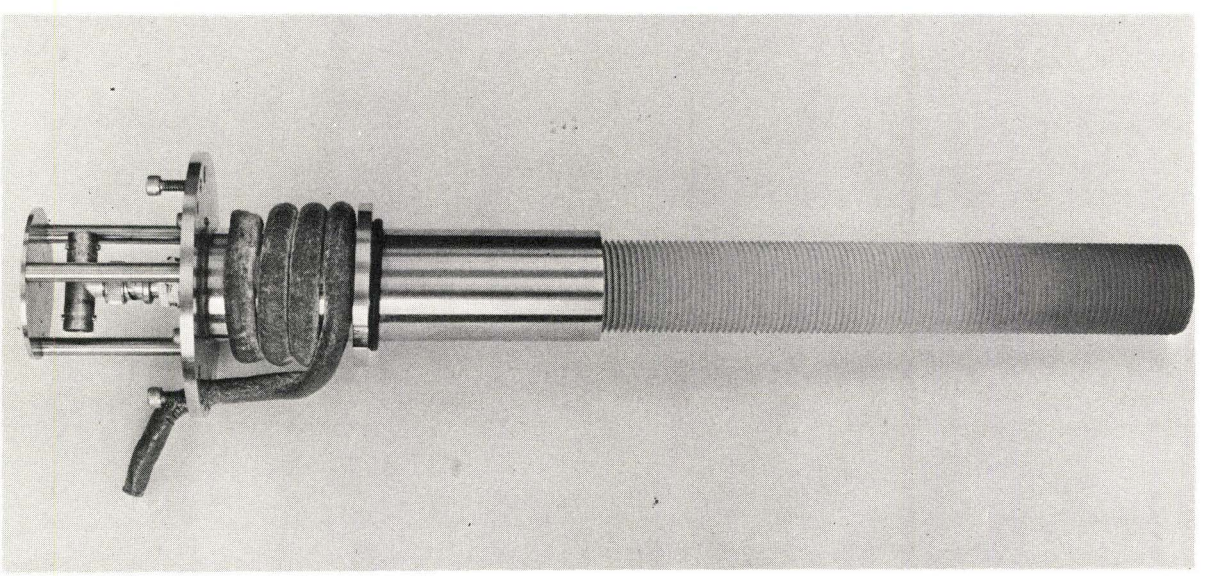

Fig. 8: Fused silica rod screwed into rod holder showing the NF 12 thread along its length.

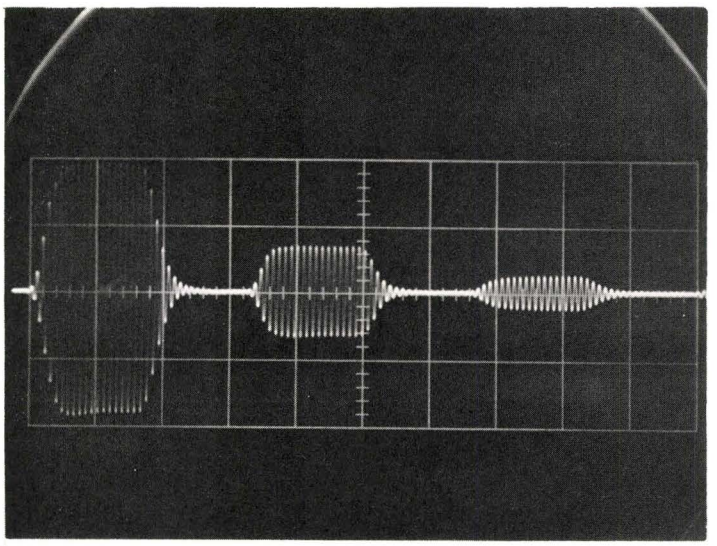

Fig. 9: Ultrasonic pulse at f = 4.5 MHz from a non-threaded fused silica delay line showing the trailing pulses. Horizontal scale = 2 μs/cm.

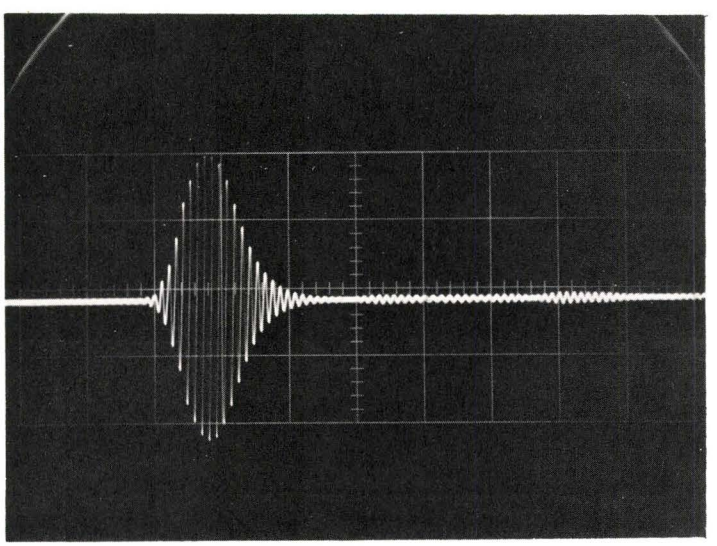

Fig. 10: Ultrasonic pulse at f = 4.5 MHz from a threaded fused silica delay line of the same diameter as above showing the reduction in trailing pulses. Horizontal scale = 2 μs/cm.

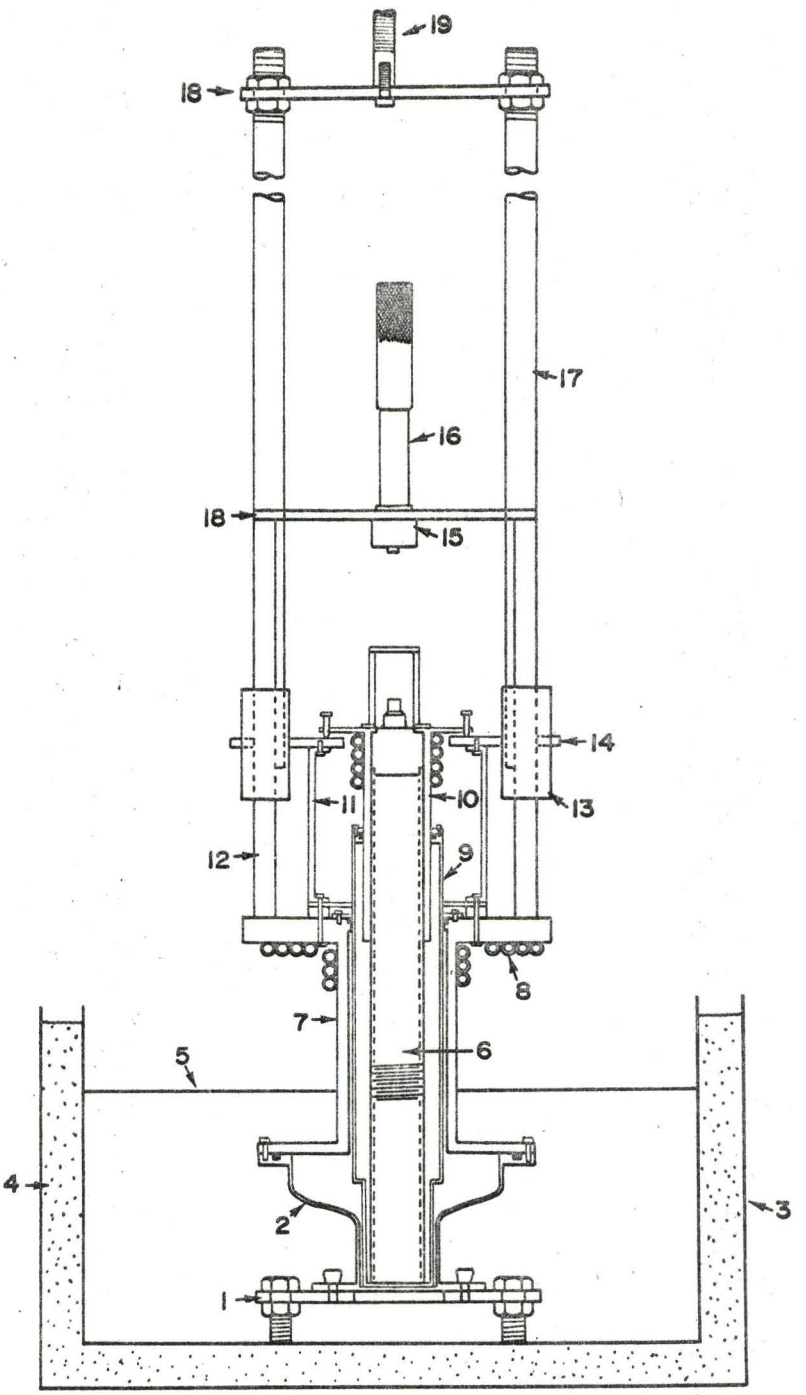

Fig. 11: High temperature apparatus.

Figure 11

Legend

1. Lower support platform.
2. Sample beaker.
3. Oil bath container
4. Insulation.
5. Oil level.
6. Fused silica rod (threaded).
7. Support platform.
8. Lead cooling coils.
9. Reflector holder.
10. Rod and electrode holder.
11. Support bracket.
12. Guide rod.
13. Guide bearings.
14. Guide platform.
15. Micrometer holder.
16. Vernier micrometer.
17. Support rods -- these are fastened at platform (14) in the same way as at platform (18).
18. Platform.
19. Threaded rod -- connected to gears (not shown).

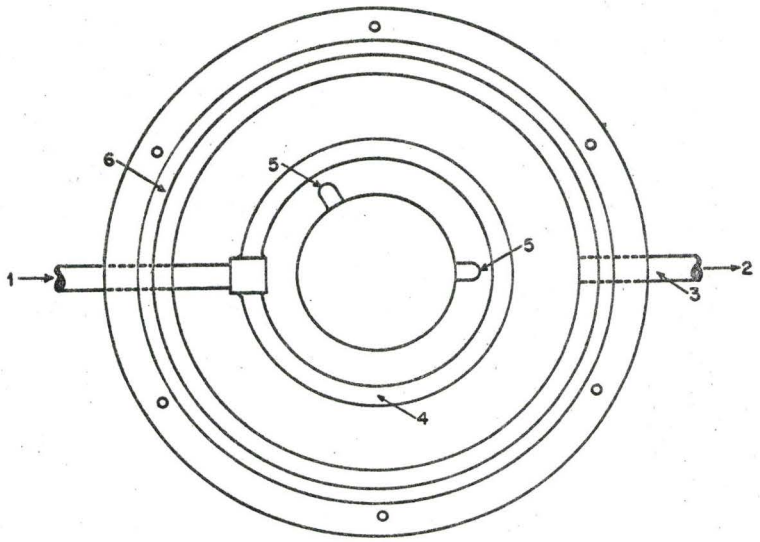

1. Argon in.
2. Argon out.
3. Copper outlet tube.
4. Copper ring with blow holes.
5. Thermocouple cut-out.
6. Viton 'O'-ring.

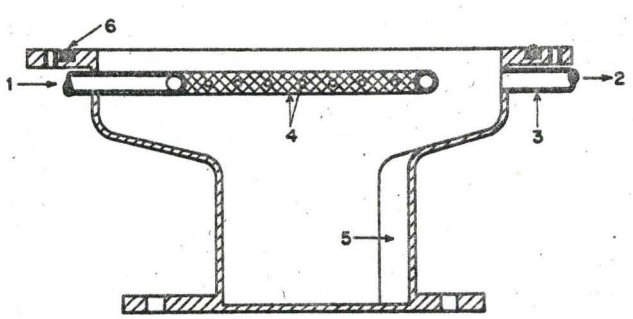

Fig. 12: Cross-sectional views of top and side of stainless steel sample beaker.

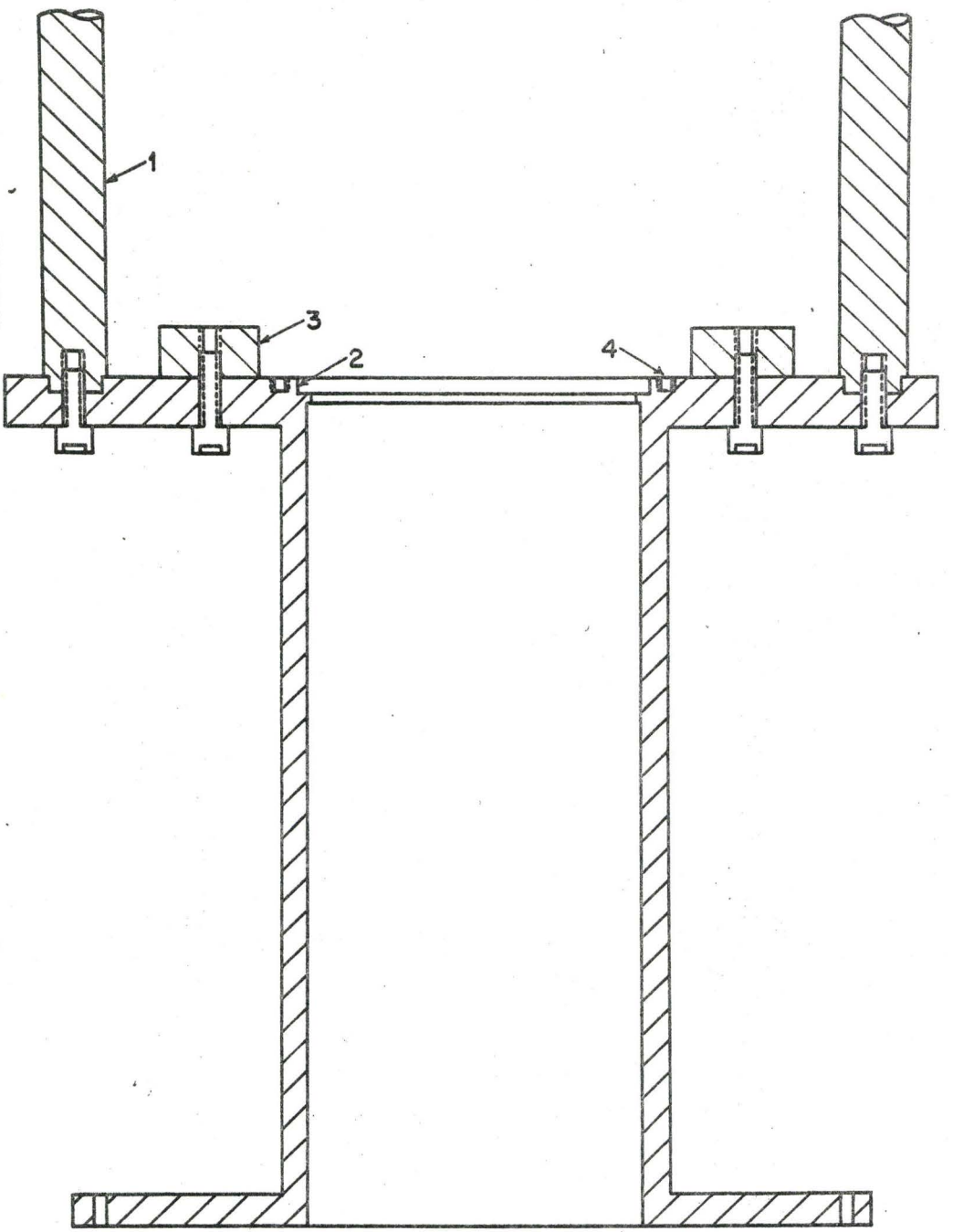

Fig. 13: Cross-section of support platform.

Figure 13

Legend

1. Guide rods.
2. 'O'-ring groove.
3. Reflector holder support pods.
4. Screw holes for 'O'-ring lid.

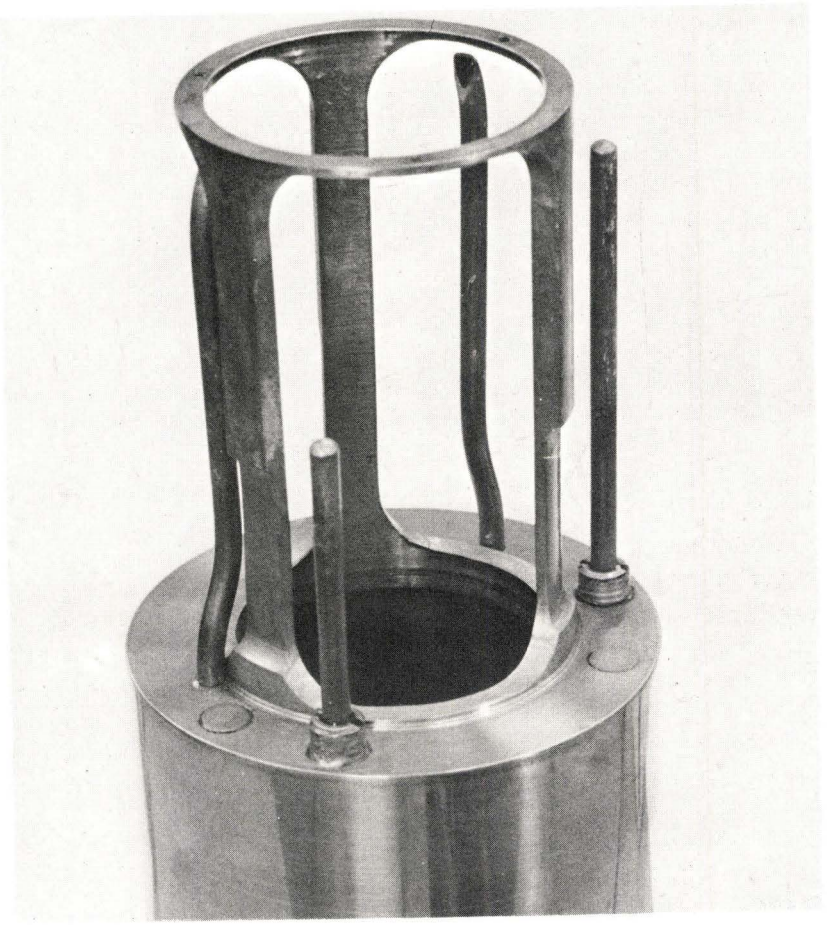

Fig. 14: Bottom end of reflector can. Reflector is not mounted.

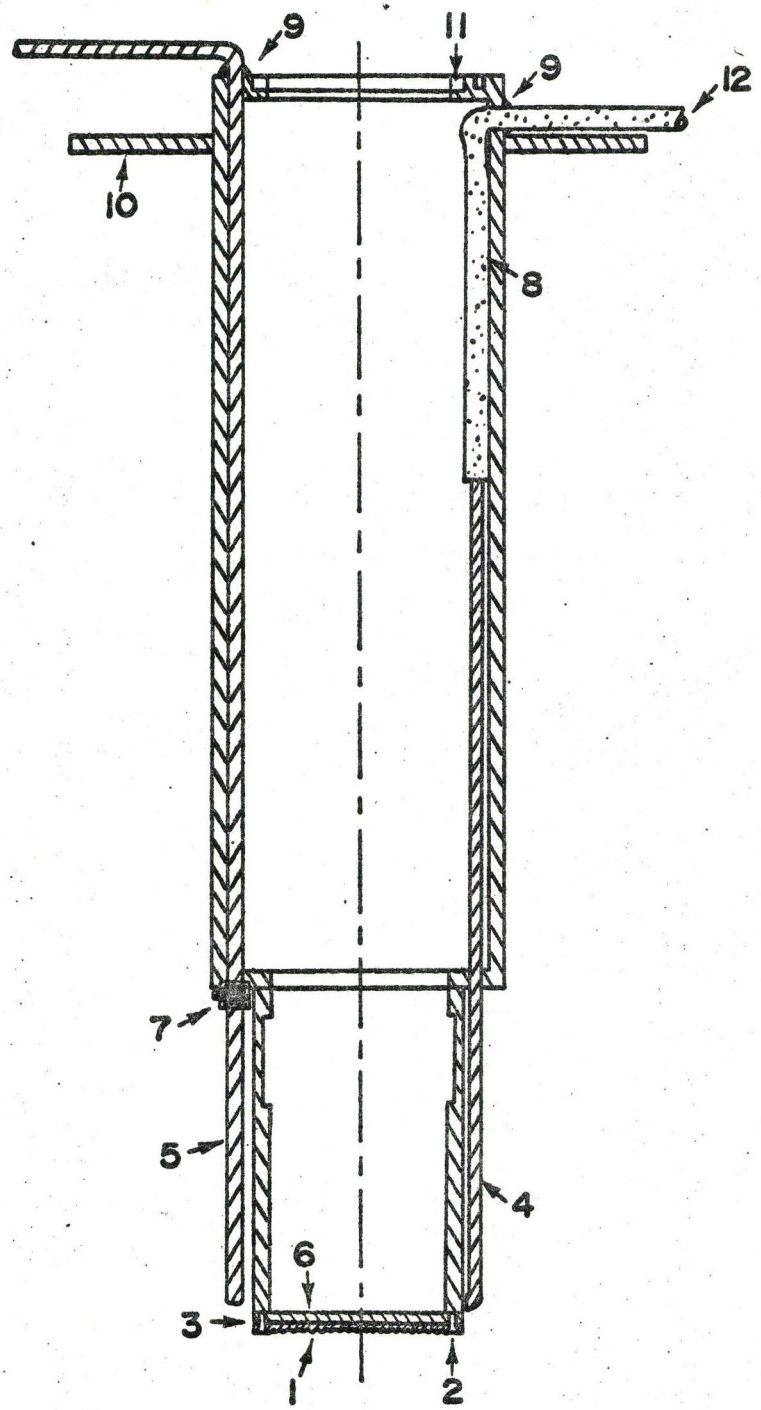

Fig. 15: Cross-section of reflector holder. Only one thermocouple and one bubble tube is shown.

Figure 15

Legend

1. Reflector.
2. Flat-headed screws.
3. Spacer.
4. Bubbler tube.
5. Thermocouple.
6. Reflector support ring.
7. Thermocouple fastener.
8. Rubber bubbler line.
9. Sealant.
10. Flared-out section (support ring).
11. 'O'-ring groove.
12. Argon inlet.

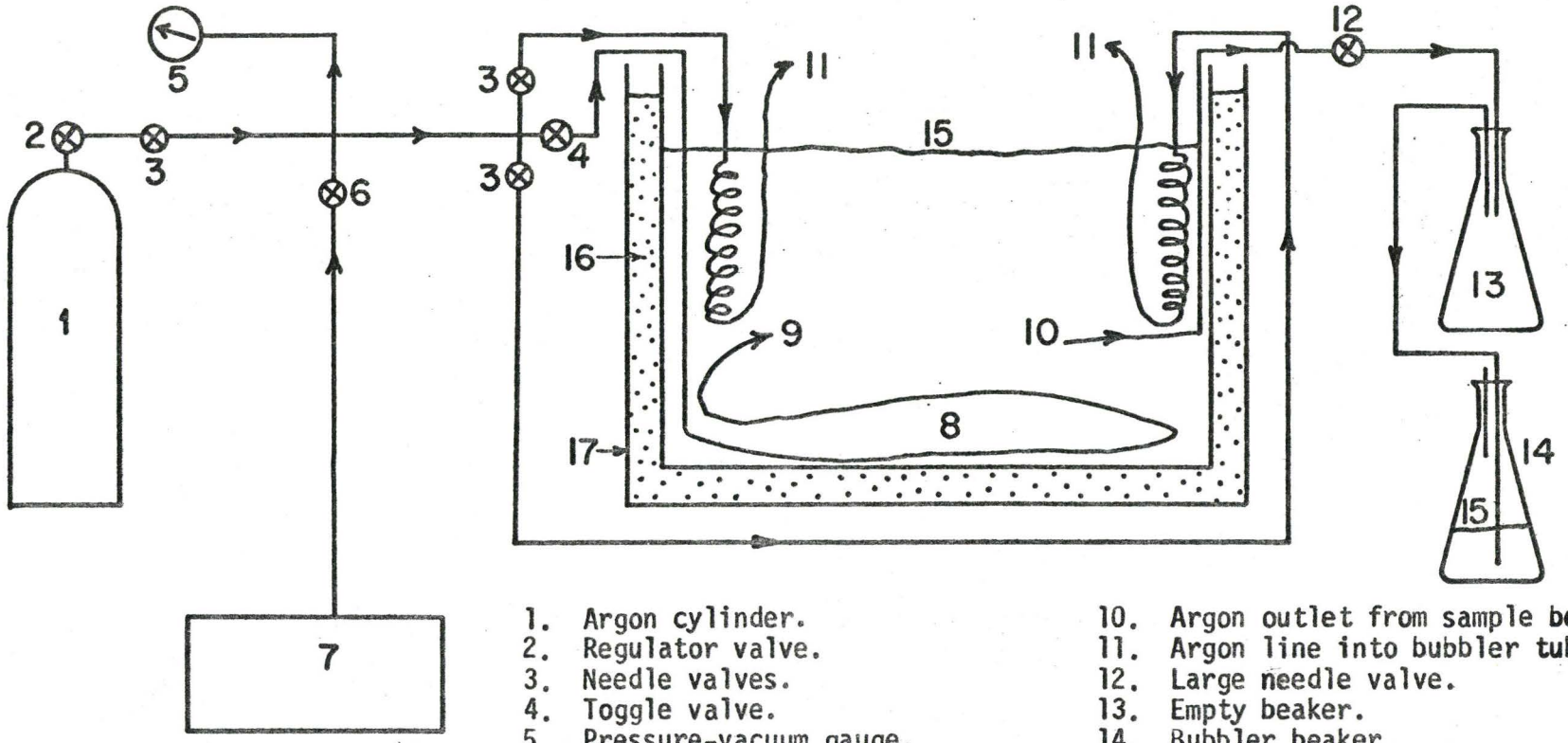

1. Argon cylinder.
2. Regulator valve.
3. Needle valves.
4. Toggle valve.
5. Pressure-vacuum gauge.
6. Valve.
7. Mechanical vacuum pump.
8. Many coils of copper tubing.
9. Argon inlet into sample beaker.
10. Argon outlet from sample beaker.
11. Argon line into bubbler tubes.
12. Large needle valve.
13. Empty beaker.
14. Bubbler beaker.
15. Oil level.
16. Heat insulation.
17. Oil bath container.

Fig. 16: Schematic of Argon supply lines and out-flushing system.

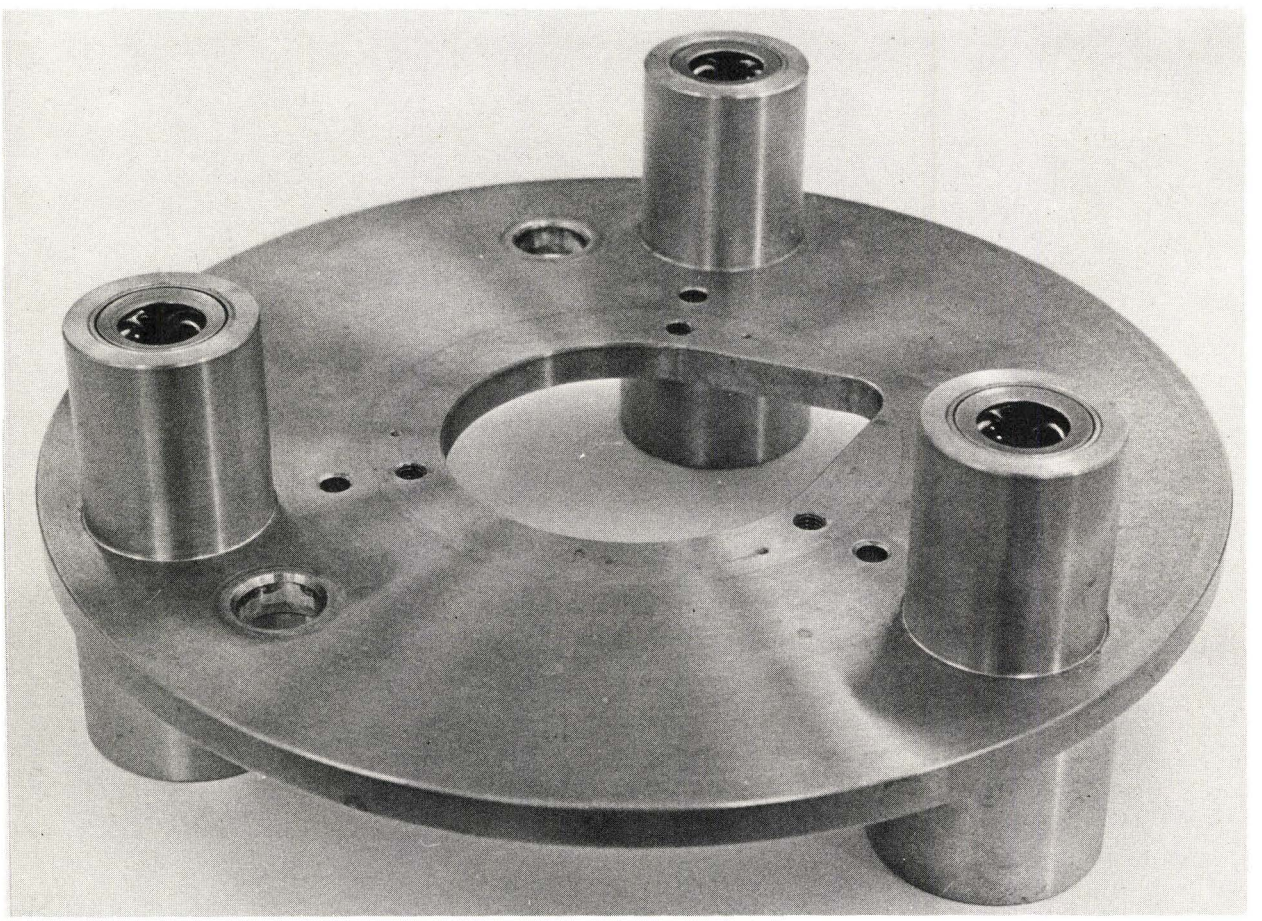

Fig. 17: Guide platform.

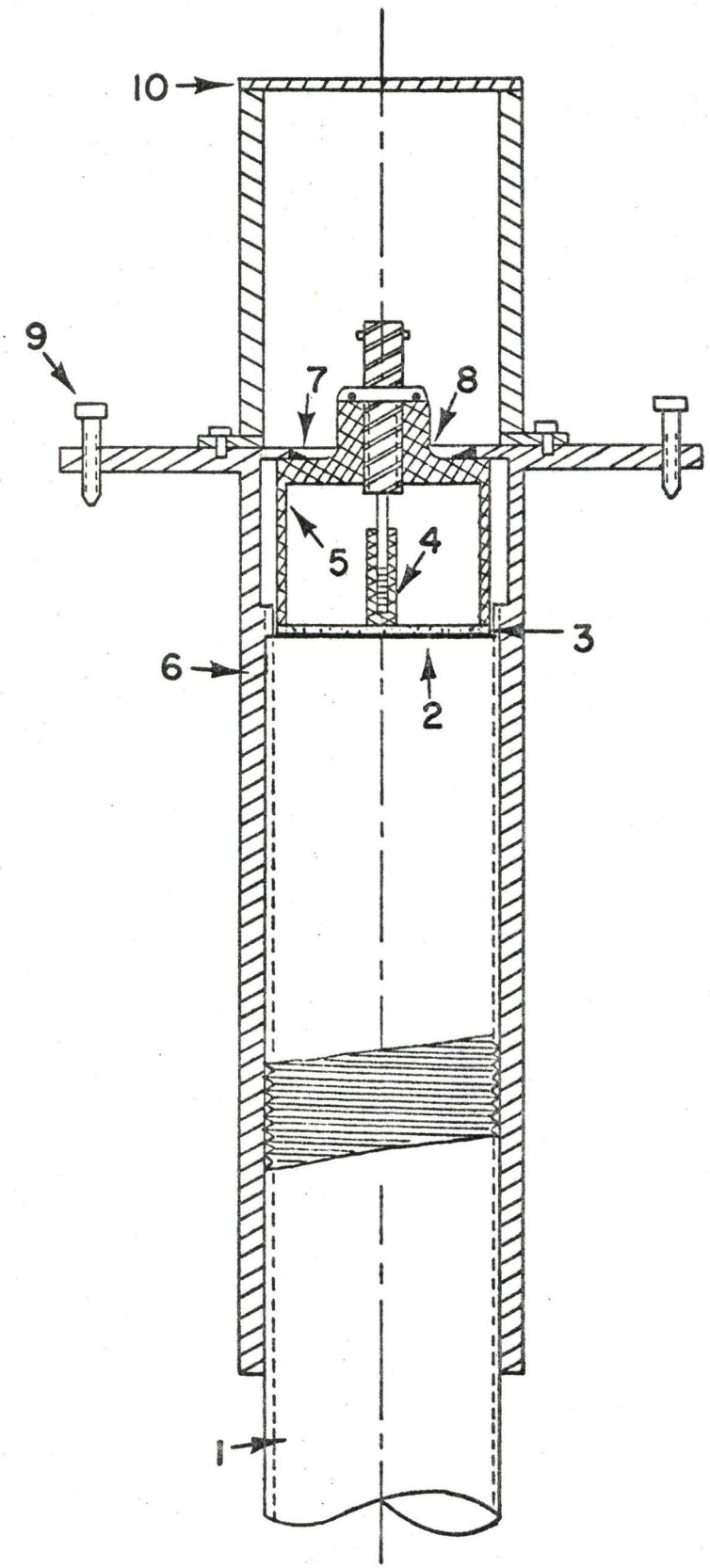

1. Fused silica rod.
2. Gallium bond.
3. Quartz transducer.
4. Center electrode.
5. Outside electrode (ground).
6. Rod holder.
7. Seal.
8. BNC connector with 'O'-ring seal.
9. Levelling screw.
10. Platform from which rod height is measured.

Fig. 18: Rod and electrode holder showing electrode arrangement.

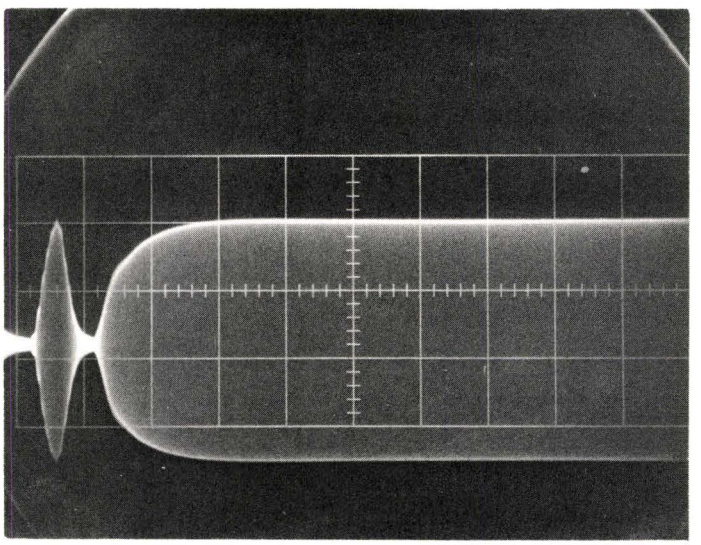

Fig. 19: Melt and comparison pulse (shown on the right) adjusted to be equal in height at f = 49.7 MHz. Horizontal scale = 5 μs/cm. R_f display mode.

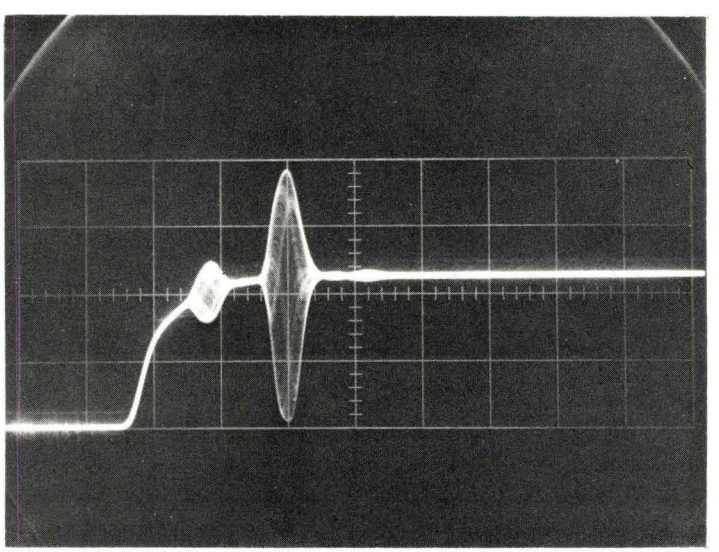

Fig. 20: Comparison pulse shown overlapping melt and "main" echos at f = 25.5 MHz. "Off" frequency condition. Horizontal scale = 5 μs/cm. Video display mode.

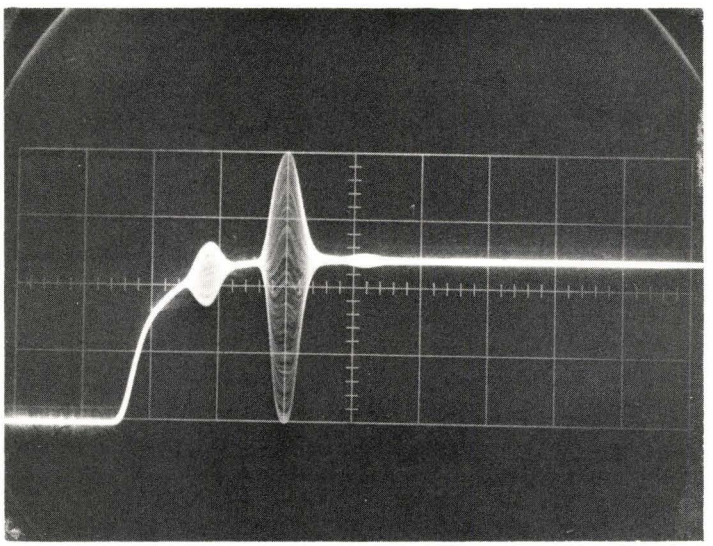

Fig. 21: Comparison pulse shown overlapping melt and "main" echos at f = 25.5 MHz. "On" frequency condition. Horizontal scale = 5 μs/cm. Video display mode.

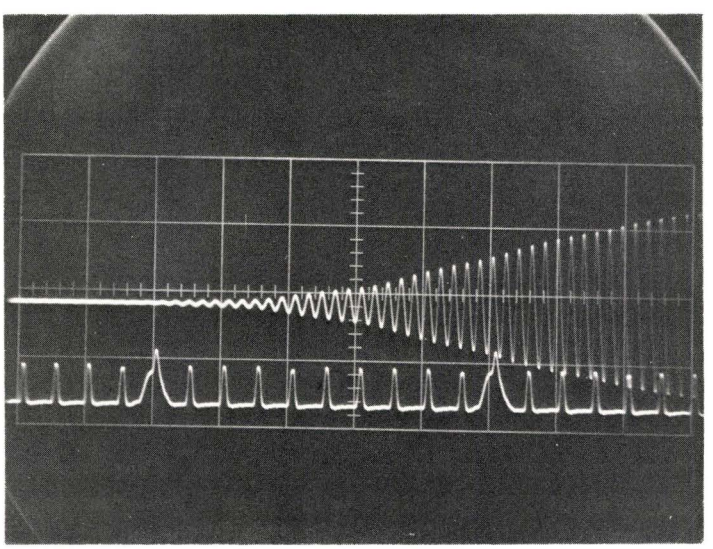

Fig. 22: Expanded view of leading edge of melt echo at f = 25.5 MHz with superimposed time-markers. Horizontal scale = 0.2 μs/cm.

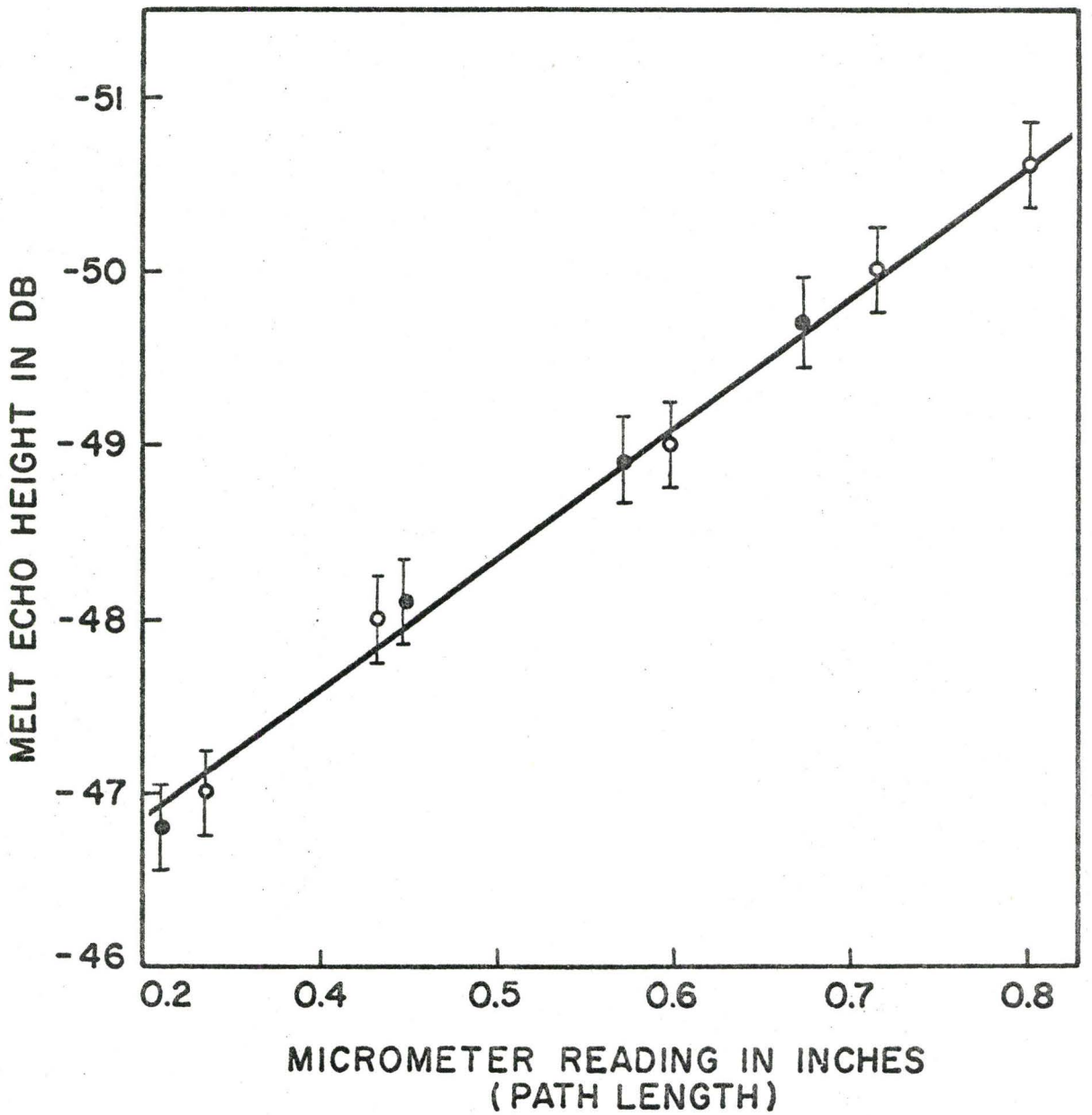

Fig. 23: Attenuation versus distance at f = 16.6 MHz. The points indicated by open circles are for increasing path length while the points indicated by closed circles are for decreasing path length.

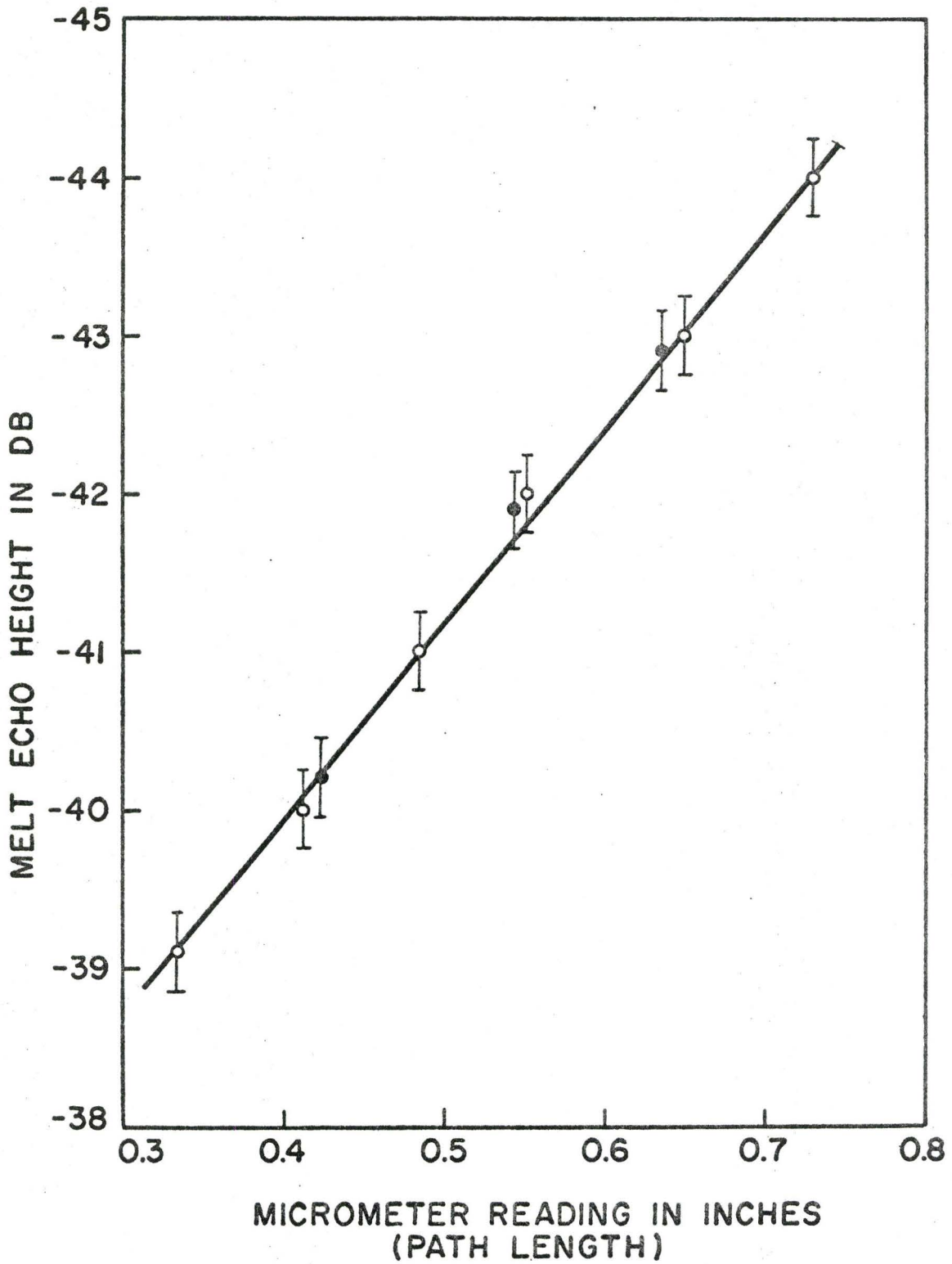

Fig. 24: Attenuation versus distance at f = 25.5 MHz. The points indicated by open circles are for increasing path length while the points indicated by closed circles are for decreasing path length.

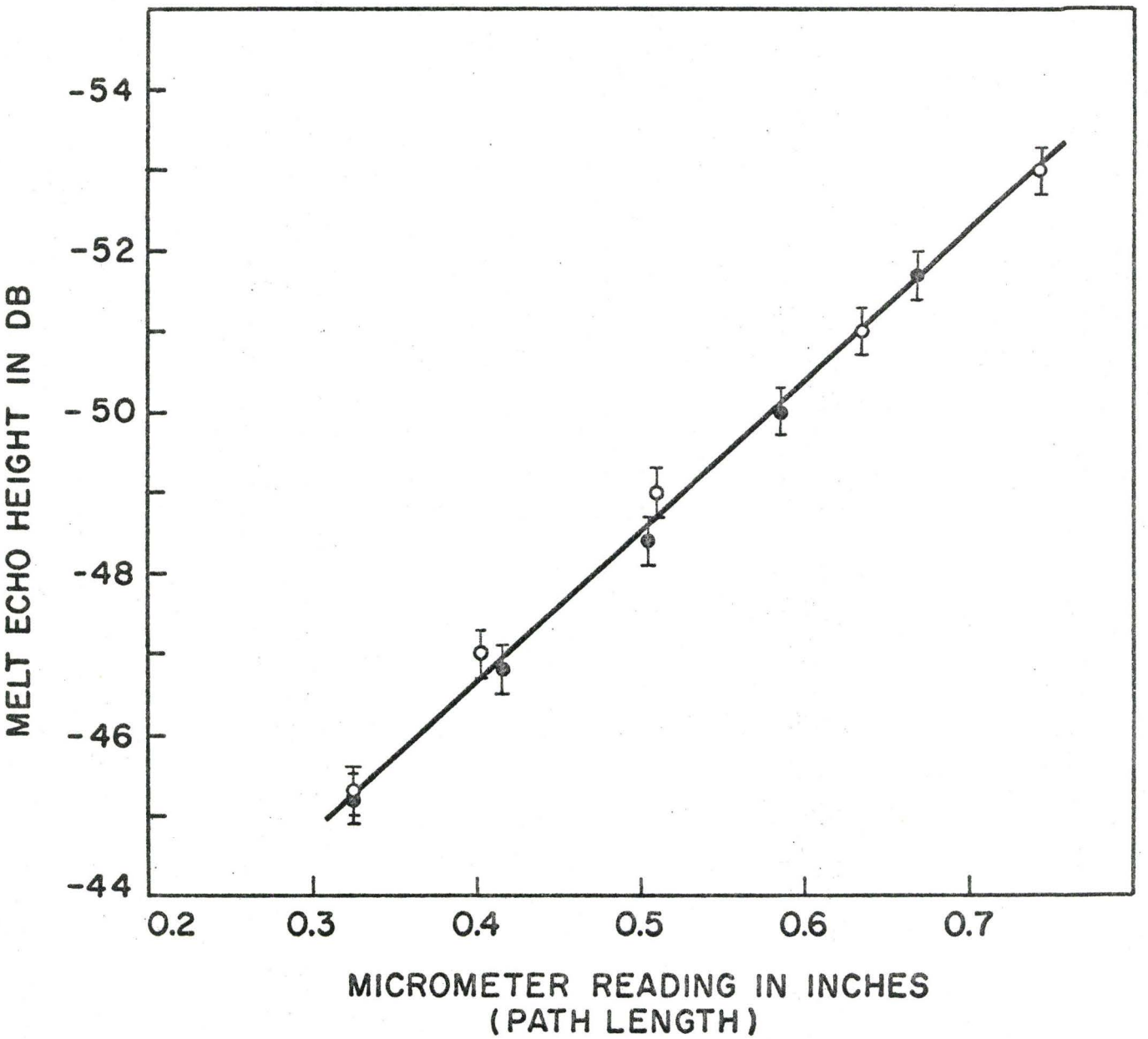

Fig. 25: Attenuation versus distance at f = 37.6 MHz. The points indicated by open circles are for increasing path length while the points indicated by closed circles are for decreasing path length.

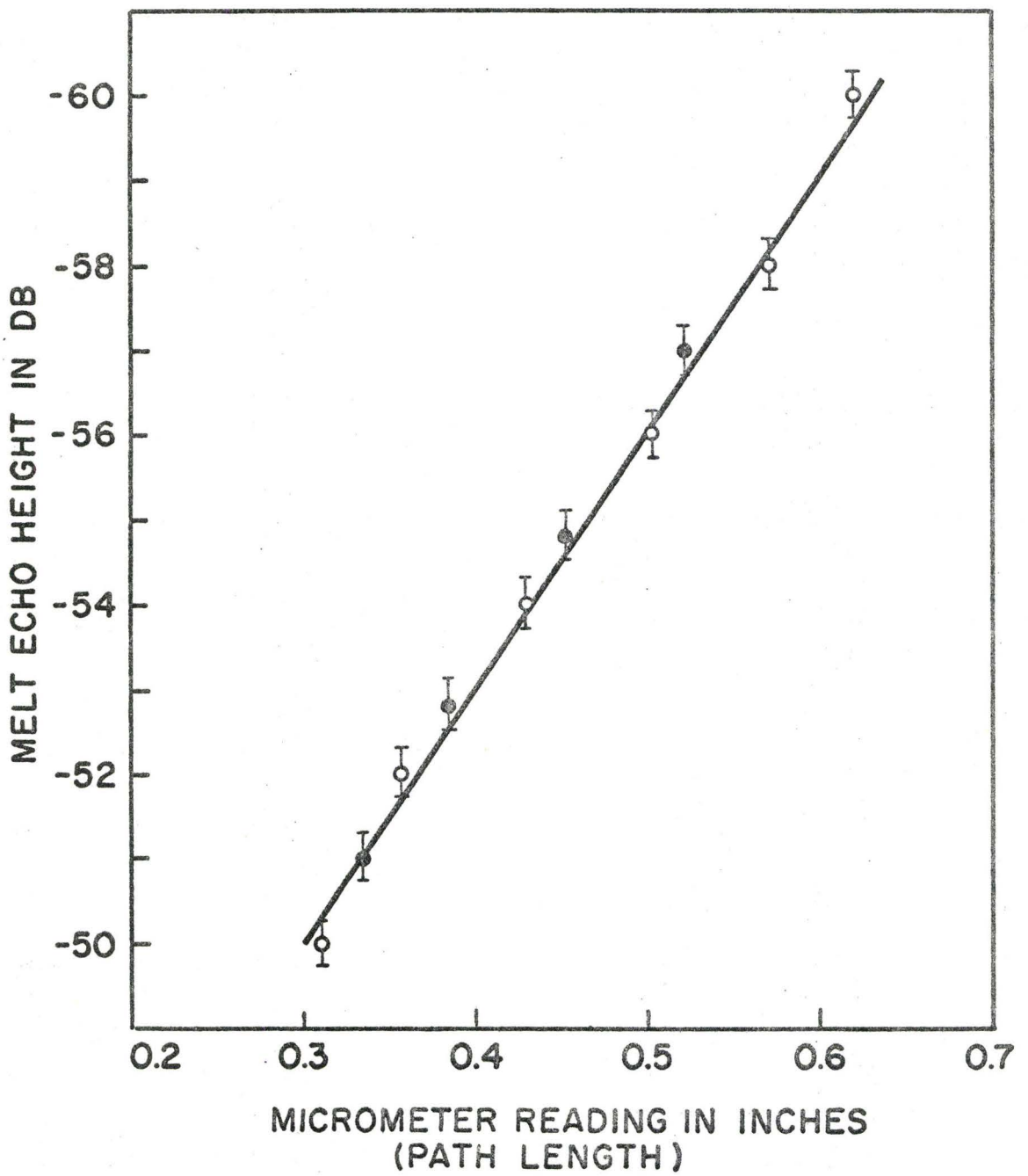

Fig. 26: Attenuation versus distance at f = 49.7 MHz. The points indicated by open circles are for increasing path length while the points indicated by closed circles are for decreasing path length.

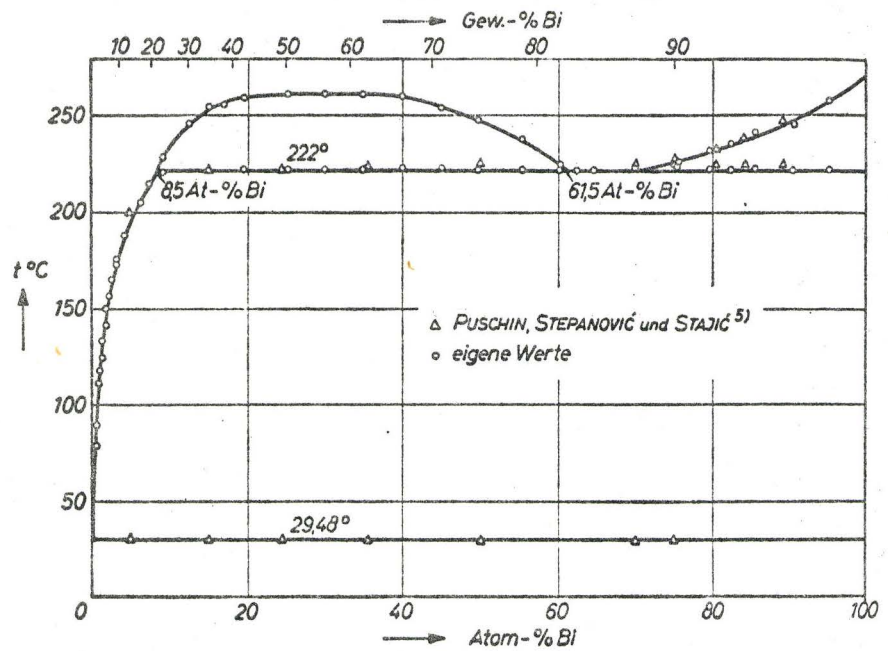

Fig. 27: Gallium-Bismuth phase diagram. Reference 56.

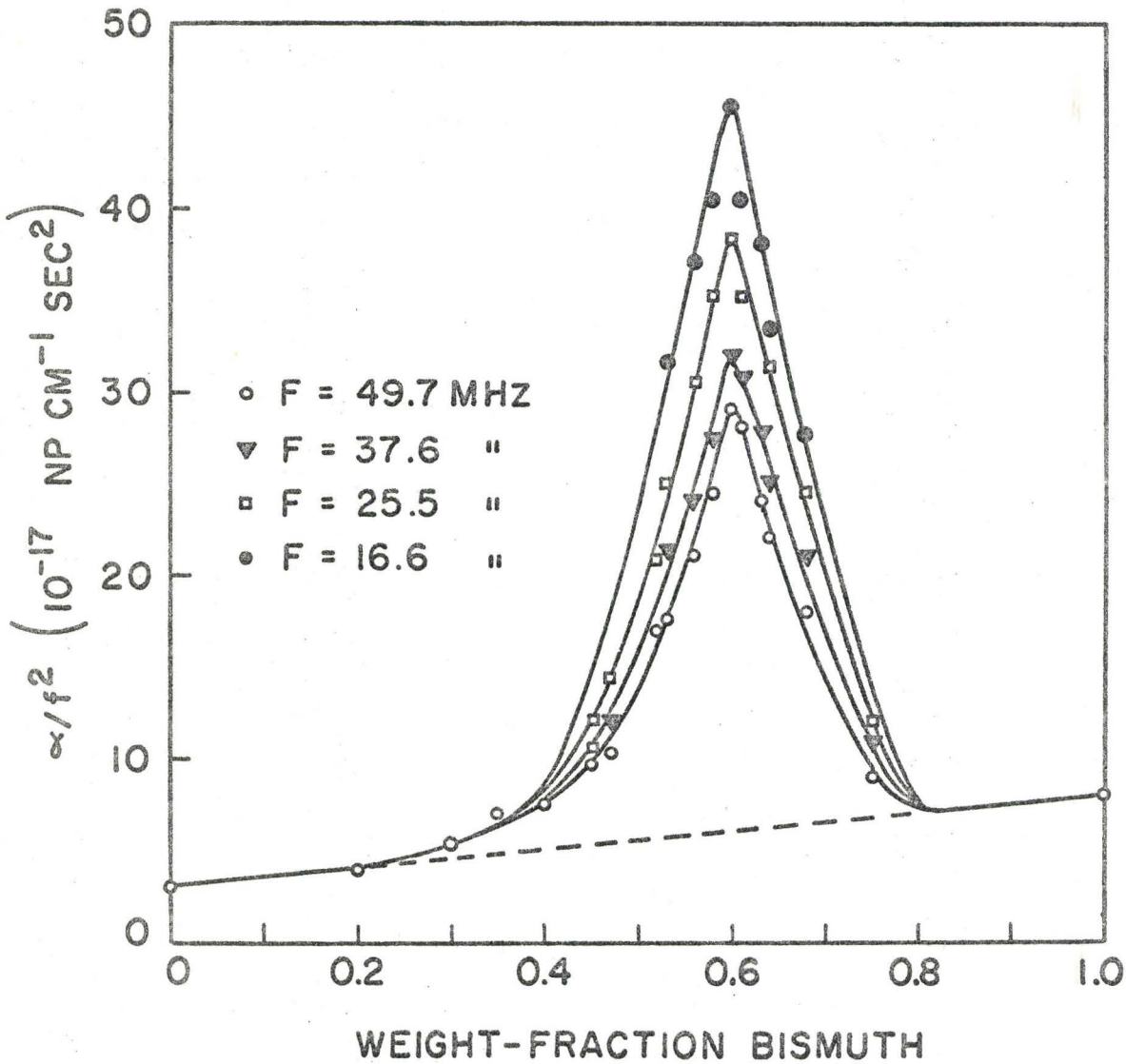

Fig. 28: Attenuation versus composition for Ga-Bi at T = 273.0°C.

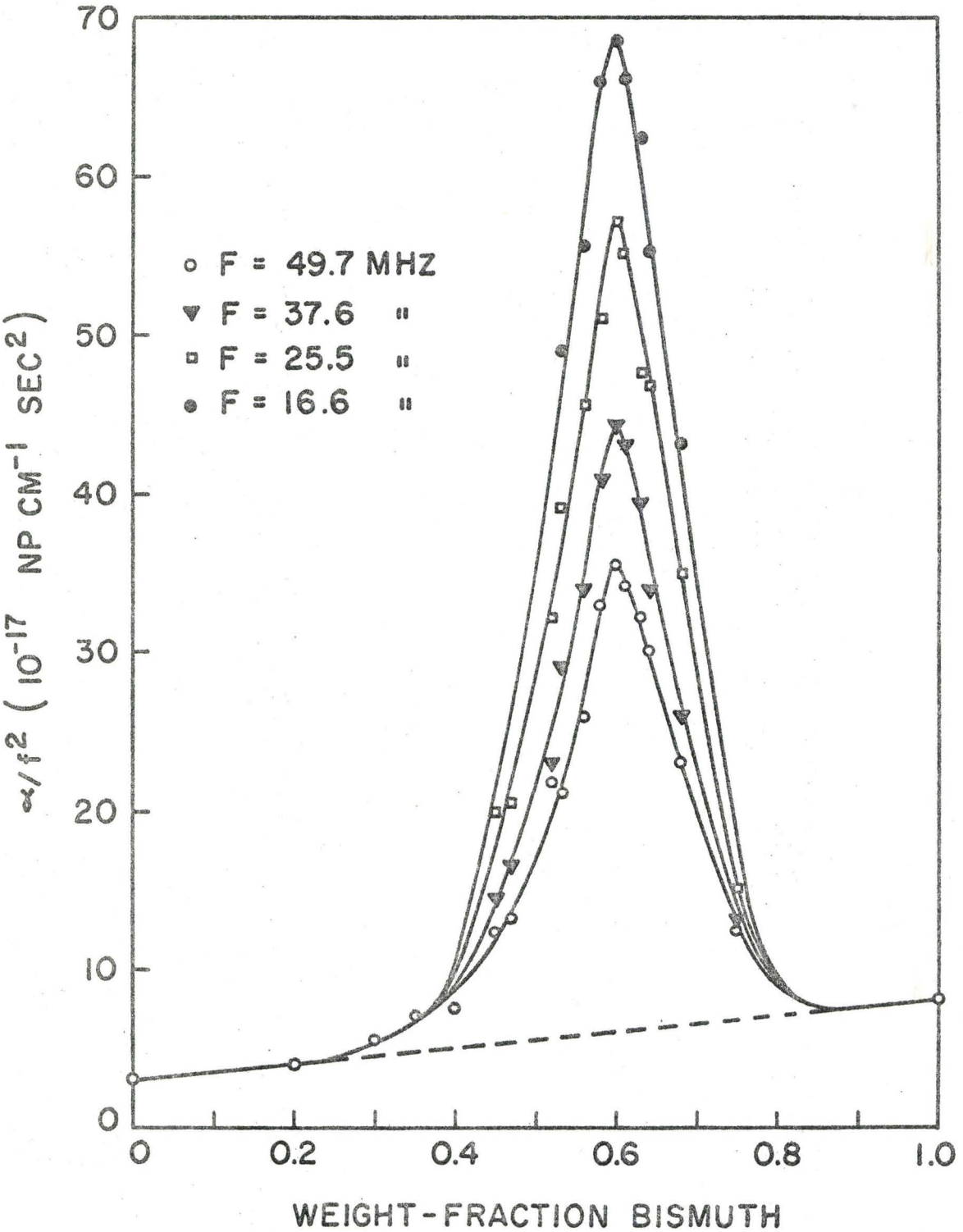

Fig. 29: Attenuation versus composition for Ga-Bi at T = 265.8°C.

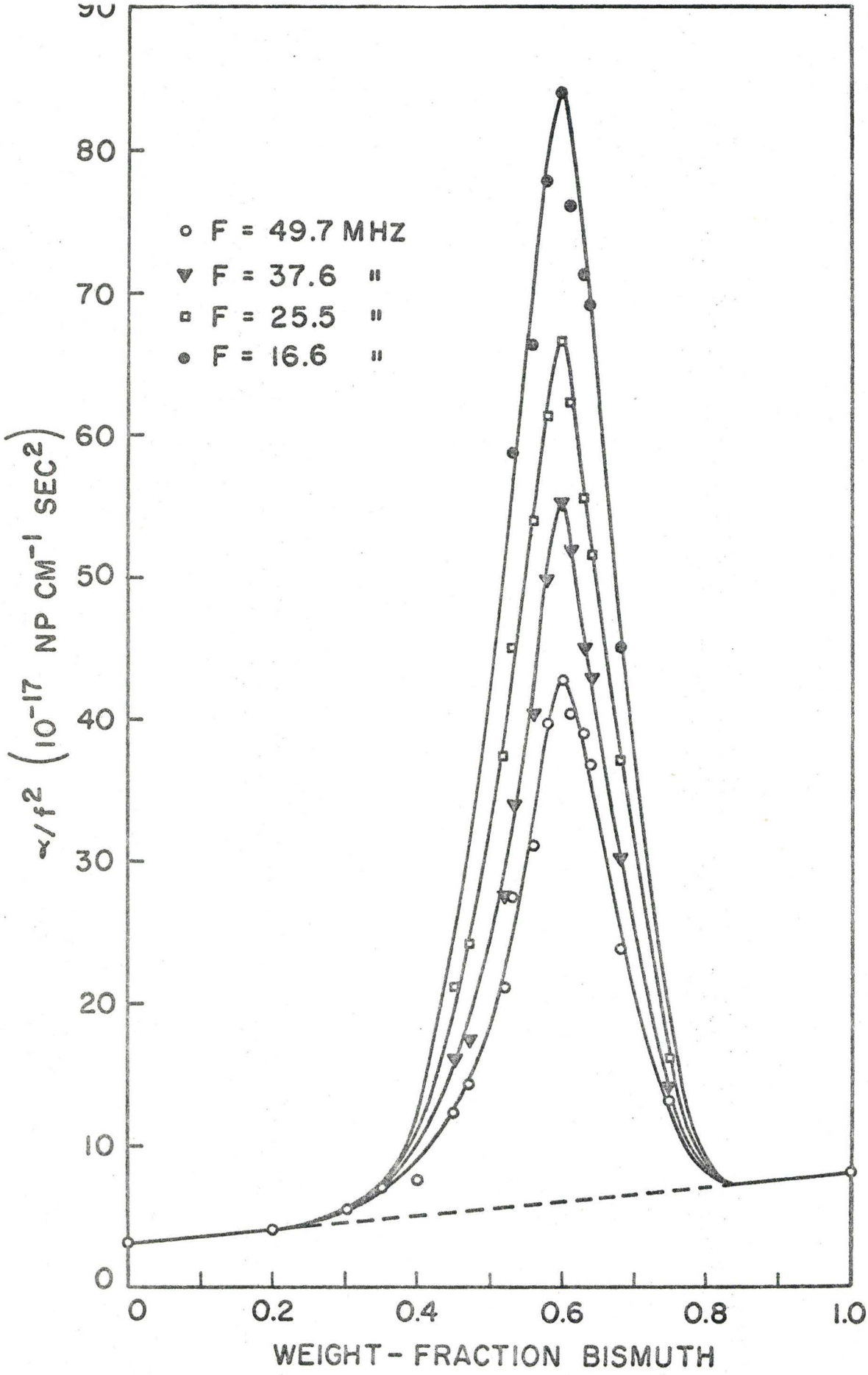

Fig. 30: Attenuation versus composition for Ga-Bi at T = 263.9°C.

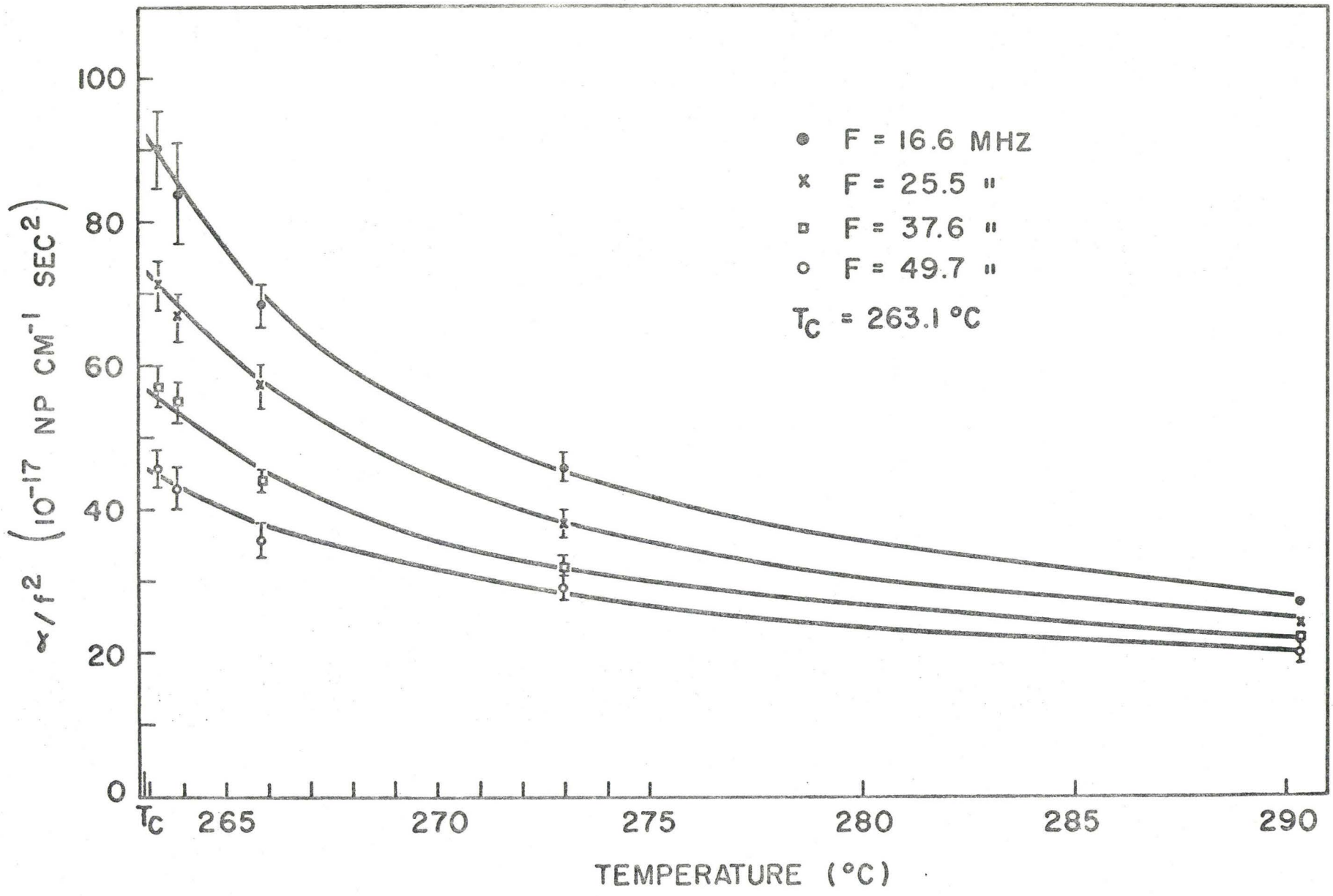

Fig. 31: Attenuation versus temperature for a Ga-Bi mixture at the critical composition.

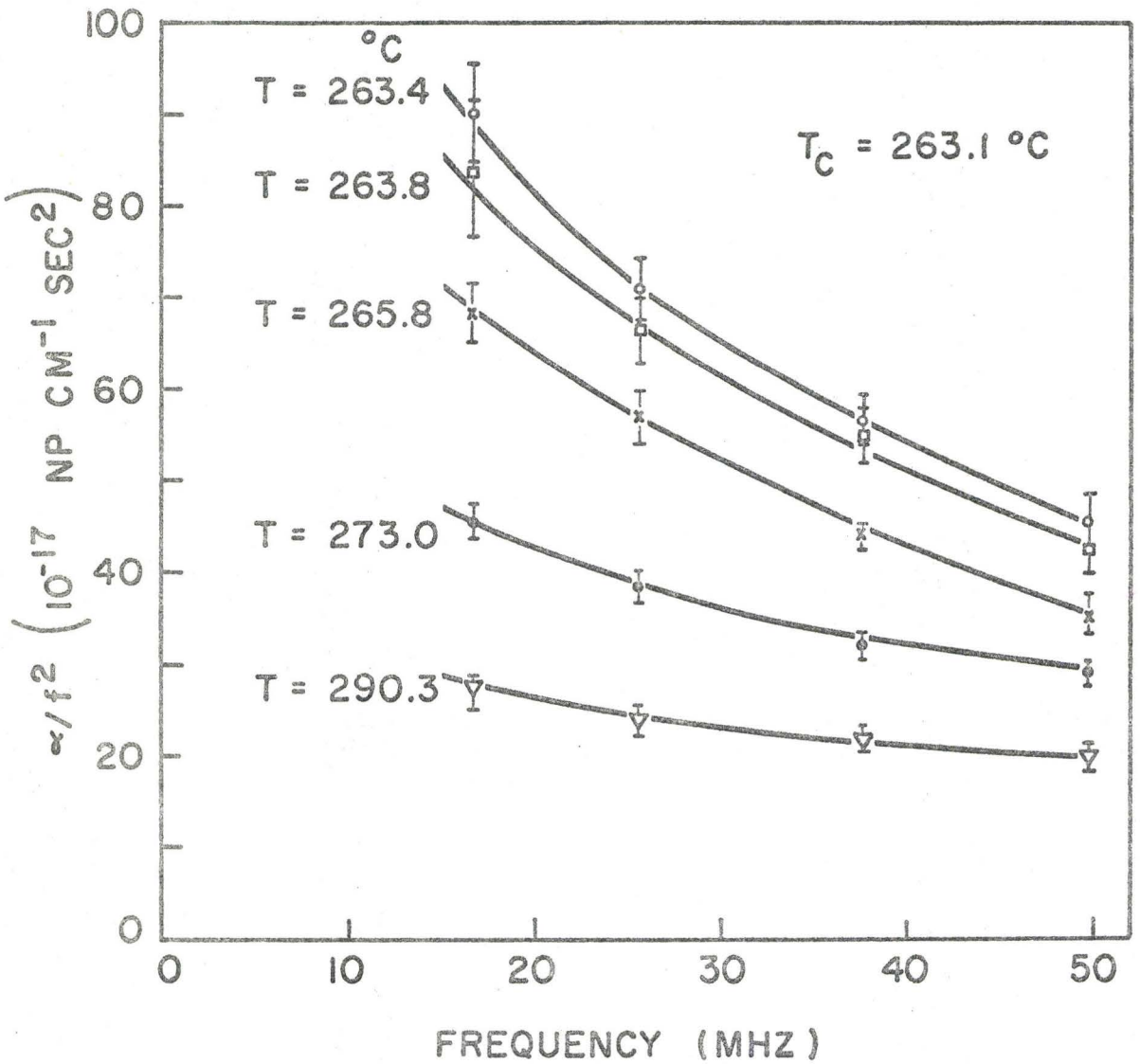

Fig. 32: Attenuation versus frequency for a Ga-Bi mixture at the critical composition.

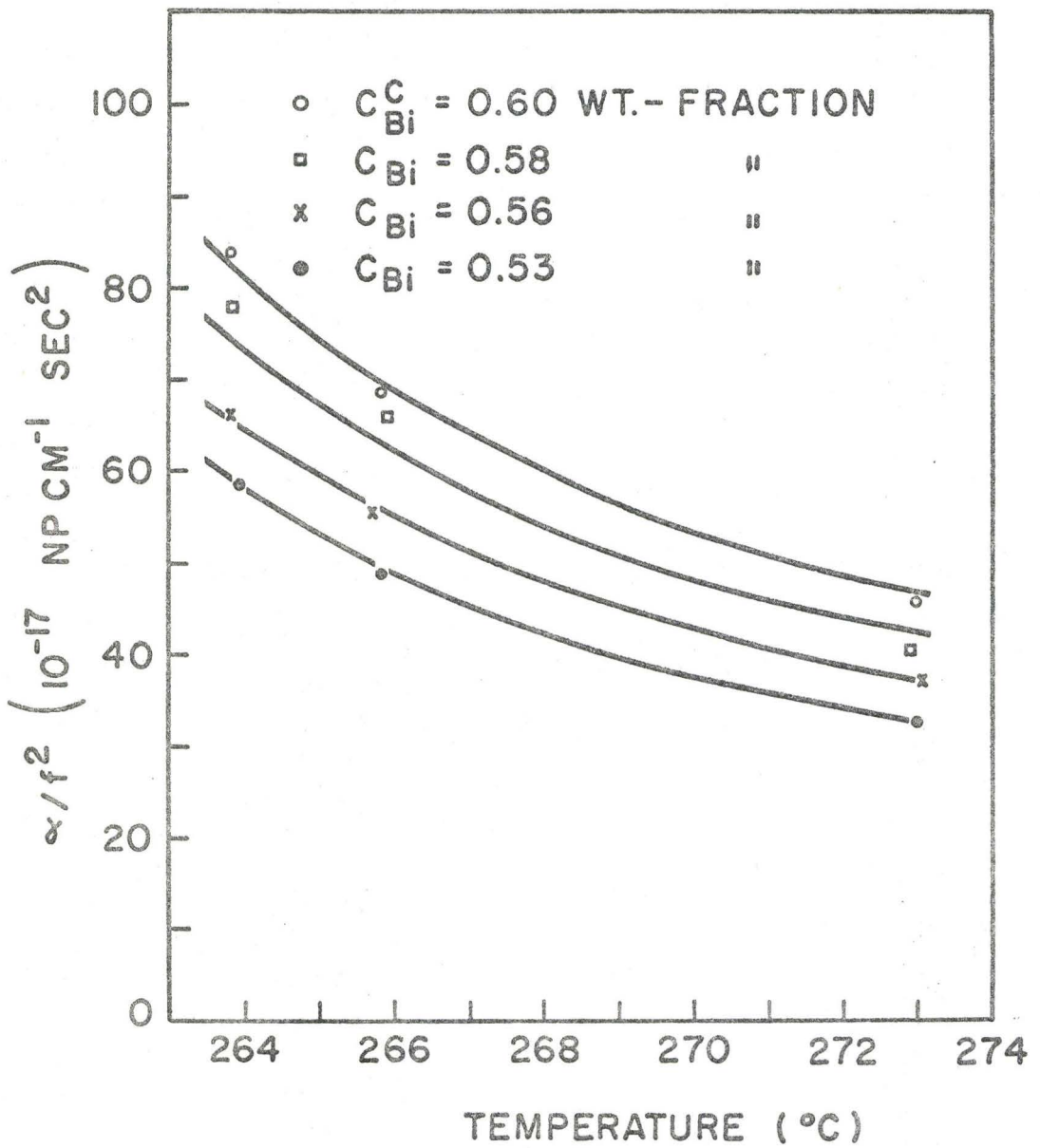

Fig. 33: Attenuation versus temperature for Ga-Bi mixtures at different compositions and at f = 16.6 MHz.

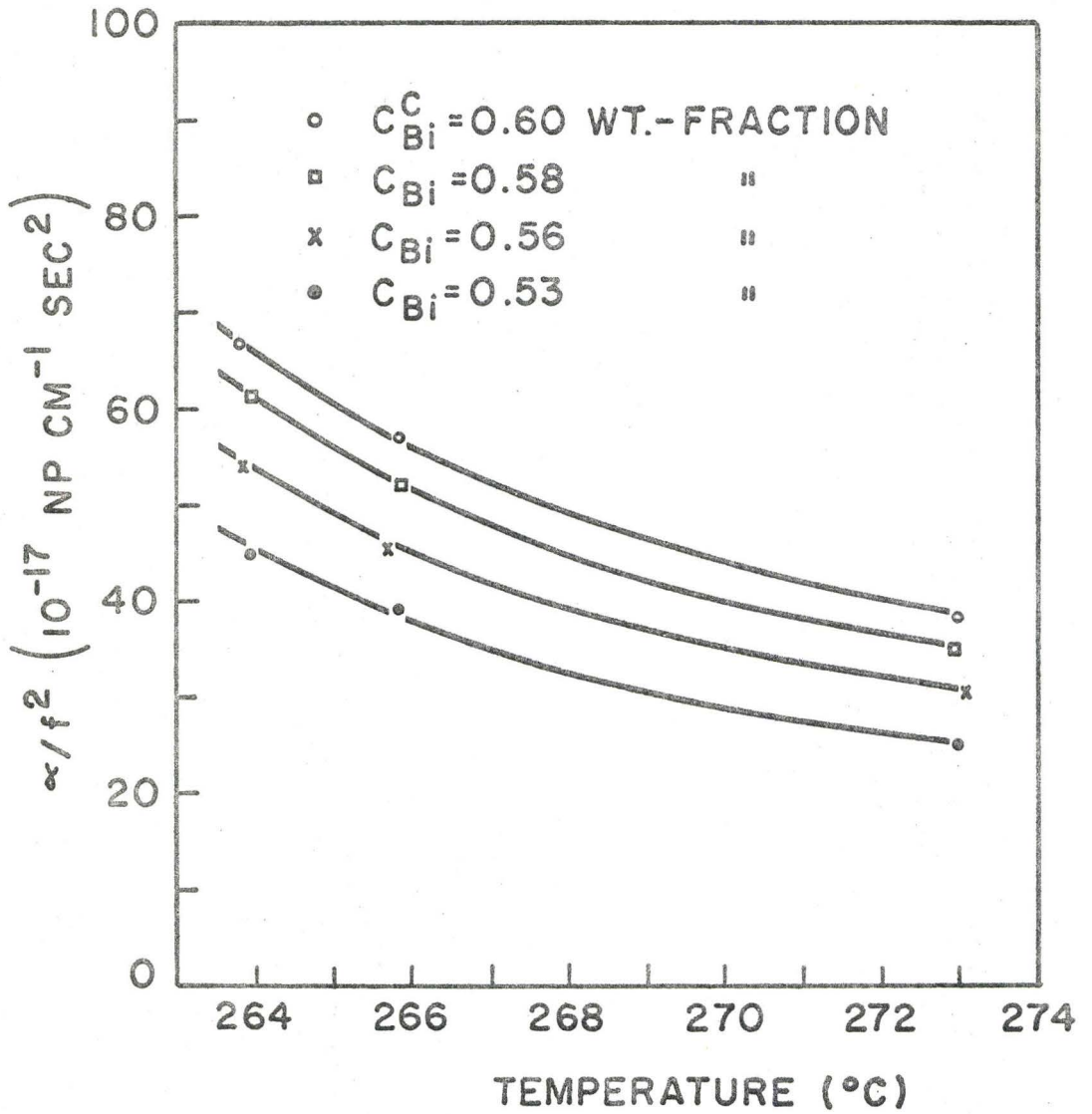

Fig. 34: Attenuation versus temperature for Ga-Bi mixtures at different compositions and at f = 25.5 MHz.

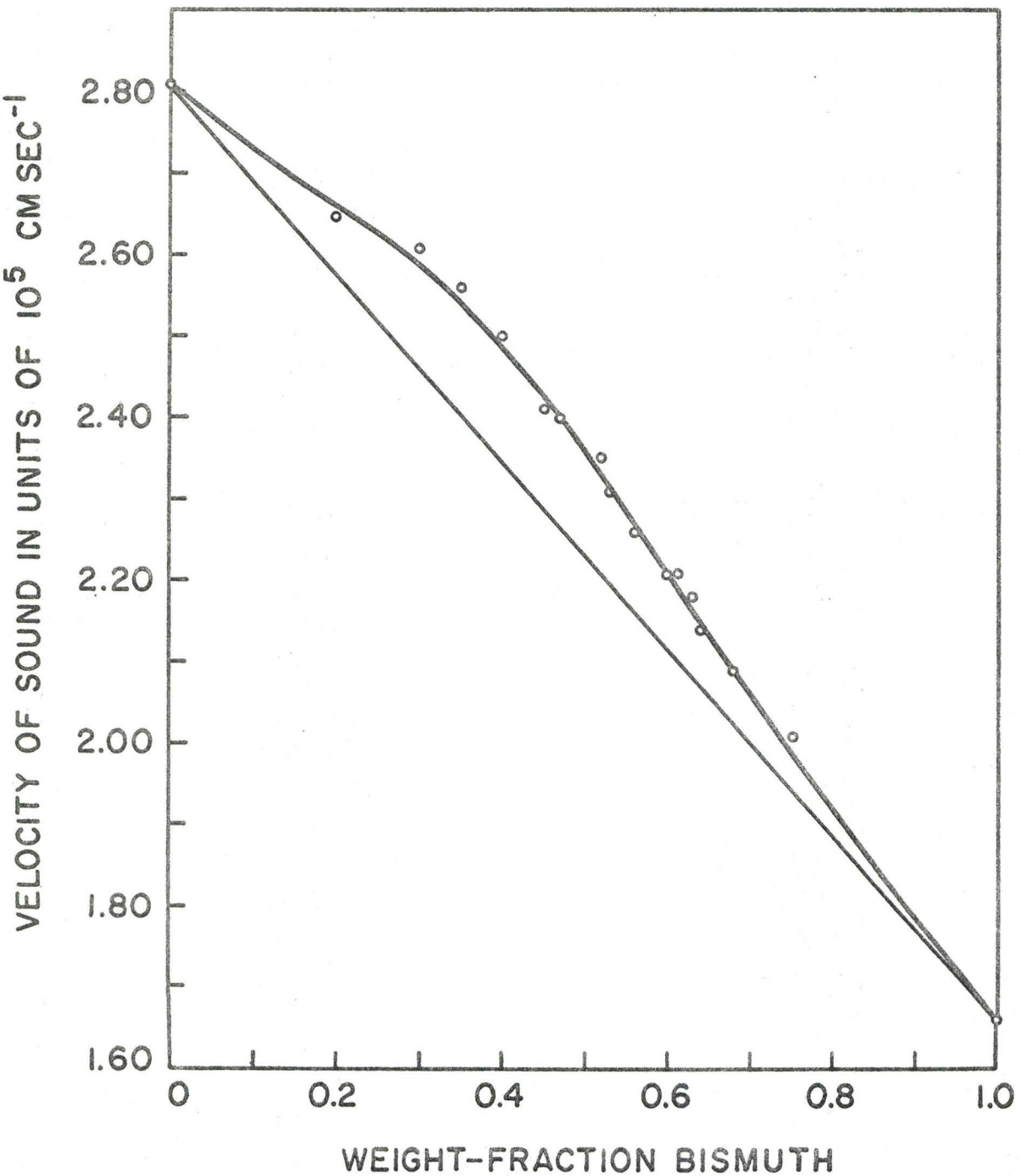

Fig. 35: Velocity of sound versus composition for Ga-Bi at f = 25.5 MHz. These values were independent of temperature from T = 263.4 to 273.0°C.

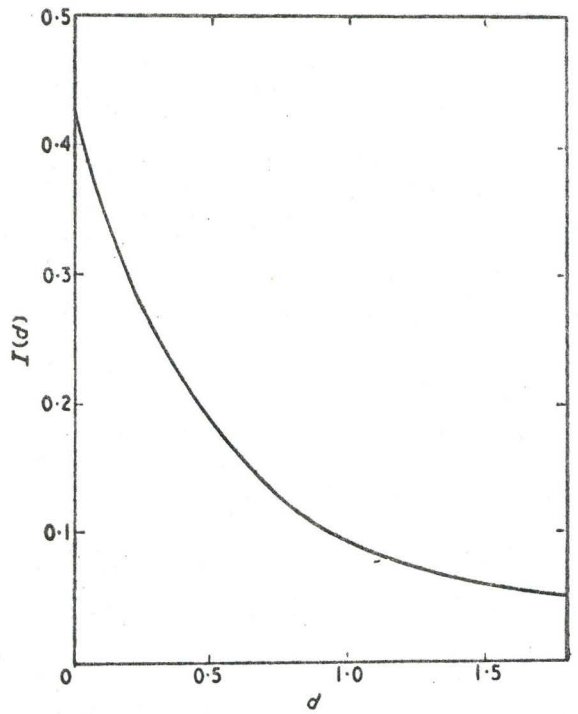

Fig. 36: Graph of Im[f(d)] versus d. Reference 33.

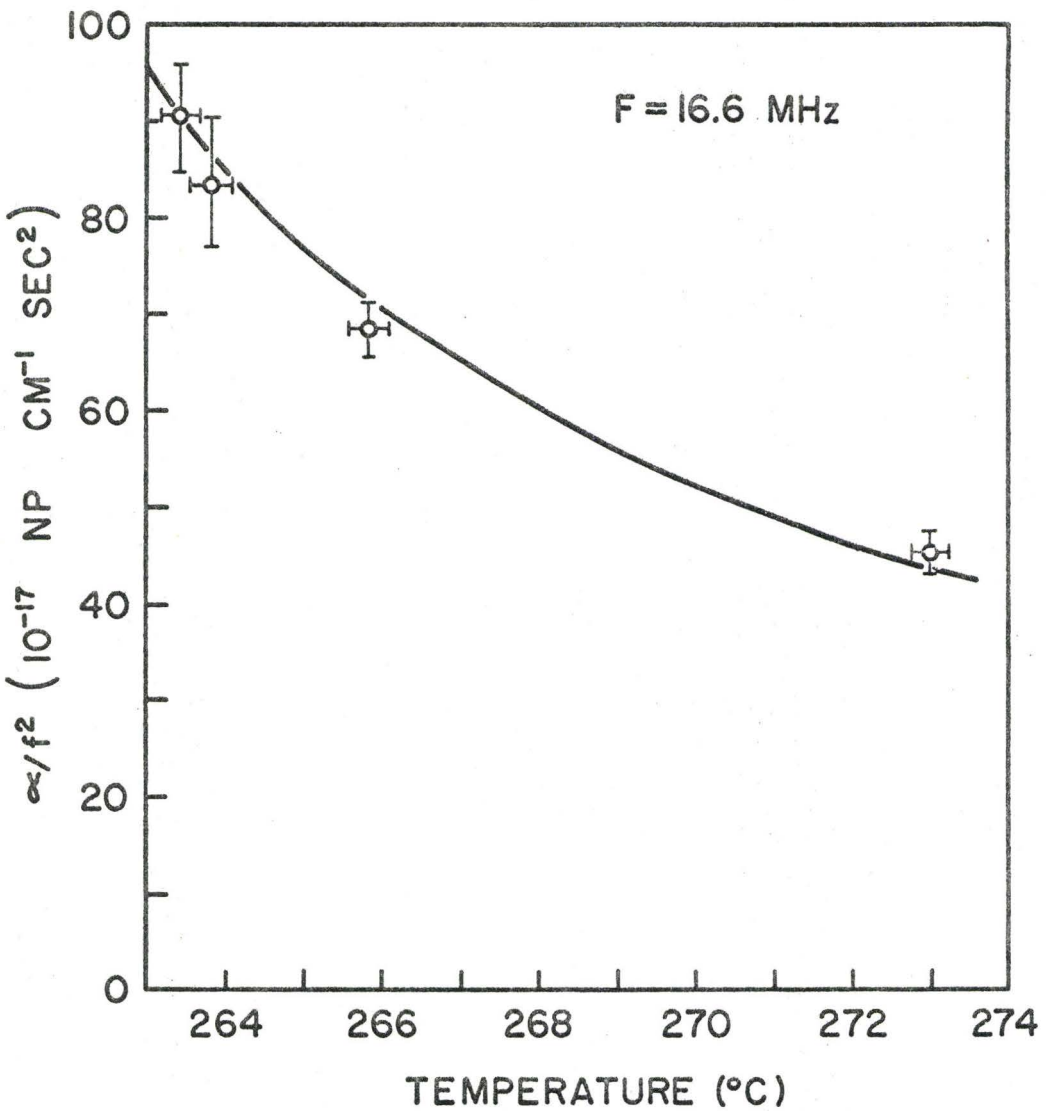

Fig. 37: Attenuation versus temperature at f = 16.6 MHz. The solid line is the "best fit" curve generated by the Fixman equations (7-1) and (7-2). The open circles represent our experimental data.

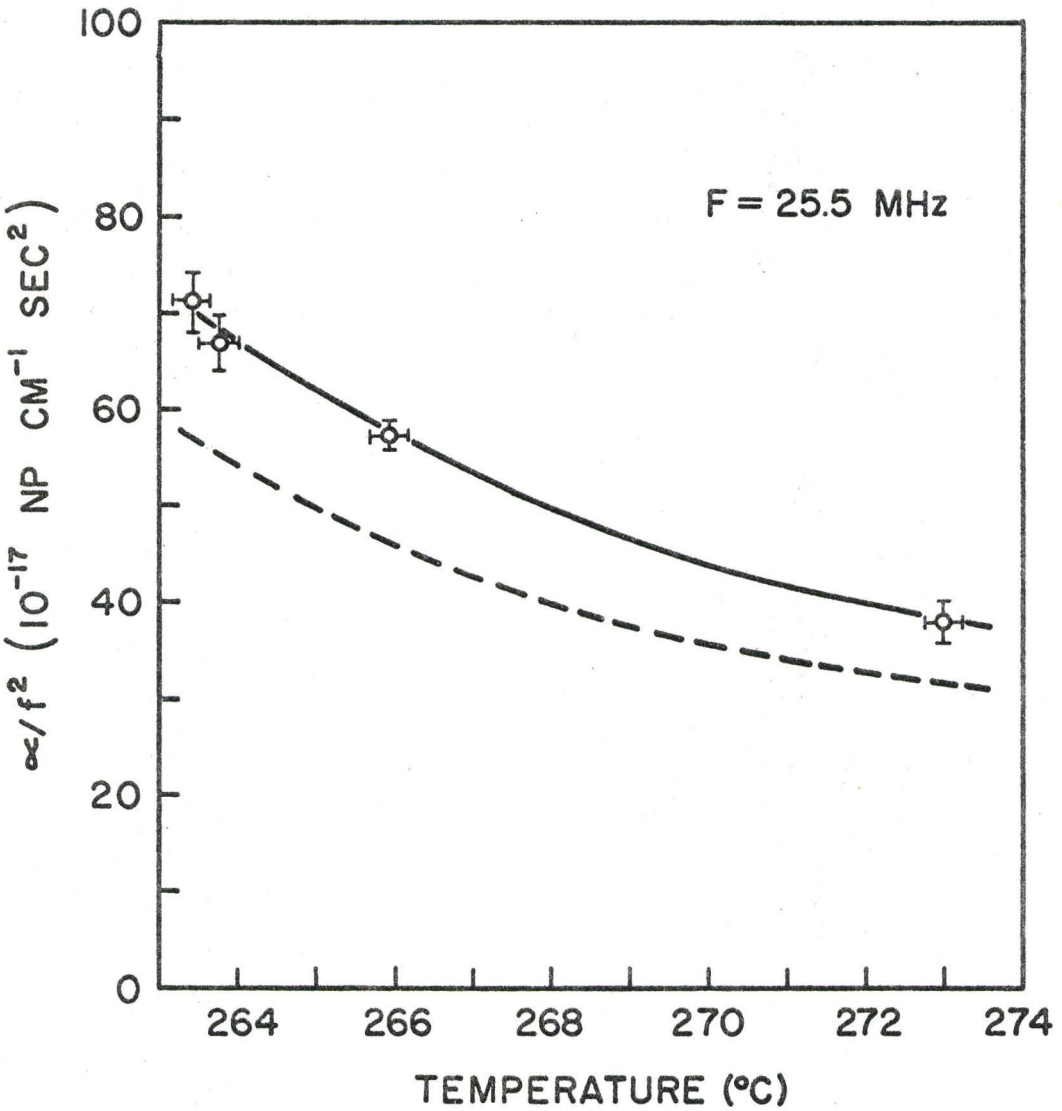

Fig. 38: Attenuation versus temperature at f = 25.5 MHz. The solid line is the "best fit" curve generated by the Fixman equations (7-1) and (7-2). The dotted line is generated by using equations (7-1) and (7-2) with the "best fit" A and C valves obtained at f = 16.6 MHz. The open circles represent our experimental data.

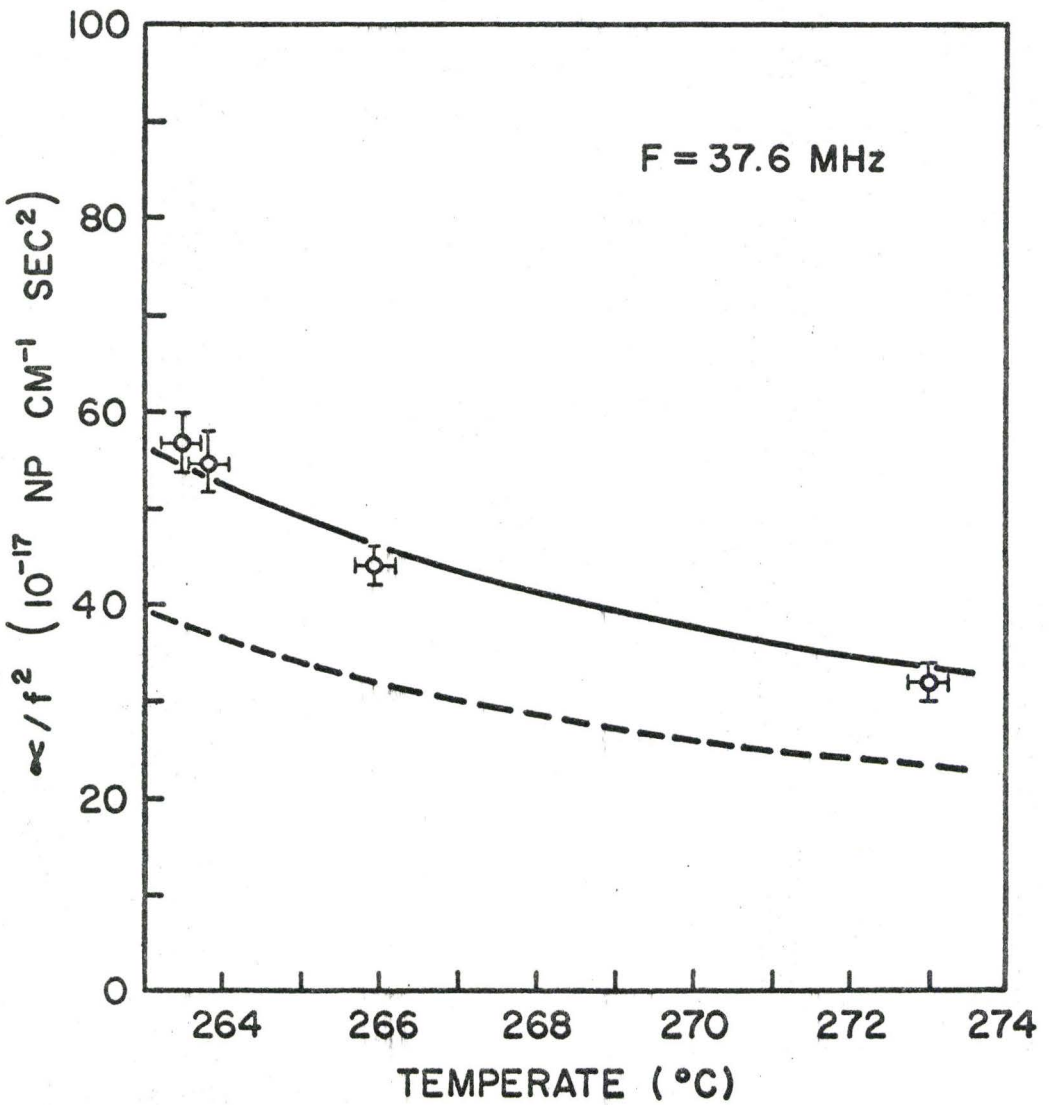

Fig. 39: Attenuation versus temperature at f = 37.6 MHz. The solid line is the "best fit" curve generated by the Fixman equations (7-1) and (7-2). The dotted line is generated by using equations (7-1) and (7-2) with the "best fit" A and C values obtained at f = 16.6 MHz. The open circles represent our experimental data.

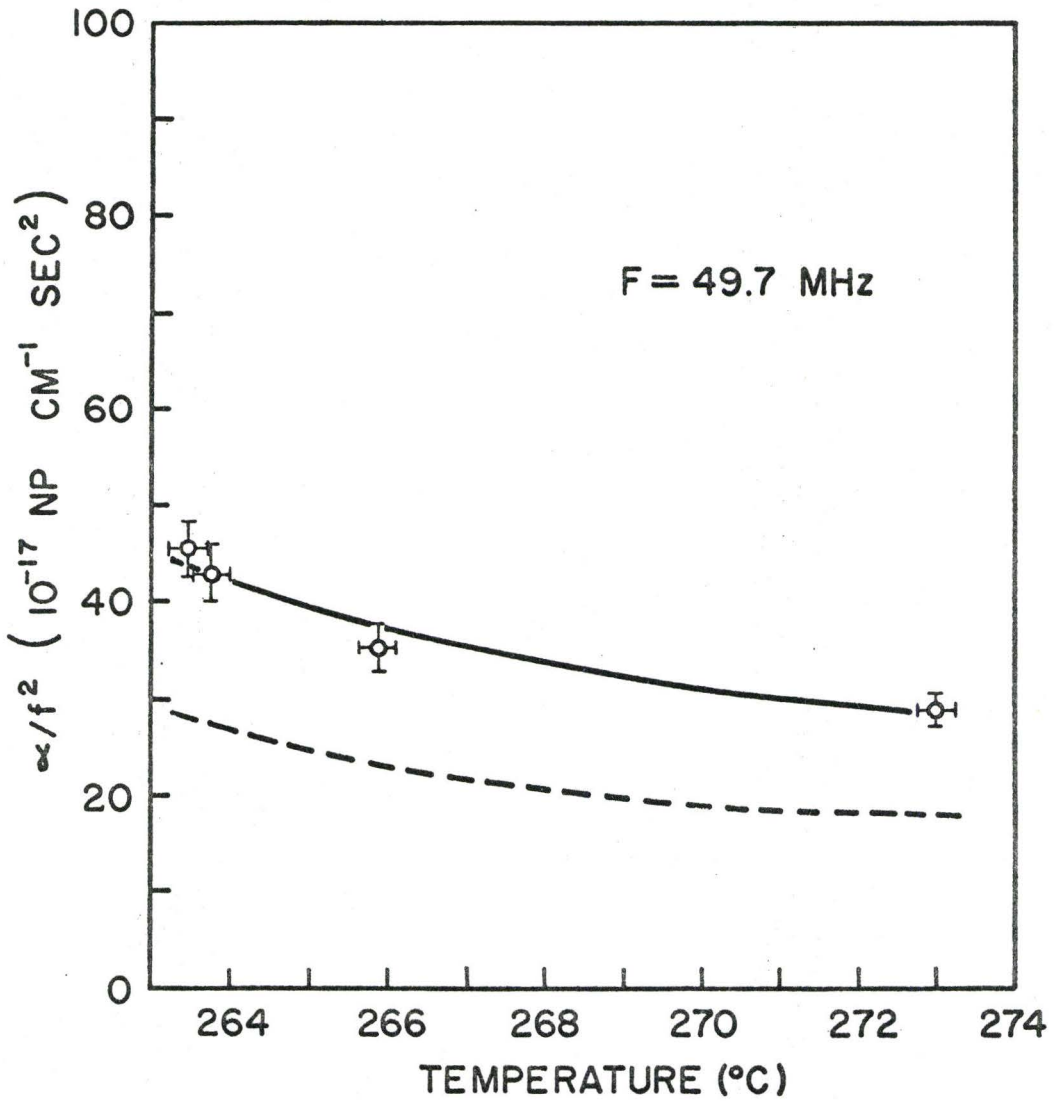

Fig. 40: Attenuation versus temperature at f = 49.7 MHz. The solid line is the "best fit" curve generated by the Fixman equations (7-1) and (7-2). The dotted line is generated by using equations (7-1) and (7-2) with the "best fit" A and C values obtained at f = 16.6 MHz. The open circles represent our experimental data.

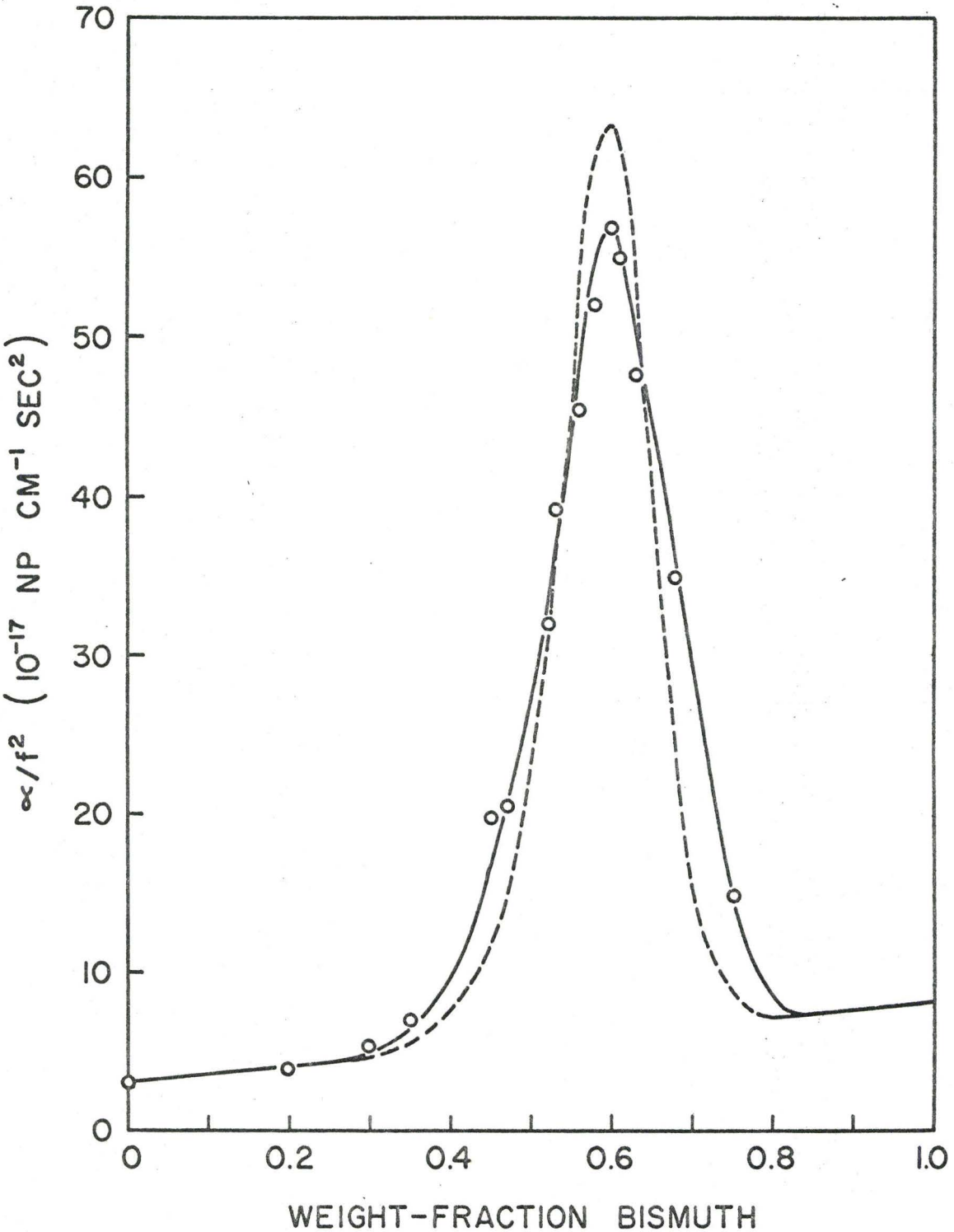

Fig. 41: Attenuation versus composition at f = 25.5 MHz and at T = 265.8°C. Solid line -- experimental; dotted line -- theoretical, (using Flory-Huggins solution model).